DESIGN OF LRB SEISMIC ISOLATORS

PERFORMANCE ASSESSMENT AND DESIGN OF LEAD RUBBER SEISMIC ISOLATORS USING A BILINEAR SPECTRUM METHOD

By

WEIXIAO SUN, B.ENG.SOC

A Thesis
Submitted to the School of Graduate Studies
in Partial Fulfillment of the Requirements
for the Degree
Master of Applied Science

McMaster University

DESCRIPTIVE NOTE

MASTER OF APPLIED SCIENCE (Civil Engineering)
McMaster University Hamilton, Ontario

TITLE: Performance Assessment and Design of Lead Rubber Seismic Isolators Using A Bilinear Spectrum Method

AUTHOR: Weixiao Sun, B.Eng.Soc. (University of Ottawa)

SUPERVISOR: Dr. John C. Wilson

NUMBER OF PAGES: ix, 105,A2,B3

ABSTRACT

Seismic isolation has been widely adopted for structural protection. This technique, which introduces a flexible layer between the structure and the support, isolates the structure from earthquake ground motions by lengthening the structural period. The lead rubber bearing (LRB) is one of the most commonly used seismic isolators. The sizes of the rubber bearing and the lead core determine its stiffness and damping characteristics. The parameters, which characterize the seismic performance of a LRB, are the elastic stiffness (k_1), post-elastic stiffness (k_2), yield strength (F_y) and the total weight (w) of the isolated structure. In this study, an assessment of the nonlinear performance of LRB isolators is carried out using a series of spectra, which are referred to as bilinear spectra, as they are based on the bilinear behaviour of LRBs. The LRB parameters are non-dimensionalized using post-to-pre elastic stiffness ratio ($n=k_2/k_1$) and yield strength to weight ratio ($r=F_y/w$) to construct the bilinear spectra. Feasible ranges of n and r have been considered according to design code recommendations. The spectra are constructed from statistical analyses of LRB responses due to sets of real earthquake ground motions. These spectra plot the displacement and the shear force response of isolated structures for various combinations of n and r, vs. the elastic period.

The results of the study show that displacement decreases as the lead content increases, as expected. However, the corresponding shear forces fluctuate over different isolated periods. An increase in the rubber bearing size increases only the shear response, but has

negligible influence on the displacement. It is also found that earthquakes with a lower ratio of PGA/PGV tend to result in higher displacement and shear force responses of the LRB compared to ground motions with higher PGA/PGV ratios.

A new chart-based method (referred to as the Chart Method) is developed by using a regression-based bilinear spectrum for estimating the LRB isolator displacement and shear force responses. The design capability of the Chart Method is compared to a more conventional method for designing LRBs, by solving several examples. The study concludes that the Chart Method has improved accuracy and versatility and can be used to evaluate the design suitability of commonly available LRB sizes.

ACKNOWLEDGEMENTS

I would like to express my sincere gratitude to my supervisor Dr. John Wilson for his valuable advice and patient guidance throughout this entire process.

I would like to thank my colleagues in the Department of Civil Engineering who have always tried to answer my questions, in particular Hamed Ebrahimian.

Finally, I would like to thank my parents Sijie and Zhongmei for all the support and encouragement they provided me during the entire graduate studies.

TABLE OF CONTENTS

LIST OF TABLES

LIST OF FIGURES

1. INTRODUCTION

1.1. OVERVIEW

Isolation strategies for seismic protection have been used since ancient days. They were however first used for major structures in the 1970's. The basic concept is to isolate structures from earthquake ground motion thus protecting the structures from damage. This is achieved by introducing an interface that lengthens the structural period and/or adds energy dissipation mechanisms. Typically, the isolated structural period is about two to three seconds, where the earthquake response spectrum is substantially reduced. This lengthed period places additional displacement demand on the isolators. For many reasons, this displacement must be controlled. Isolators are categorized as linear or nonlinear depending on whether or not a hysteresis damping mechanism is integrated into the isolator unit. Systems with linear isolators will normally need auxiliary damping. The performance of nonlinear isolators is influenced by the stiffness of the bearing and the hysteresis damping mechanism. For the most commonly used isolator, the lead-rubber bearing (LRB), the stiffness and damping are determined by the sizes of the rubber bearing and lead core, respectively. This study focuses on the performance of LRBs.

1.2. OBJECTIVES & METHODOLOGY

There are two main objectives to this study. The first is to review the characteristics of selected earthquakes and examines LRB performance characteristics, which are affected by the lead content ratio and the size of the rubber bearing. This is achieved using a series of spectra, which are the mean plus one standard deviation (84.1 percentile) of the

displacement and shear responses of bilinear modeled isolators for a group of ground motions. This type of spectrum is named a bilinear spectrum in the following content, as it plots the responses of bilinear modeled isolators.

The second part of the thesis reviews seismic isolation design methods, and introduces a chart-based LRB design method (Chart Method). The Chart Method utilizes regression-based response data to estimate the displacement and shear responses at a given structural weight to elastic stiffness ratio for a certain shaking intensity. An example is used to demonstrate the design procedure and the design accuracy is compared to that of conventional methods.

In this study two assumptions are made: 1) peak ground acceleration (PGA) to peak ground velocity (PGV) ratio less than unity can be used to identify forward directivity focusing affected earthquakes. 2) Under the same shaking intensity, the mean or mean plus one standard deviation response values of different groups of earthquakes are similar when they belong to the same PGA/PGV category (i.e. PGA/PGV< 1 or >1).

Over ten thousand nonlinear time-history analyses of seismic response of LRBs were performed using SAP2000 Version 14 (Computers and Structures, 2010). The LRBs were modeled using NLLink elements. SAP2000 input text files were created and modified using an Excel Macro (Excel, 2007), and were then semi-automatically executed using the SAP2000 Batch File Control feature. Manual verification of the SAP2000 nonlinear

response results was carried out using the method provided in Chapter 8 of Clough and Penzien (1975).

1.3. THESIS OUTLINE

There are five chapters in this thesis, with the first being an introduction. Chapter 2 provides a brief history of seismic isolation and a description of lead rubber bearings. A brief review of conventional LRB design methods is included in Chapter 2 as well.

Chapter 3 presents the fundamental parameters and the methodology that was used to select earthquake records and identify earthquakes affected by forward directivity focusing. The time-histories of selected records are compared in terms of long duration pulse-like content and spike content. The velocity spectra of selected records are compared by identifying the periods with the most energy content.

Chapter 4 presents the nonlinear time-history analysis results of various LRB systems using a series of bilinear spectra. These bilinear spectra have two uses: 1) assessing LRB design parameter influences on the performance; 2) developing a design method. Towards the end, the conventional design method is reviewed and comparisons are made with respect to the proposed Chart Method. Chapter 5 reviews the observations and summarizes the main findings of this study.

2. LITERATURE REVIEW

2.1. INTRODUCTION

This chapter will first introduce the basic concepts and history of seismic base isolation. The development of code provisions and a brief review of current applications will be presented towards the end.

2.2. HISTORY AND THEORY OF SEISMIC ISOLATION

In ancient China and Japan, it was thought that a layer of sand or steamed rice could be introduced between the base of buildings and the ground to isolate the buildings from earthquake ground motion. By doing this, the builders could have earthquake structural response control and damage limitation (Higashino and Okamoto, 2006).

Much later, in 1909, a similar concept was proposed by J.A.Calantarients, a medical doctor from the northern English city of Scarborough. He proposed to build structures on a layer of fine sand, mica, or talc that would allow the building to slide during an earthquake excitation, thereby reducing the earthquake energy transmitted to the building (Naeim and Kelly, 1999). These are some of earliest examples of the earthquake resistant design methodology now known as base isolation or seismic isolation.

The concept of base isolation is widely used in earthquake-prone regions of the world. In United States, Japan, New Zealand, and Italy, seismic isolation has been considered for application to important buildings A few demonstration projects for application on public

housing in developing countries have been completed in Chile, China, Indonesia, and Armenia (Naeim and Kelly, 1999).

The first real isolation project was done in 1969 in Skopje, Yugoslavia. Rubber bearings were utilized to protect an elementary school. The rubber block used was unreinforced and thus sideways bulging was experienced due to the weight of the structure. To eliminate the bulge effect, steel was introduced to reinforce the rubber block by using laminated multilayered combinations of steel and rubber layers. Such a structure is able to provide a high vertical stiffness with a relatively low stiffness in the horizontal direction. This isolator configuration was changed in 1975, when Robinson invented a bearing with a lead plug inserted into rubber (Skinner et al., 1993). The yielding of the intrusive lead plug provided a considerable amount of hysteretic damping to dissipate the earthquake energy. This type of isolator was tested and used in practical applications by the New Zealand Ministry of Works and Development (MWD) a few years later. This bearing type was named lead-rubber isolator or bearing and is the most common type of isolator in use today (Naeim and Kelly, 1999).

Seismic isolation has been increasingly adopted in large scale structural construction since the early 1980's. The first large-scale application of seismic isolation was done in 1981 in New Zealand; LRBs were used to protect the William Clayton Building (Fig. 2.1). In the USA, the first building to be seismically isolated was the Foothill Communities Law and Justice Center (Fig. 2.2) in Los Angeles 1985 (Higashino and Okamoto, 2006).

2.3. BASIC CONCEPT

The fundamental objective of seismic isolation is to reduce a substantial amount of the force and energy transmitted to the structure. This reduction is achieved by offering period lengthening and/or adding energy dissipation mechanisms (Skinner, et al., 1993). The reduction in force and energy is accompanied by an increase in the displacement demand (Fig. 2.3& Fig. 2.4).

The concept of earthquake resistance can be viewed as a supply and demand relationship. The conventional way to resist earthquake load was to strengthen the structure in order to provide sufficient supply. It was unrealistic to expect the amount of supply being adequate in all earthquake events. Moreover, strengthening the structure would result in an increase of demand (i.e. higher stiffness corresponds to higher spectral acceleration). Opposite to this traditional concept, seismic isolation softens a conventional structure by adding a flexible supporting mechanism to the base. This lowered stiffness elongates the natural period of motion which provides a reduction in the demand and thus the supply and demand relationship is equated in a more realistic and active way.

Ideally, the isolation system decouples structures from ground motions completely. Theoretically, this can be achieved by introducing a "soft layer" between the structure and ground. In other words, the isolated superstructure remains still while the ground is moving. Thus, earthquake energy is isolated at the isolator level. However, in reality, a complete isolation is not achievable, because of the following two reasons:

1) A material cannot feature both high vertical stiffness and strength while its lateral stiffness is zero.
2) Displacement is often limited due to space restriction or other design consideration.

For these reasons, the seismic isolation adopted in practice only partially isolates the structure, and some of the earthquake energy is still transferred to the structure.

2.4. COMPARISON WITH CONVENTIONAL DESIGN

Seismic isolation has been considered a promising technique in the earthquake resistance field. Compared with conventional design, it limits the amount of earthquake energy transmitted to the superstructure and thus less structural damage is expected.

In conventional fixed-base design, under moderate or high magnitude earthquake excitation, structures cannot remain in the elastic range. The earthquake energy is transmitted to structures and is dissipated through reinforcement yielding and concrete cracking, which lead to unavoidable structural damage (Fig.2.5). When a seismic isolator is added to structures, the isolator provides the major energy dissipation mechanism through its deformation. Thus, compared with conventional design, as illustrated in Fig. 2.5, the deformation is restrained to the isolation level only and inter-story drift can be limited (Fig. 2.5); so the structural damage is limited. After the earthquake, the damaged isolator can be replaced, if necessary, without a major structural retrofit.

While it offers a substantial reduction in structural and non-structural damage, seismic isolation also reduces the overall structural cost. In New Zealand, the reduction in structural cost has been found to be in the order of 5% -10% (Skinner, et al., 1993).

2.5. SEISMIC ISOLATION DEVICES

A seismic isolation system should consist of three basic elements: 1) A vertical-load carrying device that is flexible laterally, so that the natural period of motion of structure is lengthened; 2) A damper or energy dissipater so that the displacement trade-off can be limited; and 3) A device that provides lateral rigidity under normal service load, such as wind and traffic loads (AASHTO, 1999).

There are various kinds of isolators available in practice. Commonly used isolation systems are high-damping rubber bearings, natural rubber bearings in combination with damping systems, lead-rubber bearings and sliding bearings with or without restoring force capability (Beskos and Anagnostopoulos, 1997). In development, more high-tech materials have been adopted to construct seismic isolators. Shape memory alloys are an example of a newly developed material. In general, seismic isolation systems may be categorized into two major types: linear and bilinear isolation systems. (Skinner, et al., 1993). The major difference between linear and nonlinear isolation systems is whether or not nonlinear damping (hysteretic damping) is provided. The most commonly used isolator types have been categorized and the result is provided in Table 2.1. It is observed that lead rubber bearing, laminated-rubber isolator and high damping rubber isolator provide damping and restoring capacity at the same time. These isolator types should be

firstly considered compared to the rest, since the restoring capacity is an important design feature.

Considering the scope of this study, only LRBs will be reviewed in detail. LRB is a combination of laminated-rubber bearing and single or multiple intrusive lead plugs. The central lead plug ensures a high initial stiffness which provides structural stability under normal conditions, such as traffic load, wind load, and minor earthquake events. During normal loading, structures equipped with isolators behave as if the base is fixed. When an earthquake occurs, yielding of the lead plug dissipates energy through the hysteresis damping provided by the plastic deformation of the lead. Sample LRB configurations are illustrated in Fig. 2.6.

There are many reasons that lead is chosen as the plug material: low yielding stress (10 MPa), stable mechanical properties, and good fatigue properties. As the purpose of having a seismic isolator is to provide low lateral stiffness under design earthquake load and to remain stiff under minor loads, the relatively low yield stress (10MPa) and the elasto-plastic load-deformation relation make lead a good material for achieving this purpose (Skinner, et al., 1993). Lead was also chosen because of its relatively stable mechanical property. Lab results have shown that the property of lead varies little with ambient temperature changes and the interrelated processes of recrystallization and grain growth restore the mechanical properties of lead continuously (Robinson and Greenbank, 1976; Vlack, 1989).

2.6. SEISMIC ISOLATION CODE PROVISIONS

2.6.1. Code Provision Development in North America

In the United States, the first guideline for seismically isolated structures was published by the Structural Engineers Association of Northern California (SEAONC) in 1986. It was titled "Tentative Seismic Isolation Design Requirements". This regulation was adopted as a non-mandatory guide in design practice. It was later subjected to a considerable modification and was included in the Uniform Building Code (UBC) in 1991. UBC 91 was the first seismic isolation code provision available in North America. In 2000, the UBC was replaced by the International Building Code (IBC). The content of these code provisions are very similar. The chapter of seismic isolation design requirements in IBC was extracted and published by the American Society of Civil Engineers (ASCE). This standalone publication, ASCE-7 (ASCE-7, 2002), is the most used code provision in seismic isolation in North America (Higashino and Okamoto, 2006). In 1991, the American Association of State Highway and Transportation Officials (AASHTO) published a code provision named "Guide Specifications for Seismic Isolation Design." Unlike other provisions, this AASHTO code directly provides provisions for bridge isolation designs. Currently, efforts are being made to streamline these code provisions, in particular to apply them to smaller and more common structures (Higashino and Okamoto, 2006).

2.6.2. Description of Code Provisions

The design procedures permitted in all major code provisions are similar. This study focuses on the seismic response of an isolated single-degree-of-freedom (SDOF) system.

For this reason, the AASTHO guide specification for bridge isolation design (AASHTO, 1999) was considered the base code provision. In this design provision, four analysis procedures were defined:

- Uniform Load Method
- Single Mode Spectral Method
- Multimode Spectra Method
- Time-History Analysis Method (Linear and Non-linear)

With the exception of the nonlinear time-history analysis method, analyses should be performed based on an equivalent linear model. The equivalent linear model is obtained by a bilinear model linearization procedure, which will be discussed in detail in the following content. As defined in AASHTO, nonlinear time-history analysis is required when the structural effective period is greater than 3 seconds or the effective damping, which is expressed as a percentage of critical damping, exceeds 30%. This analysis procedure is performed on the actual load-deformation relation, which requires prior knowledge of the hysteresis curves of the isolation system. In design practice, the actual hysteresis curve is normally simplified to a bilinear relation (Fig. 2.7) with small loss in accuracy (Hwang et al., 1994).

On one hand, nonlinear time-history analysis provides good design accuracy. However, on the other hand the complexity of it prevents its adoption in routine office design. In contrast, methods based on equivalent linear model are much simpler. Equivalent linear

models are obtained by simplifying the highly nonlinear damping into a critical viscous damping ratio (Hwang, 1996; Hwang and Chiou, 1996; Hwang and Sheng, 1993, 1994). This process is achieved by equating the areas under the LRB's hysteresis curve and a viscous damping loop (Fig.2.8). This process simplifies the bilinear hysteresis curve of LRB to an effective stiffness and an equivalent viscous damping ratio. Higashino and Okamoto (2006) provided a study, in which five major seismic isolation design code provisions were reviewed and compared. Table 2.2 provides a summary of the comparison on the limitation of equivalent linear analysis method application amongst the five code provisions. Among these five, the Japanese code provision defines the most specific limitations of application of equivalent linear model. In the US code provision, IBC 2003, the applicable effective structural period is restricted to be under three seconds and the height of the structure is limited to 19.8 m. IBC 2003 also specifically defines the seismicity limitation of application as spectral acceleration (S_a) $\leq$0.6 g.

2.7. APPLICATIONS IN NORTH AMERICA

The application of seismic isolation has drawn a lot of attention in the last decade. Several detailed studies (Buckle and Mayes, 1990; Jangid and Datta, 1995; Kelly, 1986) have reviewed the applications taking place in North America.

The first building equipped with a seismic isolation system was the Foothill Communities Law and Justice Center in California (Fig. 2.2). This project was completed in 1985. It was equipped with 98 high-damping rubber bearings below the basement level (Buckle et al., 2003). The second building application was the City and County Building in Salt

Lake City (Fig. 2.9). This project was completed in 1989 and it was the first project in the world to use a seismic isolation technique for a building retrofit. This five story building with a clock tower is approximately 75m in height and it is isolated with 208 lead-rubber isolators and 239 natural rubber bearings (Walters, 1986). Figure 2.10 shows the plan view. In general the building application of seismic isolation in North America mainly involves public and institutional buildings. As of 2005, there were approximately 80 isolated buildings (Higashino and Okamoto, 2006).

The first bridge application of seismic isolation was a retrofit. The bridge was the Sierra Point Overhead (Fig. 2.11), located on US 101 near San Francisco. It was constructed in the 1950's and the retrofit was completed in 1985. It was subjected to the 1989 Loma Prieta earthquake and survived without being damaged (Buckle et al., 2006). It is also noteworthy that LRBs have been the most commonly-used system in the bridge seismic isolation in North America (Buckle, et al., 2003). Buckle et al (2006) notes that even a poorly designed isolation system can provide a considerable amount of protection. As of 2005, over 175 bridges were isolated in the United States (Higashino and Okamoto, 2006).

Seismic isolation has also been extended to industrial and non-building structures. These include water tanks, emergency power units, large scientific equipment, chemical storage tanks, and storage stands for rocket motor units (Bleiman, 1993).

2.8. SUMMARY AND DISCUSSION ON REVIEW

Seismic isolation is a promising solution to reduce earthquake damage and its application has been considerably increased since it was first adopted in earthquake retrofitting in North America in the 1980's. Structures equipped with isolators are, to a certain degree, decoupled from ground excitation. This technique is being used worldwide in building and bridge protections. The application has been extended to industrial and non-structural elements protection in the past decade. Many types of seismic isolation devices are currently used. They are categorized as being either linear or nonlinear isolator, depending on whether or not a nonlinear energy dissipation mechanism is included in the isolation unit. The lead rubber bearing isolator is the most widely used device in bridge and building protection.

In seismic isolation code provisions, methods based on a bilinear model and equivalent linear model are permitted. Among all methods of analysis, the nonlinear time-history analysis method is the most accurate and is capable of calculating the exact structural response to specified earthquakes. Other methods, which are based on equivalent linear model, however, are simplified and more suitable for routine office design. While using equivalent linear model, it must be realized that the accuracy of equivalent linear model decreases as the deformation nonlinearity increases in the isolators. Most current constructed isolators were designed based on equivalent linear model and thus they are in potential risks of failure under design earthquakes. There could be only one reason that the constructed based on these simplified methods have not failed is that the earthquake experienced has not reached to the design demand (Bommer and Acevedo, 2004).

To improve the equivalent linear model based methods appearing in codes, considerable time has been invested on generating more appropriate bilinear model linearization equations to achieve a better accuracy (Dicleli and Buddaram, 2006, 2007; Hwang, 1996). However, considering the complicated nature of earthquakes and high non-linearity in isolator response, the limitations inherent in the bilinear model linearization process are unavoidable.

Table 2. 1 Stiffness and damping of common isolator components (Skinner, et al., 1993)

	Linear	Non-linear
Restoring Force	• Laminated-rubber bearing • Flexible piles or columns • Springs • Rollers between curved surfaces (gravity)	• High-damping rubber bearing • Lead-rubber bearing • Buffers • Stepping (gravity)
Damping	• Laminated-rubber bearing • Viscous damper	• High-damping rubber bearing • Lead-rubber bearing • Lead-extrusion damper • Steel dampers • Friction (e.g.PTFE)

Table 2. 2 Applicability of the equivalent linear analysis method in five codes (Higashino and Okamoto, 2006)

	USA	Japan	China, Mainland	China, Taiwan	Italy
Limitation on site seismicity	S_1<0.6g	-	-	-	-
Limitation on soil class	A,B,C,D	1,2	I,II,III	1,2	-
Maximum plan dimension	-	-	-	-	50m
Maximum height of superstructure	19.8m	60m	40m	-	20m
Maximum number of stories	4	-	T_f<1s	-	5
Location of devices	-	Base only	Base only	-	-
Maximum mass-stiffness centers eccentricity	-	3%	-	-	3%
Tension in isolator	Allowed	Not Allowed	Not Allowed	Not Allowed	Not Allowed
Yield strength	-	>3%W	-	-	-
Period of T_{eff}	$3T_1$~3s	T_2>2.5s	-	<2.5s	$3T_1$~3s
Maximum value of T_v	-	-	-	<0.1s	-

Where:

T_1= period of motion calculated based on elastic stiffness
T_2= period of motion calculated based on post-elastic stiffness
T_f= period of motion for fixed-base
S_1= mapped spectral acceleration of 5% damped response at 1-sec

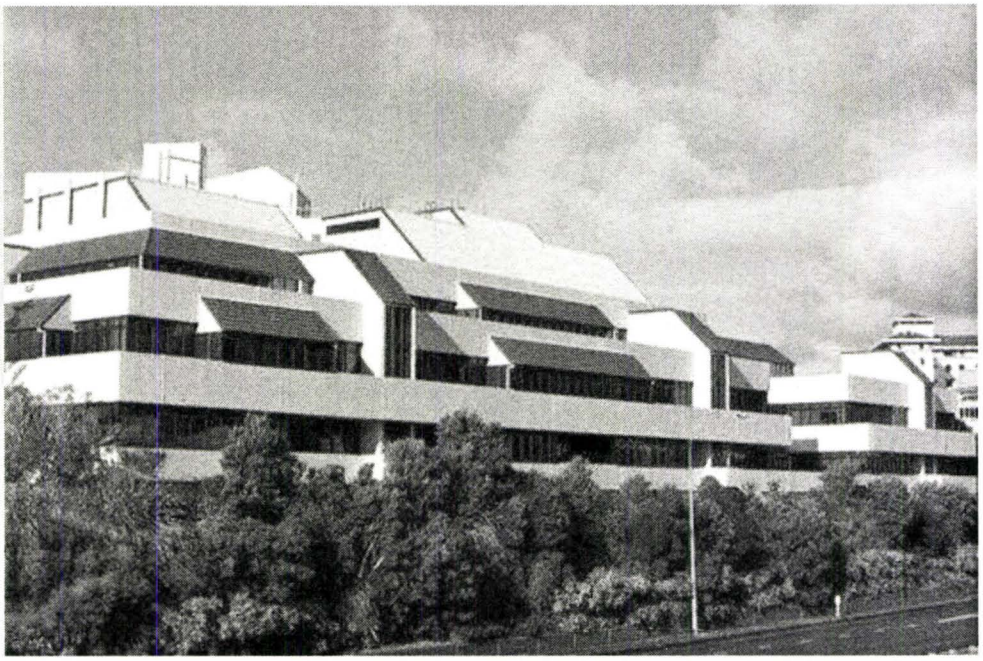

Figure 2. 1 William Clayton Building (The University of Waikato, 2007)

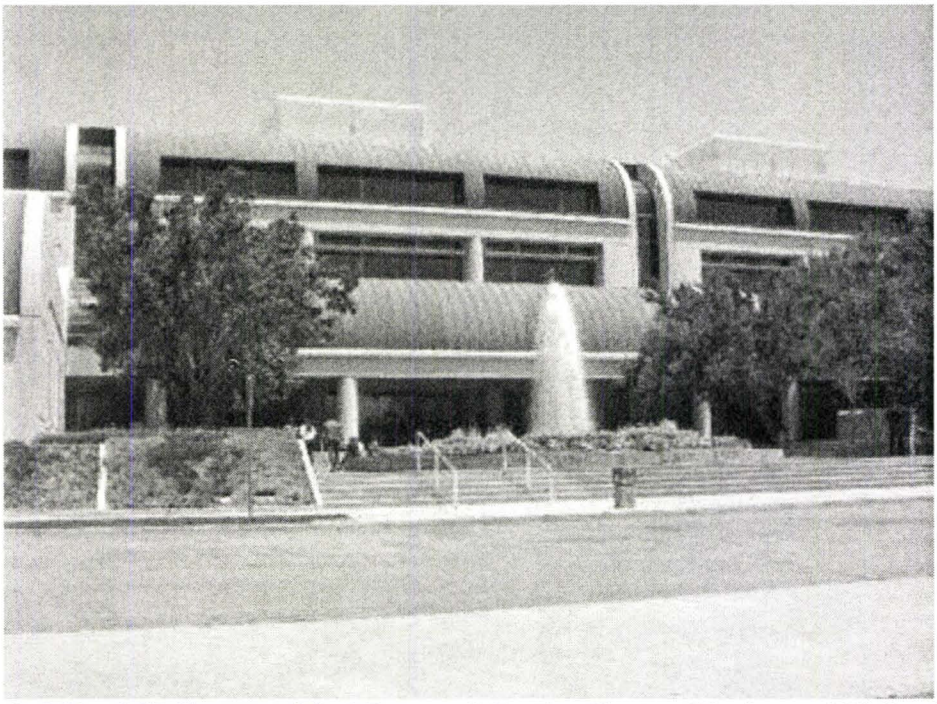

Figure 2. 2 Foothill Communities' Law and Justice Center (Naeim and Kelly, 1999)

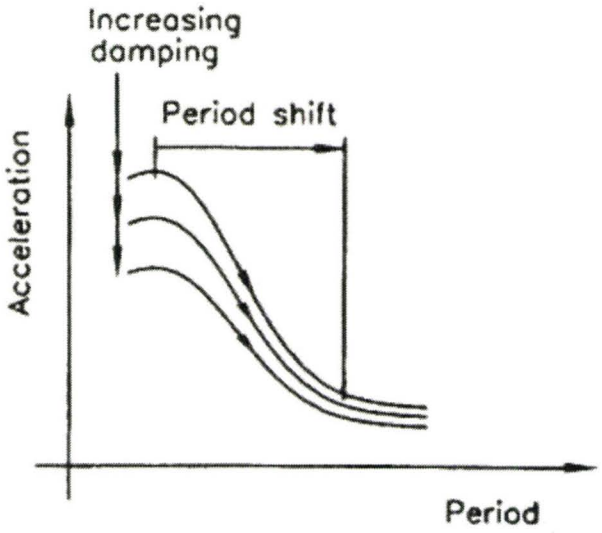

Figure 2. 3 Increased period and damping decrease the seismic acceleration response (Skinner, et al., 1993)

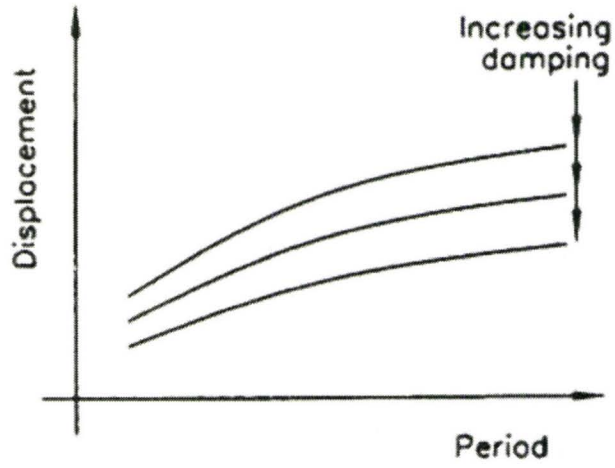

Figure 2. 4 Increased period increases the seismic displacement response, but compressed by increased damping (Skinner, et al., 1993)

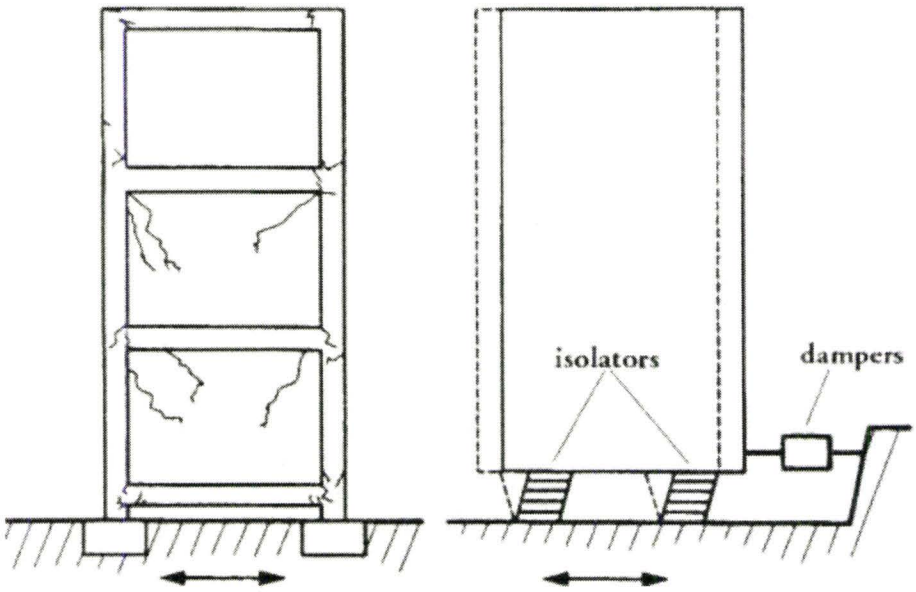

Figure 2. 5 Comparison of fixed-base (left) and isolated structures (right) (Skinner, et al., 1993)

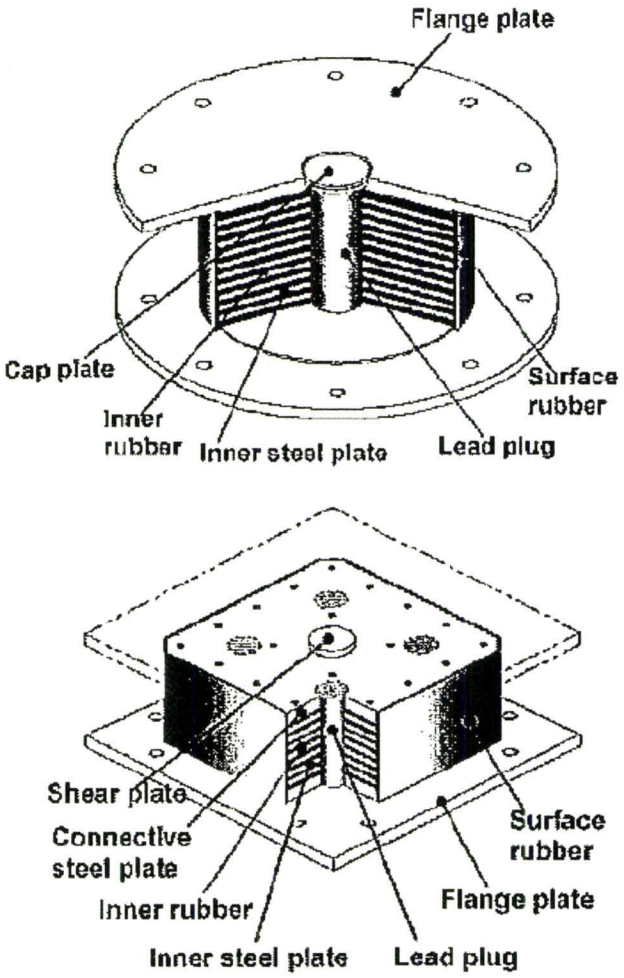

Figure 2. 6 Sample configurations of lead rubber bearing (Higashino and Okamoto, 2006)

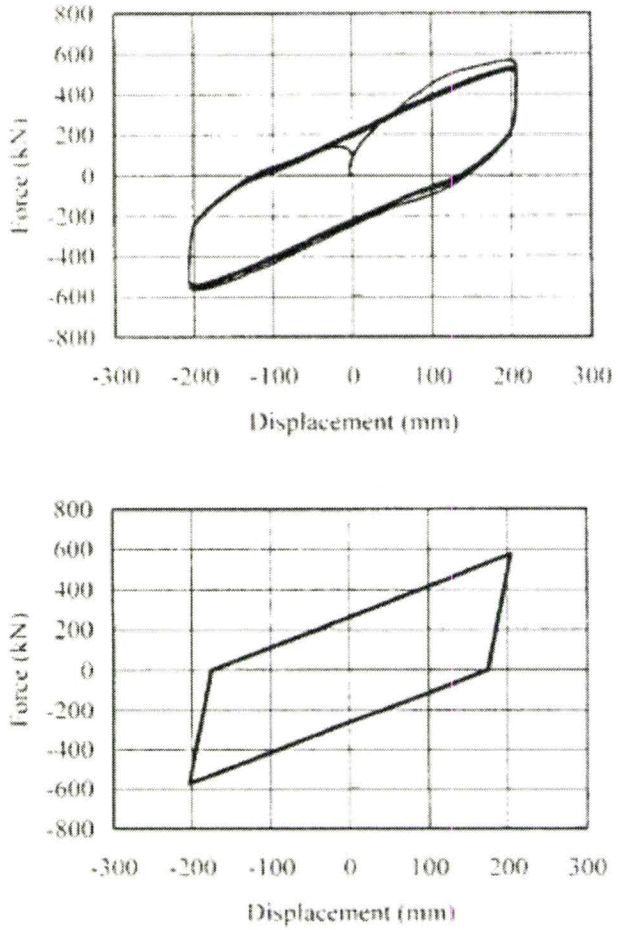

Figure 2. 7 Example hysteresis loop of lead rubber bearings (Higashino and Okamoto, 2006)

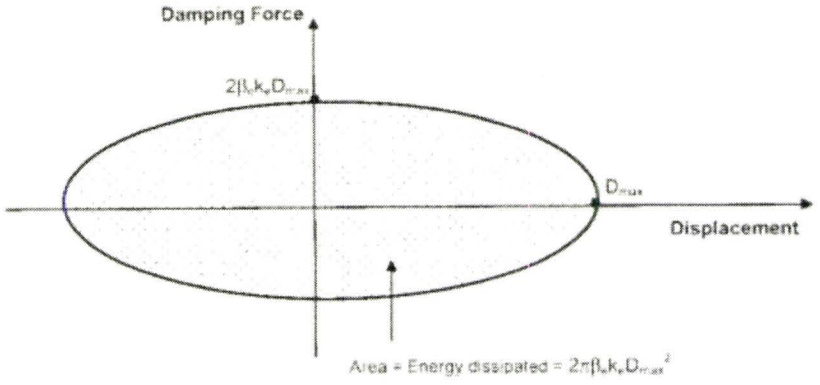

Figure 2. 8 Force-displacement loop for viscous damper (Buckle, et al., 2006)

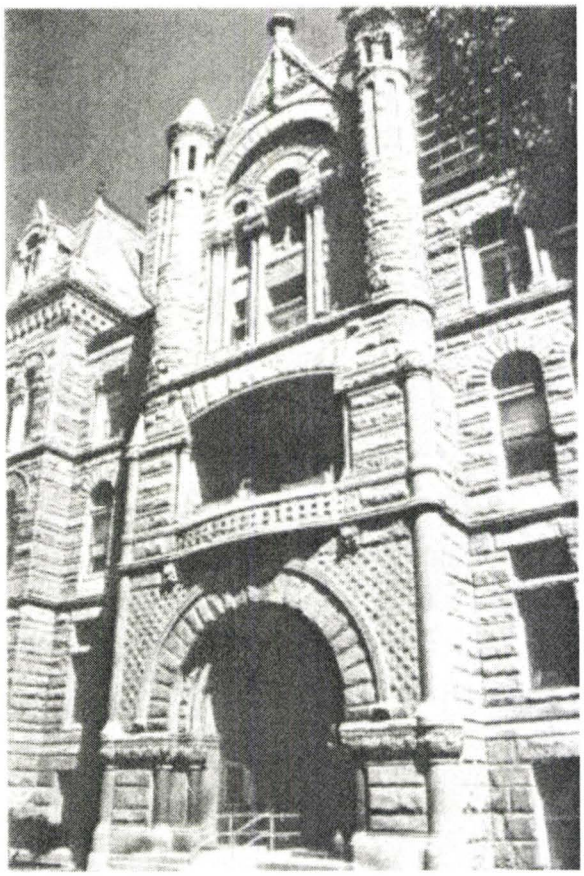

Figure 2. 9 Salt Lake City and County Building (Bailey and Allen, 1988)

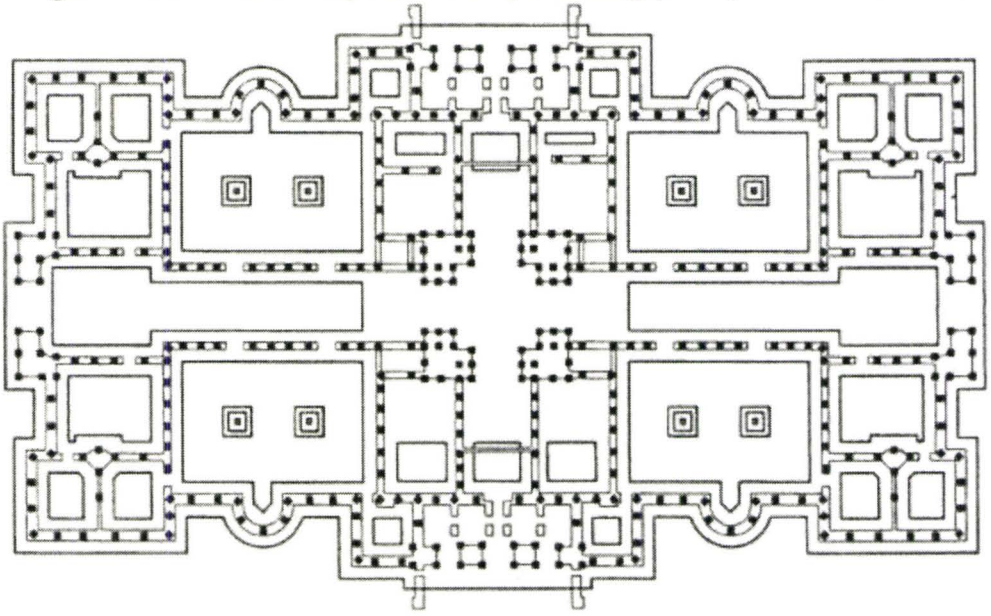

Figure 2. 10 Plan view showing locations of isolators on exterior and interior walls (Bailey and Allen, 1988)

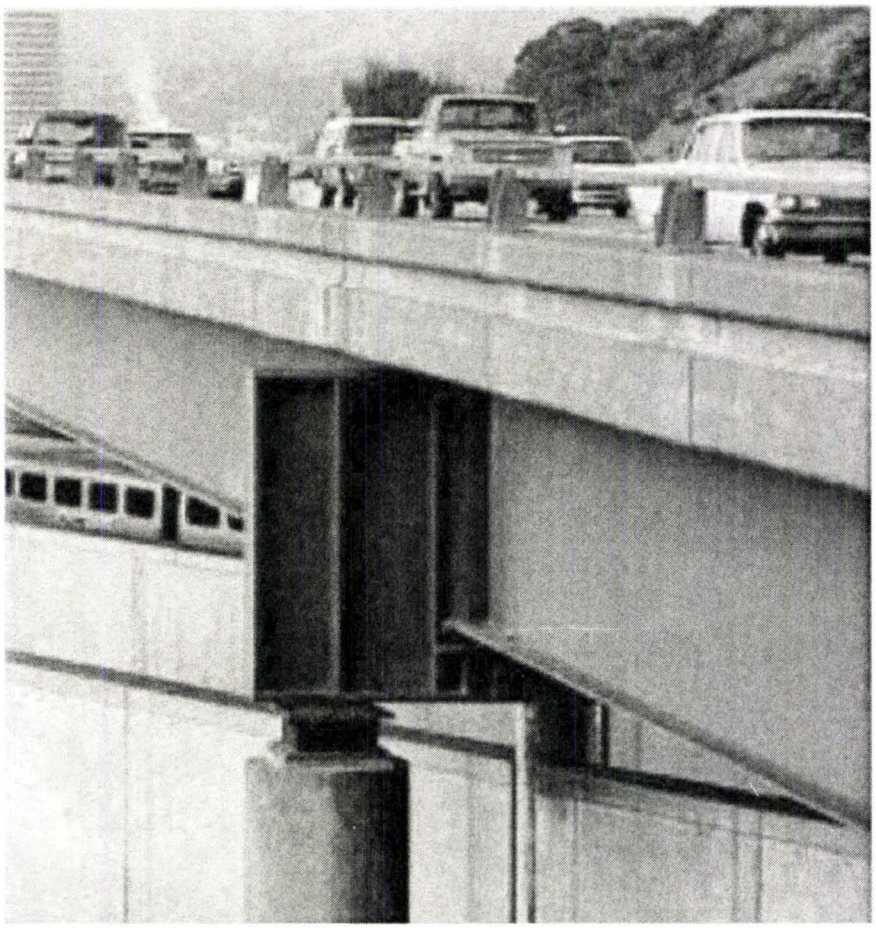

Figure 2. 11 Sierra Point Overhead, San Francisco, retrofitted with lead rubber bearings (Buckle, et al., 2006)

3. CHARACTERIZATION OF SELECTED GROUND MOTION RECORDS

3.1. INTRODUCTION

This chapter reviews earthquake characterization parameters and characteristics of earthquake forward directivity. Earthquake acceleration time-histories are selected based on the review findings. The characteristics of the selected earthquakes are presented towards the end and comparisons are made in terms of pulse-like wave content, damage potential and frequency content. The selected earthquake time-histories are used for nonlinear time-history analysis in Chapter 4.

3.2. CHARACTERIZATION PARAMETERS OF EARTHQUAKES

In seismic code provisions, design-level earthquakes are defined based on a probabilistic or a deterministic basis. The probabilistic hazards are defined in terms of probability of exceedance in 50 years. The commonly used probabilities are 10%, 5% and 2% probability of exceedance in 50 years. These probabilities correspond to ground motions that have return periods of approximately 500, 1000 and 2500 years, respectively. The deterministic demands are defined as spectral response with a level of confidence from a previous earthquake on a known fault within the region (FEMA-356, 2000). In ASCE-7 (2002), these demands are calculated based on the mapped spectral acceleration of 5% damped response at short period (S_s) (i.e. less than 1-sec) or at 1-sec (S_1). For seismically isolated structures, the design and maximum considered earthquake refers to the mapped spectral acceleration at 1-sec (S_1).

In all major code provisions in North America, the earthquake shaking intensity is only characterized using spectral acceleration (S_a) (ASCE-7; FEMA-356; IBC). However, in practice, time-domain parameters are often used to study the earthquake characteristics. The parameters are peak ground acceleration (PGA), peak ground velocity (PGV) and peak ground displacement (PGD). PGA correlates well with the low shaking intensity. However, for higher intensities of ground shaking, PGV tends to correlate with shaking intensity better than PGA (Boatwright et al., 2001; Kaka and Atkinson, 2004).

Velocity time-histories and displacement time-histories are obtained from the numerical integration of the acceleration time-histories. Velocity and displacement time-histories are generally smoother, and spikes, which are observed in acceleration time-histories, are removed. Thus the structural response to an earthquake is usually better reflected by the velocity and displacement time-histories. As velocity is the parameter most directly related to kinetic energy, which is relevant to structural damage, PGV is sometimes said to be a more suitable parameter than PGA for estimating earthquake damage potential measure (Wald et al., 1999). It should be noticed that the debate between using PGV and PGA has drawn a lot of attention in the past decade and is yet by no means settled. Using PGA in representing earthquake damage potential, however, still plays an important role in engineering practice, largely for historical reasons and for convenience.

3.3. EARTHQUAKE FORWARD DIRECTIVITY

When an earthquake ground motion occurs, the ground rupture propagates from the epicenter along the fault trace. Along the axis of the fault, in-phase shear waves

accumulate and energy focusing occurs. This is known as earthquake forward directivity. Ground motions affected by forward directivity focusing, where in-phase shear waves accumulate, contain long duration pulses in acceleration, velocity and displacement time-histories. This long duration wave can generate large roof displacement and high shear force which may be especially problematic for isolated structures (Bray and Rodriguez-Marek, 2004; Chopra and Chintanapakdee, 2001; Jangid and Kelly, 2001). Directivity focusing is often observed in near-fault ground motions (Chopra and Chintanapakdee, 2001; Iwan, 1997; Malhotra, 1999). However, when an earthquake is affected by the forward directivity, the fault distance is not the only consideration, the direction is also important. Malhotra (1999), shows that ground motions affected by directivity focusing tend to have low PGA/PGV (or A/V) ratio. The reverse of this is one assumption in this study, in which forward directivity can be captured using records with low A/V ratios. An A/V ratio of unity was used to separate earthquakes affected by directivity (PGA in units of g and PGV in units of m/s). For an earthquake with A/V <1, the ground motion is considered as directivity affected and pulses are expected to exist in the time-histories

3.4. SELECTED RECORDS AND SCALING

The process of selecting and scaling earthquake records is important in earthquake resistant design (Kalkan and Chopra, 2010). The number of time-history records required to complete a nonlinear time-history analysis is specified in some code provisions. For example in IBC (2003), a minimum of three pairs (i.e. orthogonal orientations) of records must be used. Numerous studies have investigated the best approach to select suitable ground-motions for individual nonlinear time-history analysis (Amiri and Dana, 2005;

Iervolino and Cornell, 2005; Kalkan and Chopra, 2010; Naeim et al., 2004). Kalkan and Chopra (2010) suggested considering the local influences, as follows:

- Magnitude range of anticipated significant events
- Distance range of the site from the causative faults
- Site-conditions
- Basin effects
- Directivity effects

Following this procedure, the seismic responses are site specific. However, an alternative earthquake records selection method, which is generally used in probabilistic seismic demand analysis (Carballo and Cornell, 2000; Chapman, 1995), focuses on the general seismic responses. Instead focusing on individual seismic response of each time-history, this method focuses on statistical results of a group of earthquakes. Different groups of earthquakes when properly classified will have similar structural response statistics. A second assumption used in this work is that the mean plus one standard deviation (84.1 percentile) response values of different groups of earthquake should be similar if they are in the same A/V category (i.e. A/V<1 or >1). In other words, the statistical value of a group of earthquakes is independent of the contained records, when they are from the same A/V category. Ground motions are selected to test these assumptions.

A total of 37 earthquake records are selected and divided into two groups, Group A and Group B, with each group being further separated according to A/V<1 and A/V>1. The detailed information of these records is shown in Table 3.1 and 3.2. Group A contains 20

records and Group B contains 17 records. Group A has a lower average value of PGA (0.17g) and PGV (0. 47 m/s) compared to that of Group B, where average PGA and PGV are 0.70g and 1.29m/s, respectively. These two groups of earthquakes were prepared for different design earthquake level scalings, as shown in Table 3.3. Earthquake scaling, so-called accelerogram scaling, is the process by which earthquake records are manipulated to produce design spectrum compatibility (Naeim and Kelly, 1999). The time-domain method, which manipulates time-history amplitudes, is used in this study to scale the earthquakes. Thus, considering code provision compatibility and research accuracy purposes, both PGA and PGV are considered for earthquake records selection and scaling. Three PGA and four PGV values were considered to explore the isolator responses under two design earthquake levels, namely *moderate* and *severe* design earthquakes. The details are provided in Table. 3.3. Group A (with the lower values of PGA & PGV) is used for time-history analysis for *moderate* design earthquake level and Group B is used for *severe* design earthquake level time-history analysis. Another purpose of having Group A and Group B is to validate the earthquake selection procedure. The details will be presented in Chapter 4.

3.5. CHARACTERISTICS OF SELECTED EARTHQUAKES

Characteristics of selected ground motions are presented and discussed in this section. Fig. 3.1 to Fig. 3.10 show the time-history plots from Group A, where records with A/V <1 are shown in Fig. 3.1 to Fig. 3.5 and records with A/V>1 are shown in Fig. 3.6 to Fig. 3.10. Sample velocity spectra are provided together with their time-histories in Fig. 3.11

to Fig. 3.16. Three major observations are drawn from comparison of the selected time-history records.

The first observation is the pulse-like wave content. When ground motions with A/V<1 (Fig.3.1 to Fig.3.5) and ground motions with A/V>1 (Fig.3.6 to Fig.3.10) are compared, the former ones have distinct pulse-like wave, which can be visualized in terms of both acceleration and velocity time-histories. This pulse-like wave requires steady energy dissipation over a longer duration of time, in other words, numerous yields are anticipated. This characteristic makes these records high in damage potential.

Secondly, high acceleration spikes are observed in the A/V>1 time-histories. For example this behaviour is seen in Westmoreland 1981 (Fig. 3.8) at the 6 sec mark and in Coalinga 1983 (Fig. 3.10) at the 4 sec mark. The acceleration spike is very short in duration and the energy can be dissipated instantaneously. As a result, such an earthquake appears high in PGA; however, it can cause much less structural excitation than an earthquake with an equivalent PGA but has steadier waves. Therefore, the acceleration spike content can be very misleading to the damage potential measure if PGA is used for earthquake scaling.

Lastly, differences are found in period content. The velocity spectra show that earthquakes with A/V<1 tend to have high spectral velocity at two to three seconds (Fig.3.11c to Fig. 3.13c). Conversely, high spectral velocity content exists at one to two seconds for higher A/V>1 records (Fig.3.14c to Fig.3.16c). A seismic isolation system will lengthen a structure's natural period of motion to typically about three seconds. This

period coincides with the long period content of A/V<1 earthquakes. Thus, under earthquake excitation, the response of isolated-structure can be amplified. This makes seismic isolated structures vulnerable to low A/V earthquakes.

Table 3. 1 Group A selected earthquake records

	Earthquake	Year	Station	M_w	Closest Distance (km)	PGA (g)	PGV (m/s)	A/V
(A/V<1)	Chichi, Taiwan	1999	TCU031	7.6	26.8	0.122	0.434	0.28
	Imperial Valley	1979	412 El Centro Array #10	6.5	8.6	0.171	0.475	0.36
	Kocaeli, Turkey	1999	Arcelik	7.4	17	0.149	0.395	0.37
	Cape Mendocino	1992	89486 Fortuna	7.1	23.6	0.116	0.300	0.38
	Taiwan SMART1	1986	64 SMART1 O04	7.3	39	0.126	0.319	0.39
	Superstition Hills	1987	Kornbloom Road (temp)	6.7	19.7	0.136	0.311	0.43
	Northern California	1954	1023 Ferndale City Hall	n/a	31.5	0.159	0.339	0.46
	N. Palm Springs	1986	5071 Morongo Valley	6.0	10.1	0.205	0.409	0.50
	Loma Prieta	1989	1601 Palo Alto SLAC Lab	6.9	36.3	0.194	0.375	0.51
	Duzce, Turkey	1999	Duzce, Duzce-180	7.1	8.2	0.348	0.600	0.58
(A/V>1)	Northridge	1994	90091 LA - Saturn St	6.7	30.0	0.439	0.390	1.12
	Duzce, Turkey	1999	Duzce, Bolu	7.1	17.6	0.728	0.564	1.29
	Cape Mendocino	1992	89324 Rio Dell Overpass	7.1	18.5	0.549	0.421	1.30
	Kobe, Japan	1995	0 Nishi-Akashi	6.9	11.1	0.509	0.373	1.36
	Westmoreland	1981	5169 Westmoreland Fire Sta	5.8	13.3	0.496	0.344	1.44
	N. Palm Springs	1986	5072 Whitewater Trout Farm	6.0	7.3	0.612	0.315	1.94
	Victoria Mexico	1980	6604 Cerro Prieto	6.1	34.8	0.621	0.316	1.96
	San Fernando	1971	279 Pacoima Dam	6.6	2.8	1.160	0.543	2.13
	Landers	1992	24 Lucerne	7.3	1.1	0.785	0.319	2.46
	Coalinga	1983	1651 Transmitter Hill	5.8	9.2	1.083	0.397	2.72

Table 3. 2 Group B selected earthquake records

	Earthquake	Year	Station	M_w	Closest Distance (km)	PGA (g)	PGV (m/s)	A/V
(A/V<1)	Imperial Valley	1979	5155 Meloland Overpass	6.5	0.5	0.296	0.905	0.32
	Chichi, Taiwan	1999	TCU120	7.6	8.1	0.225	0.631	0.36
	Northridge	1994	0655 Jensen Filter Plant	6.7	6.2	0.424	0.106	0.37
	Superstition Hills	1987	5051 Parachute Test Site	6.7	0.7	0.455	0.112	0.38
	Kocaeli, Turkey	1999	Yarimca	7.4	2.6	0.349	0.621	0.39
	Erzincan, Turkey	1992	95 Erzincan	6.9	2.0	0.515	0.839	0.43
	Parkfield	1966	1013 Cholame #2	6.1	0.1	0.476	0.751	0.46
	Duzce, Turkey	1999	Duzce, Duzce-270	7.1	8.2	0.535	0.835	0.50
	Cape Mendocino	1992	89156 Petrolia	7.1	9.5	0.662	0.897	0.51
	Landers	1992	24 Lucerne	7.4	1.1	0.721	0.976	0.58
(A/V>1)	Chichi, Taiwan	1999	TCU084	7.6	10.4	1.157	0.115	1.12
	Kobe, Japan	1995	0 KJMA	6.9	0.6	0.821	0.813	1.29
	San Fernando	1971	279 Pacoima Dam	6.6	2.8	1.226	0.113	1.30
	Cape Mendocino	1992	89005 Cape Mendocino	7.1	8.5	1.497	0.127	1.36
	Northridge	1994	24207 Pacoima Dam	6.7	8.0	1.285	0.104	1.44
	Northridge	1994	24436 Tarzana	6.4	17.5	1.779	0.114	1.94
	Morgan Hill	1984	57217 Coyote Lake Dam	6.2	0.1	1.298	0.808	1.96

Table 3. 3 Considered design earthquake levels for accelerogram scaling

Considered Scaling Parameters	Considered Design Levels	
	Moderate	Severe
PGV	0.3 m/s	1.0 m/s
	0.5 m/s	1.5 m/s
PGA	0.5 g	1.0 g
		1.5 g

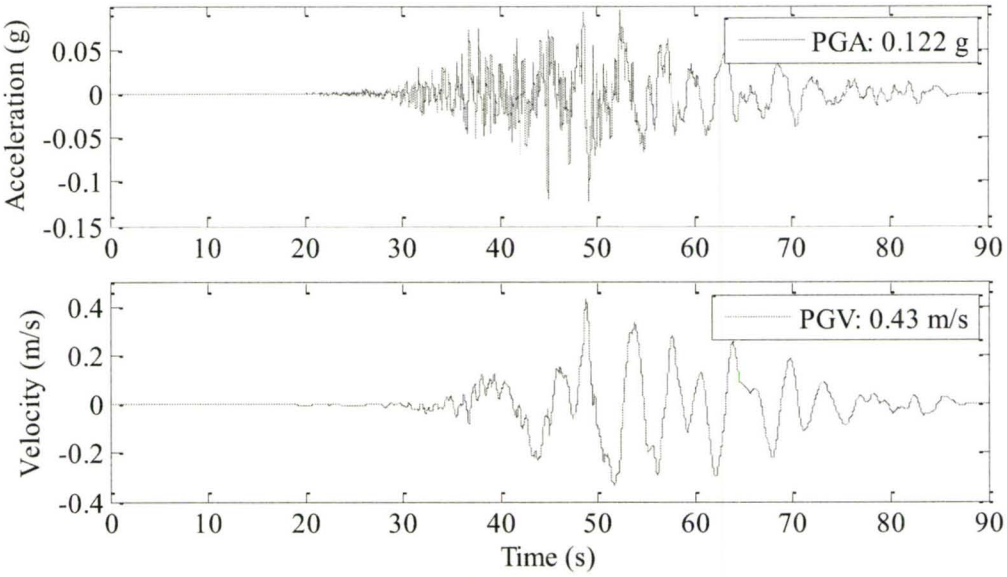

Chichi, 1999
(TCU031)

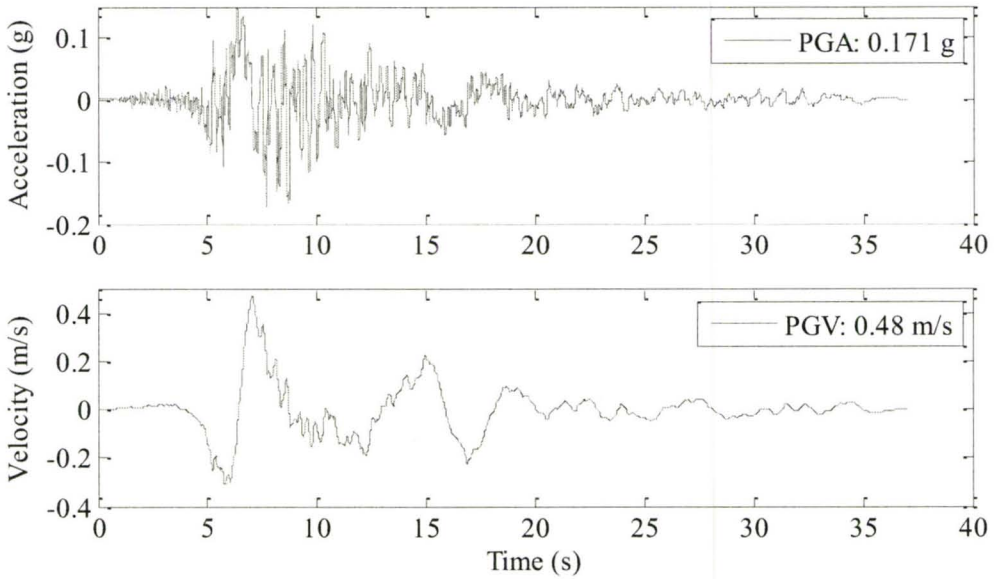

Imperial Valley, 1979
(412 El Centro Array #10)

Figure 3. 1 Time-history plots for Group A, A/V<1

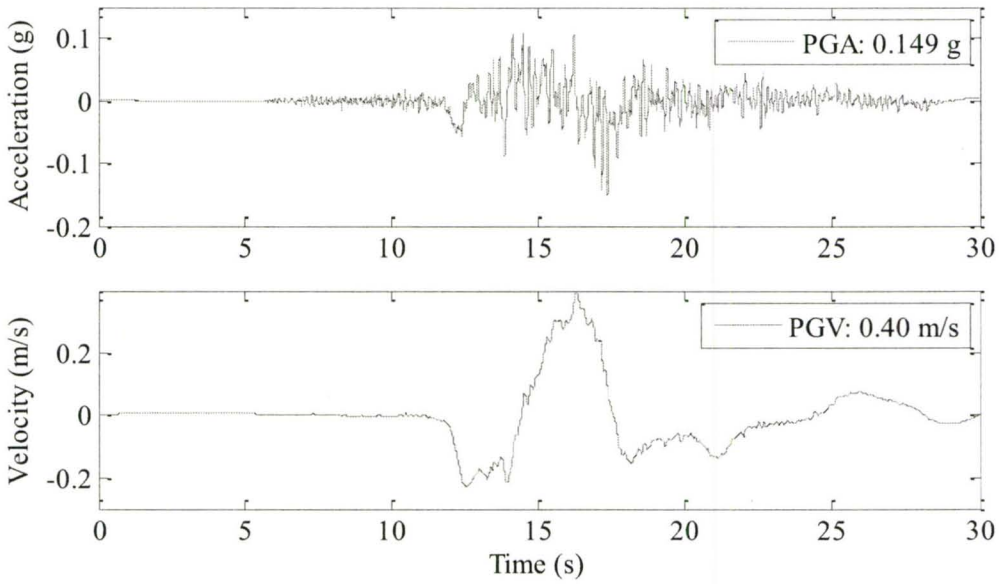

Kocaeli,1999
(Arcelik)

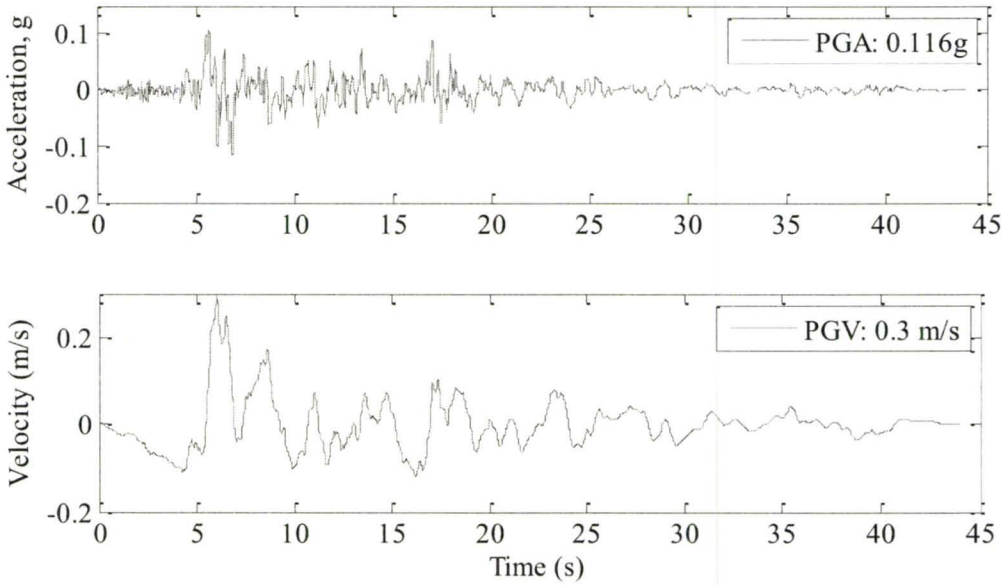

Cape Mendocino, 1992
(89486 Fortuna)

Figure 3. 2 Time-history plots for Group A, A/V<1 (Cont'd)

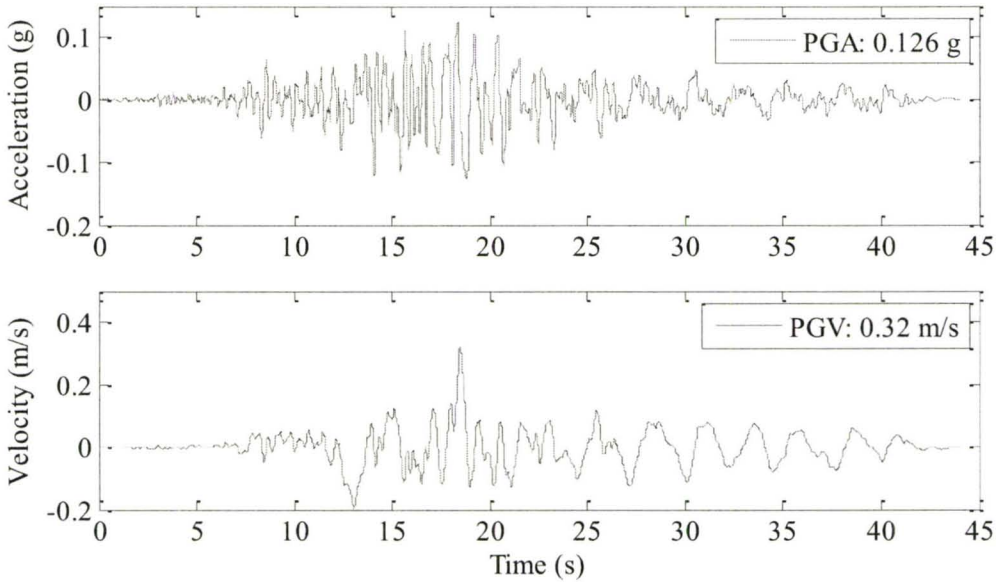

Taiwan SMART1,1986
(64 SMART1 O04)

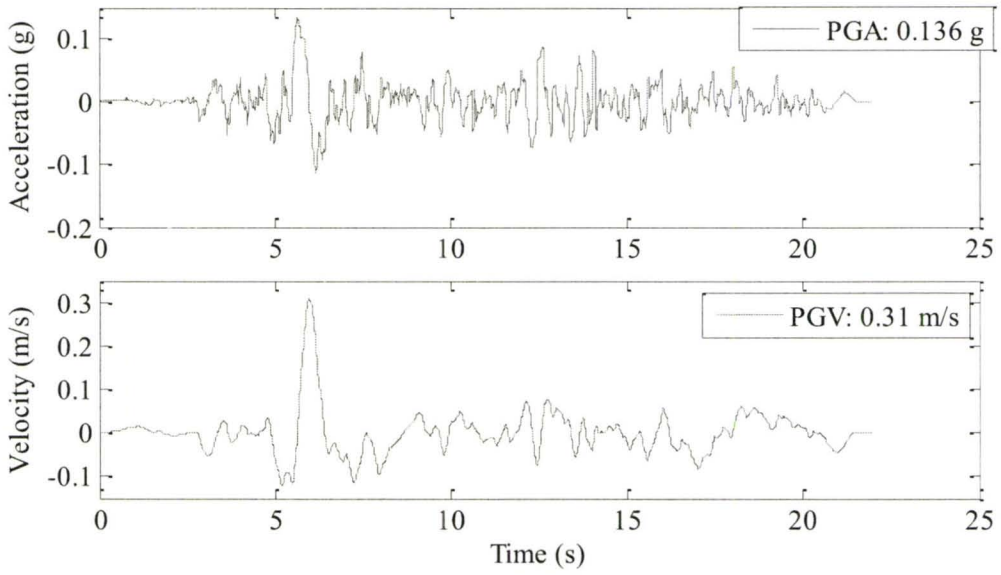

Supertition Hills, 1987
(Kornbloom Road)

Figure 3. 3 Time-history plots for Group A, A/V<1 (Cont'd)

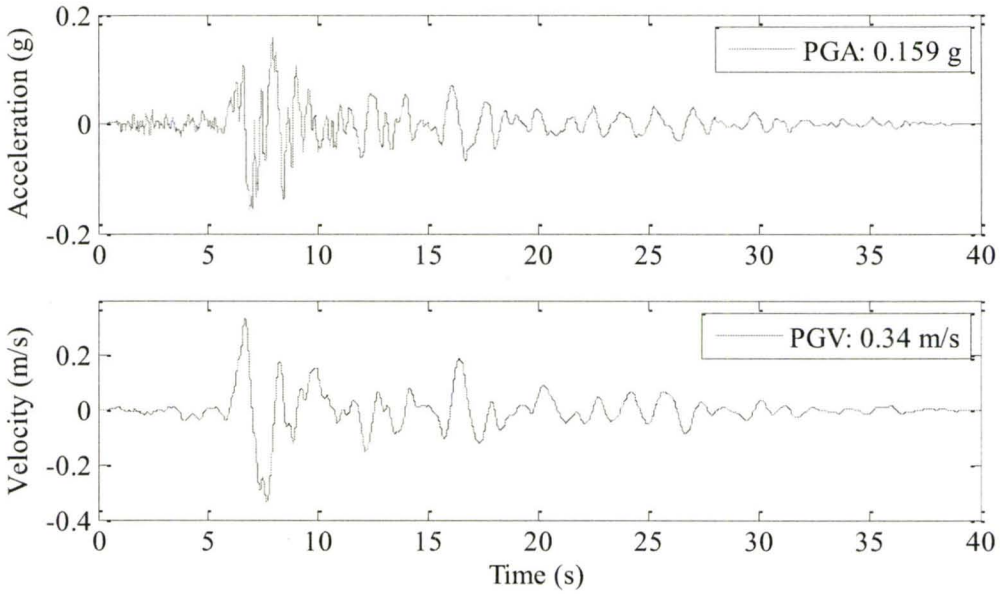

Northern California, 1954
(1023 Ferndale City Hall)

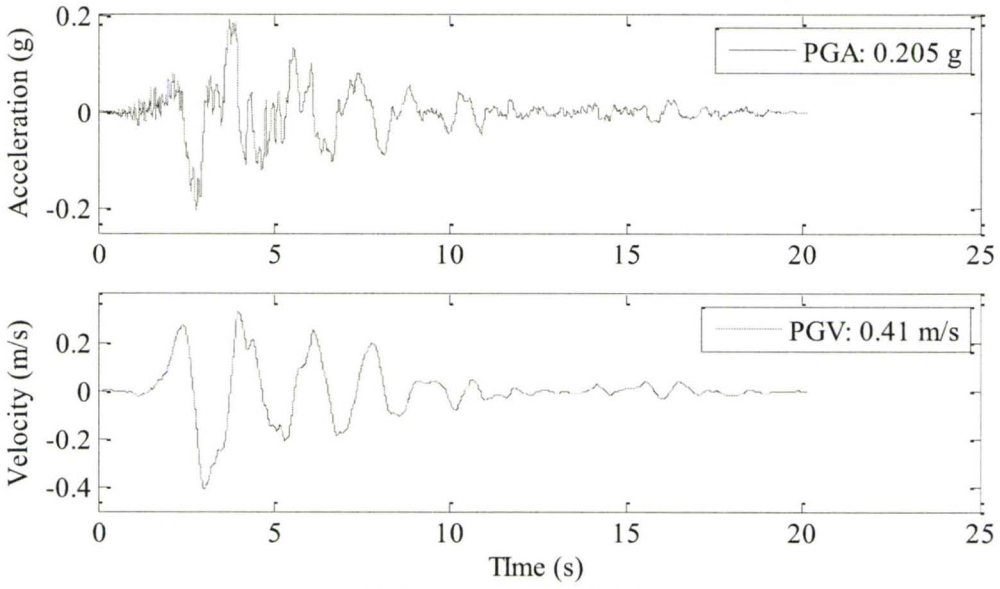

N.Palm Springs, 1986
(5071 Morongo Valley)

Figure 3. 4 Time-history plots for Group A, A/V<1 (Cont'd)

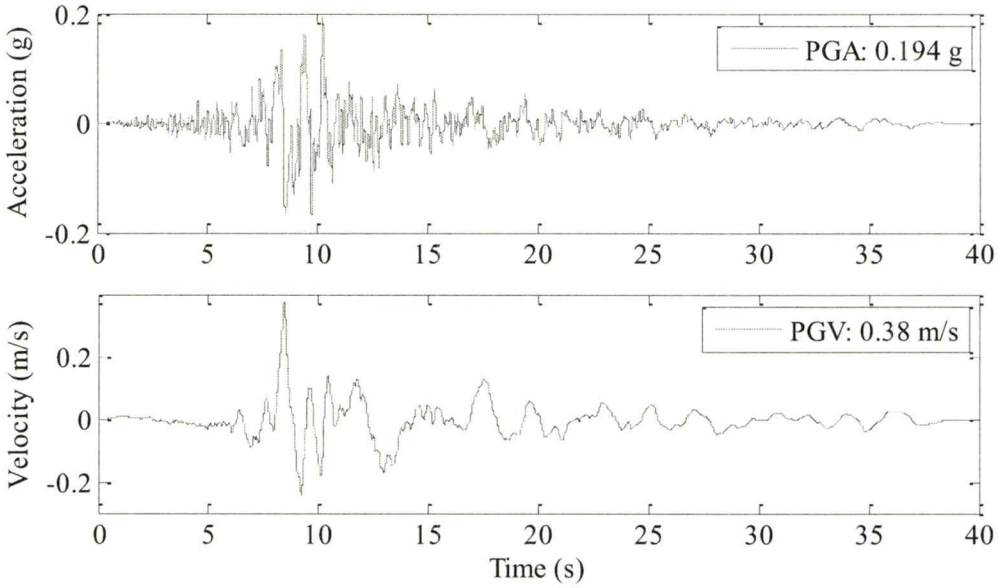

Loma Prieta, 1989
(1601 Palo Alto - SLAC Lab)

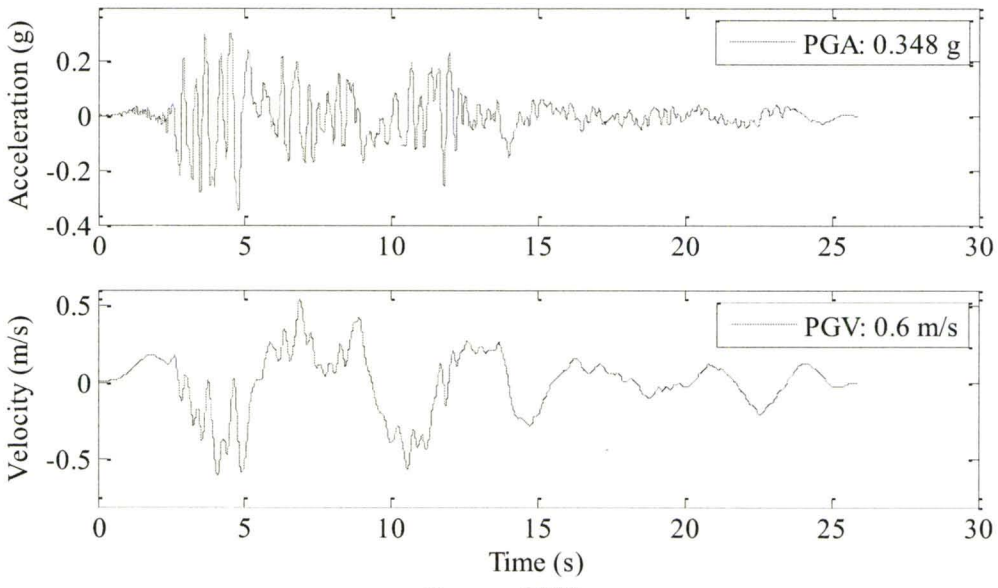

Duzce, 1999
(Duzce)

Figure 3. 5 Time-history plots for Group A, A/V<1 (Cont'd)

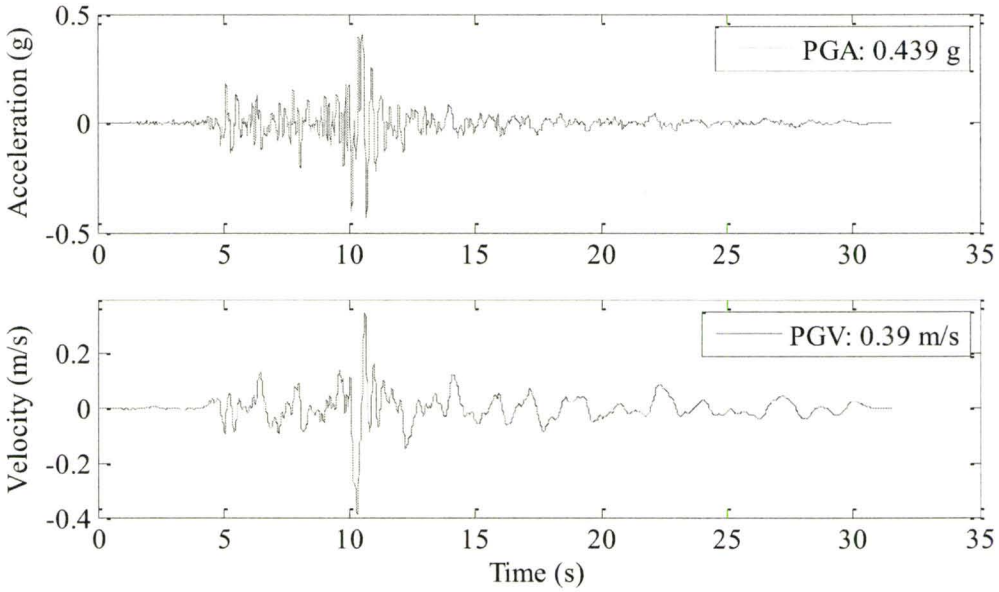

Northridge,1994
(90091 LA- Saturn St)

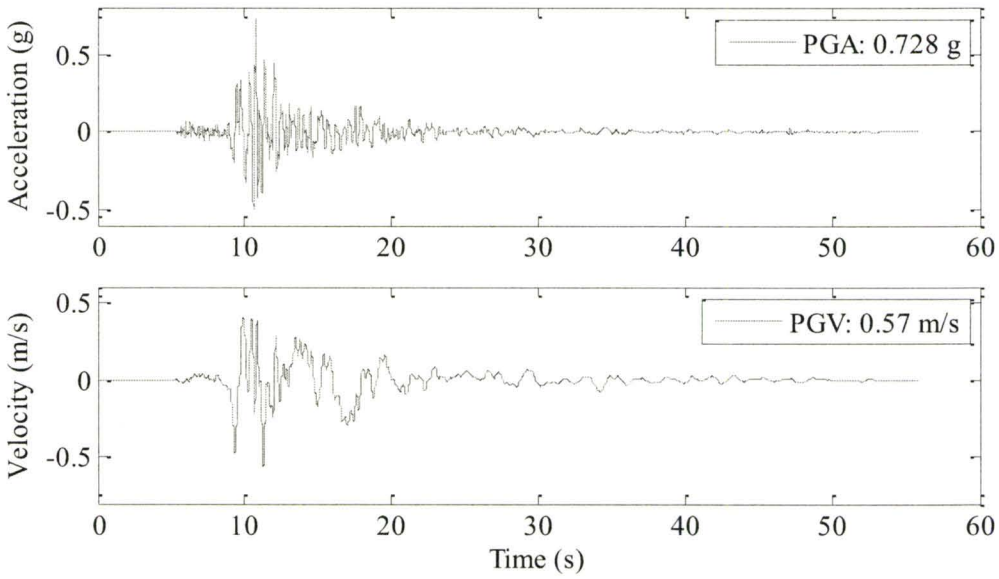

Duzce, 1999
(Duzce)

Figure 3. 6 Time-history plots for Group A, A/V>1

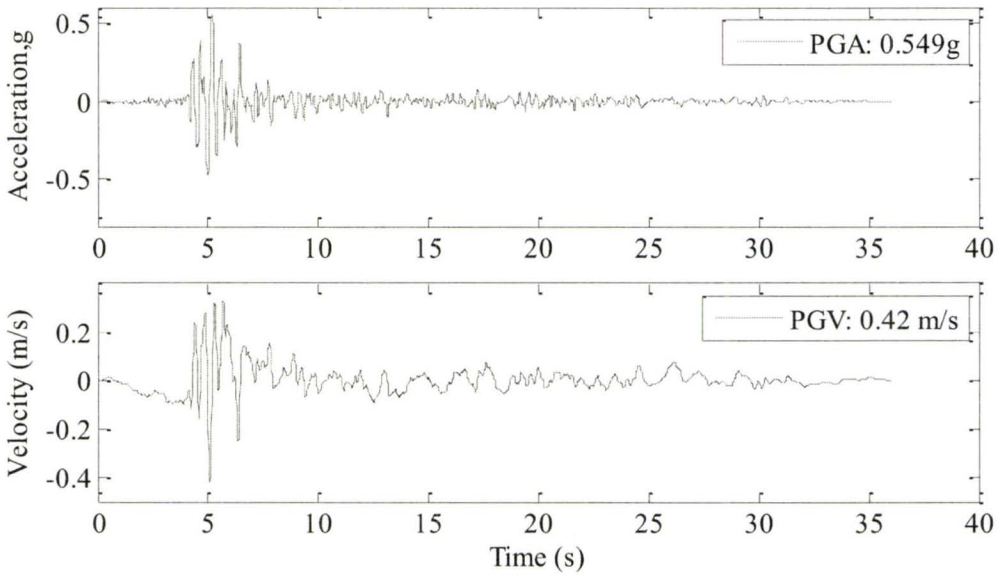

Cape Mendocino, 1992
(89324 Rio Dell Overpass)

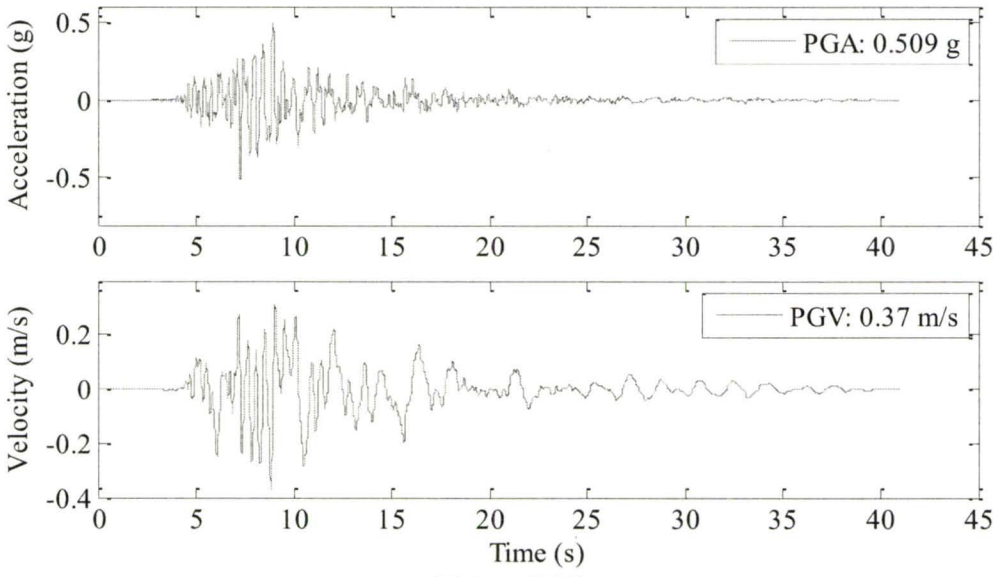

Kobe, 1995
(0 Nishi-Akashi)

Figure 3. 7 Time-history plots for Group A, A/V>1 (Cont'd)

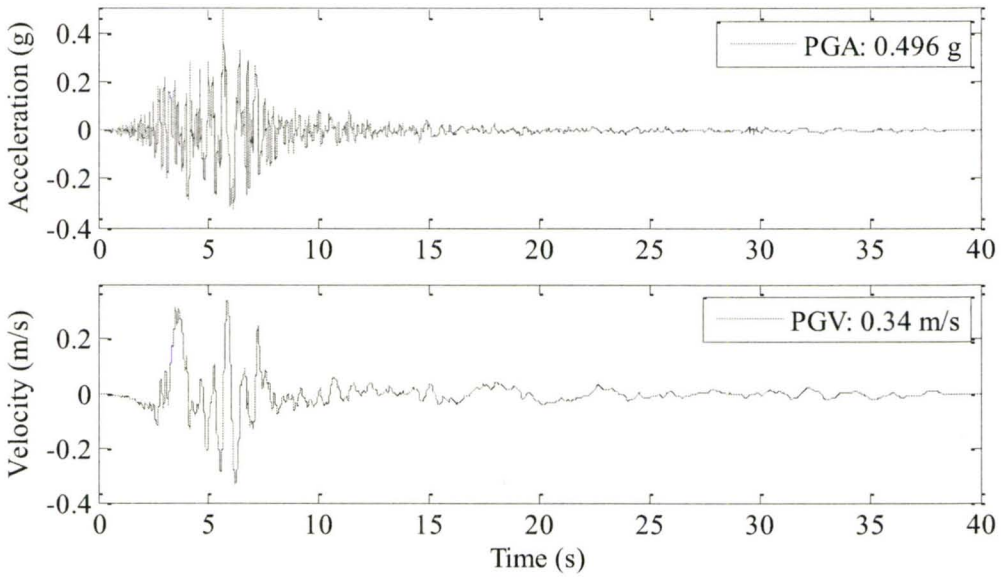

Westmoreland, 1981
(5168 Westmoreland Fire Sta)

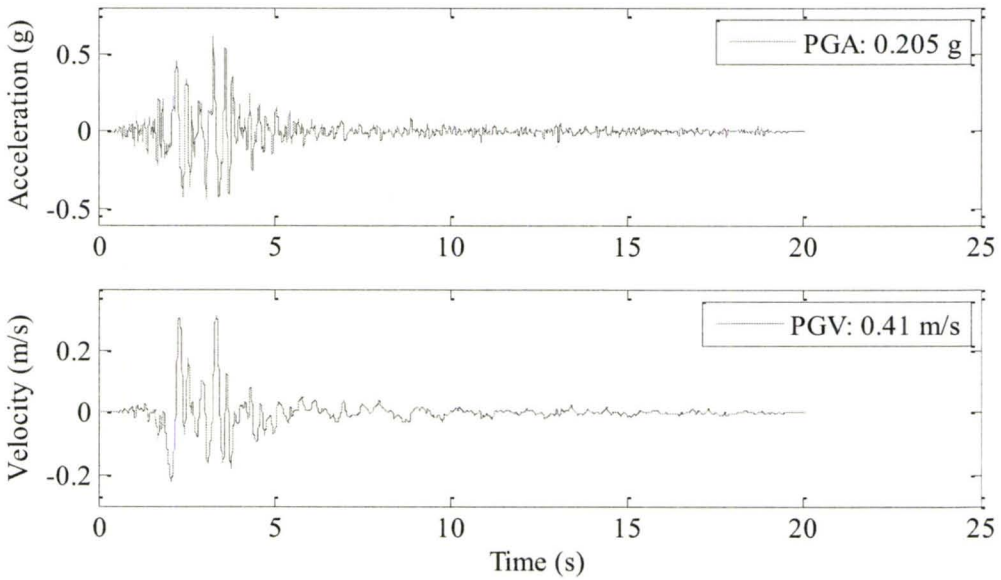

N. Palm Springs, 1986
(5072 Whitewater Trout Farm)

Figure 3. 8 Time-history plots for Group A, A/V>1 (Cont'd)

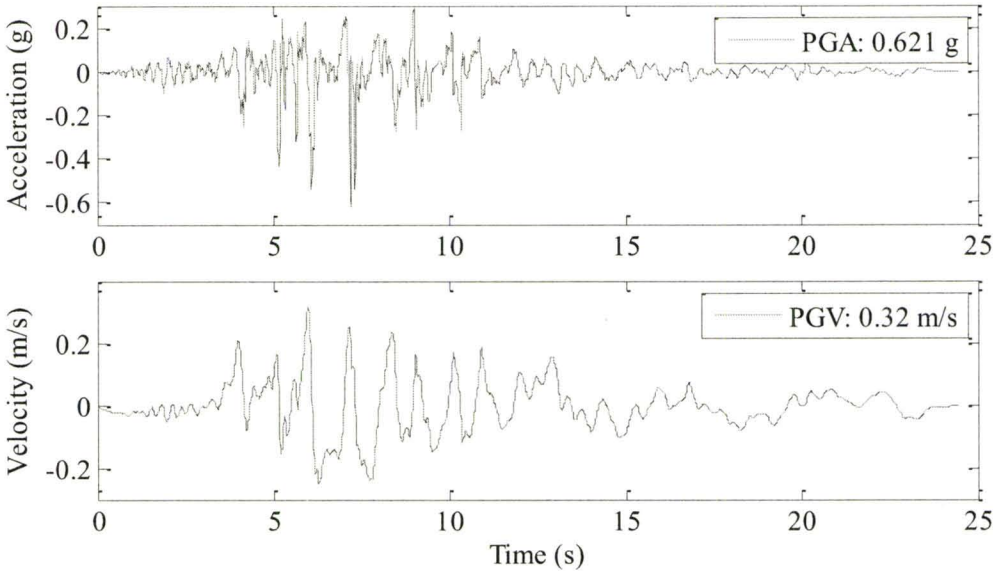

Victoria Mexico, 1980
(6604 Cerro Prieto)

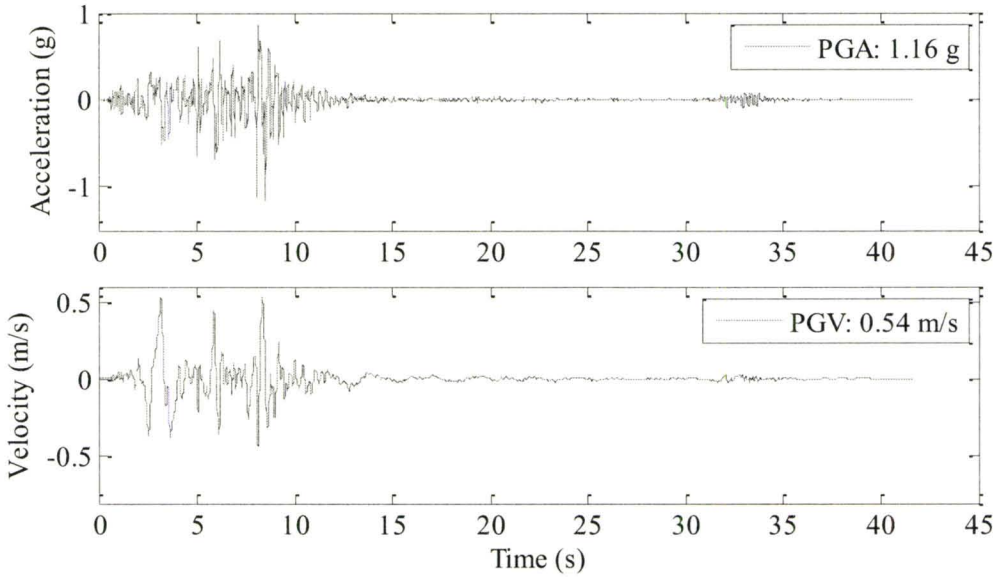

San Fernando, 1971
(279 Pacoima Dam)

Figure 3. 9 Time-history plots for Group A, A/V>1 (Cont'd)

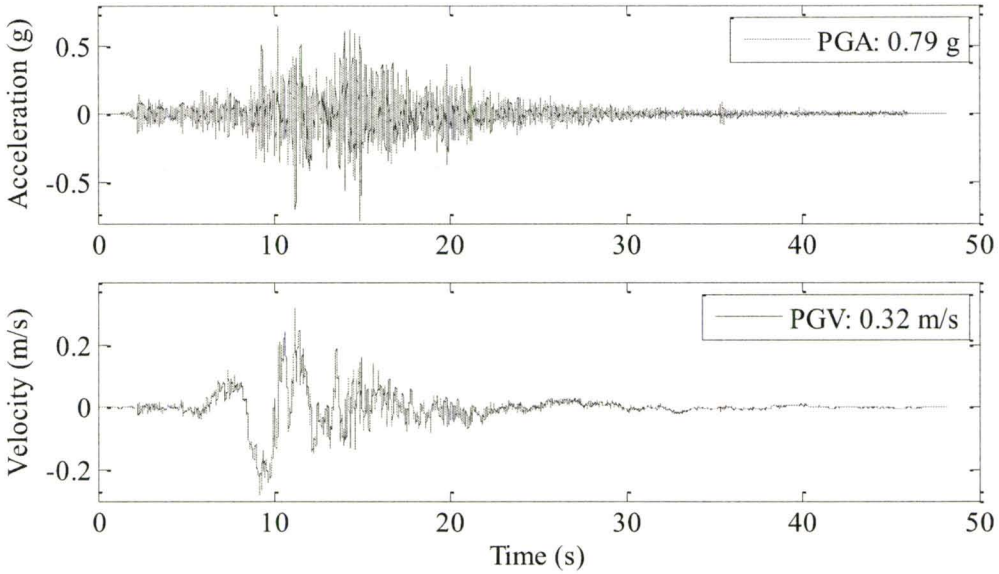

Landers, 1992
(24 Lucerne)

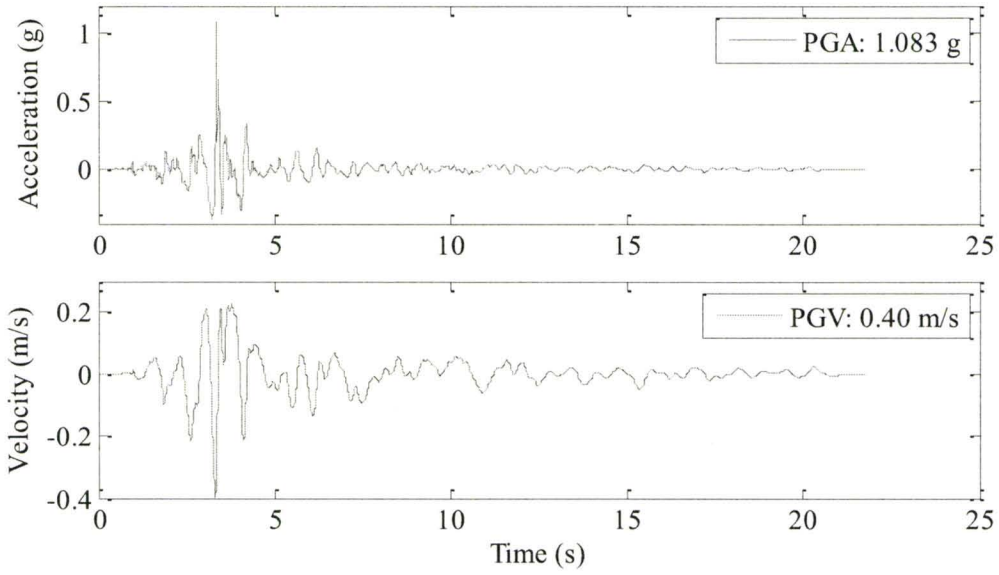

Coalinga, 1983
(1651 Transmitter Hill)

Figure 3. 10 Time-history plots for Group A, A/V>1 (Cont'd)

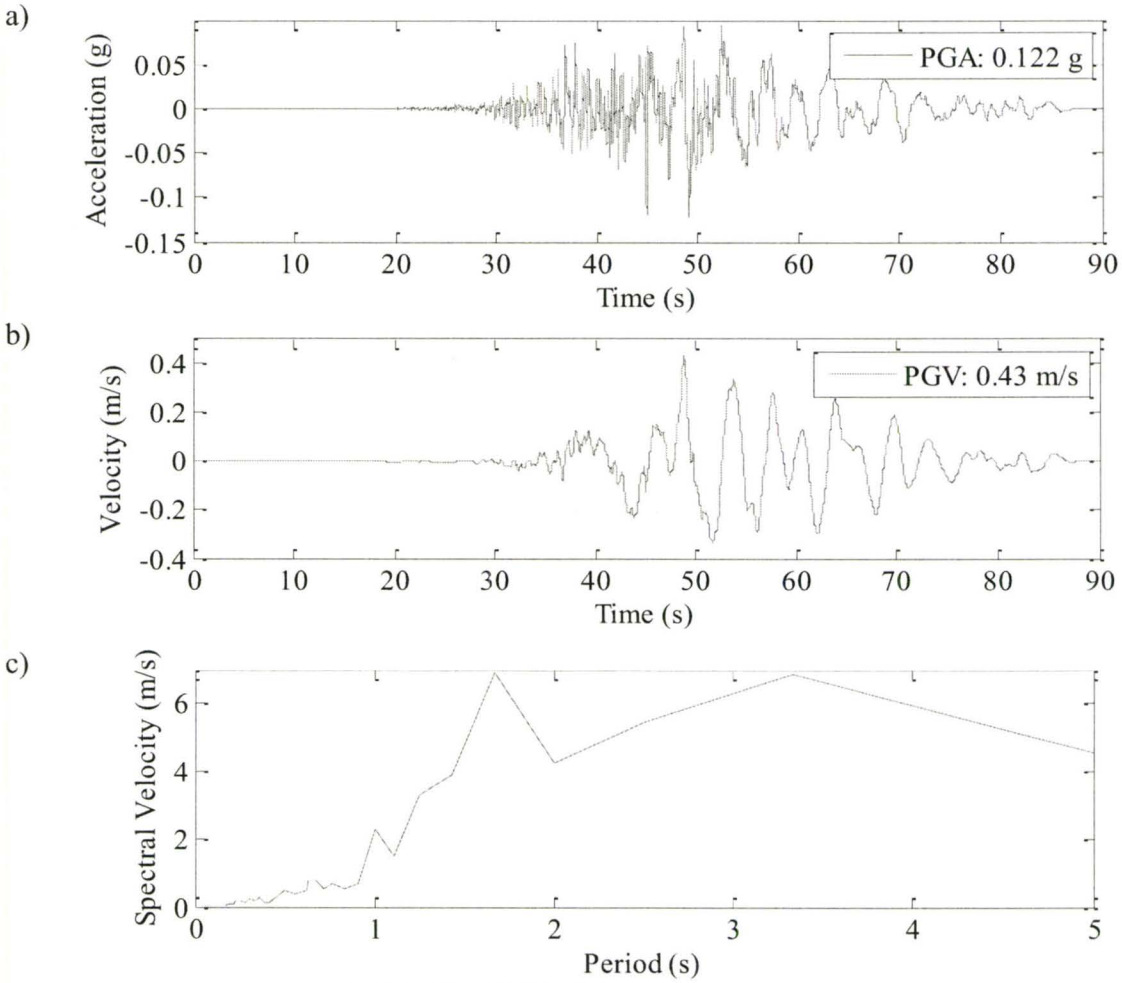

Figure 3. 11 Chi-Chi (TCU031) ground motion, A/V<1

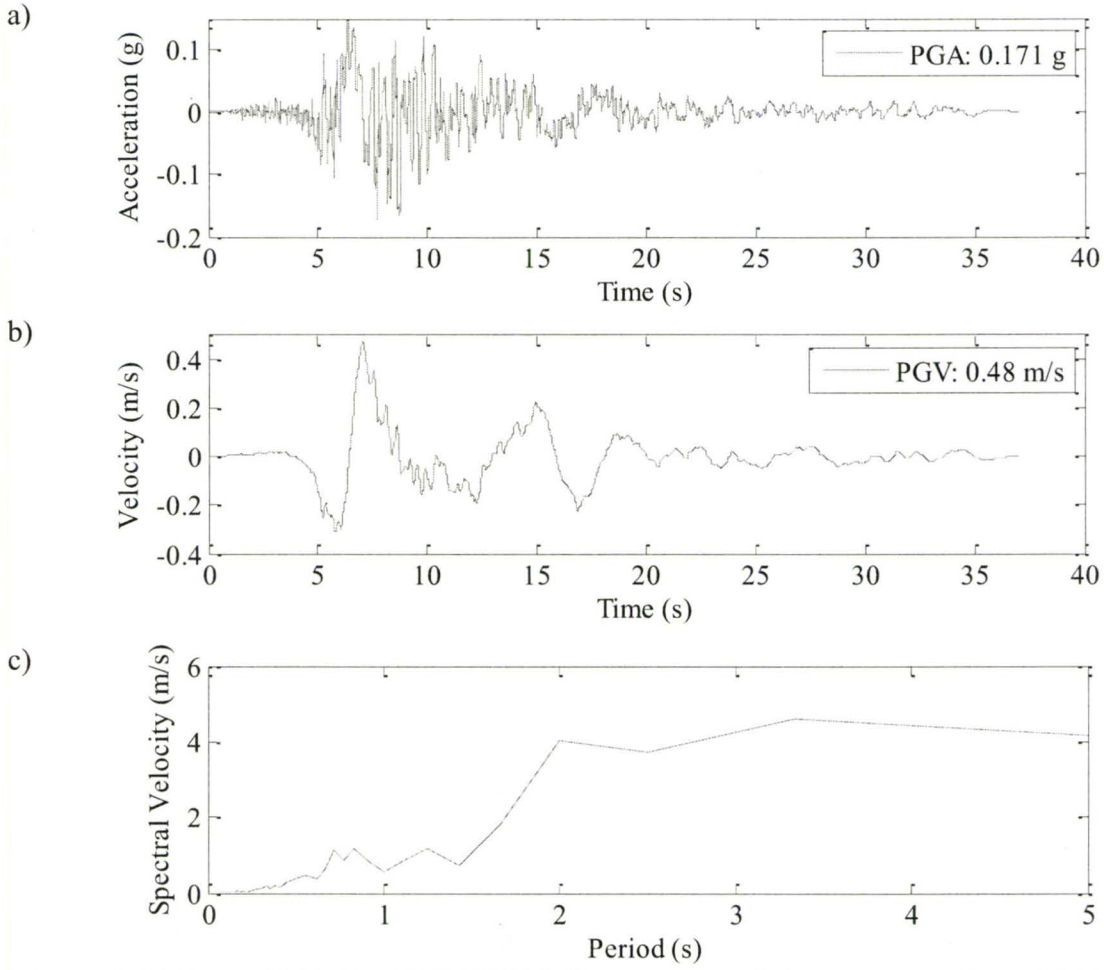

Figure 3. 12 Imperial Valley 1979 (412 El Centro Array #10) ground motion, A/V<1

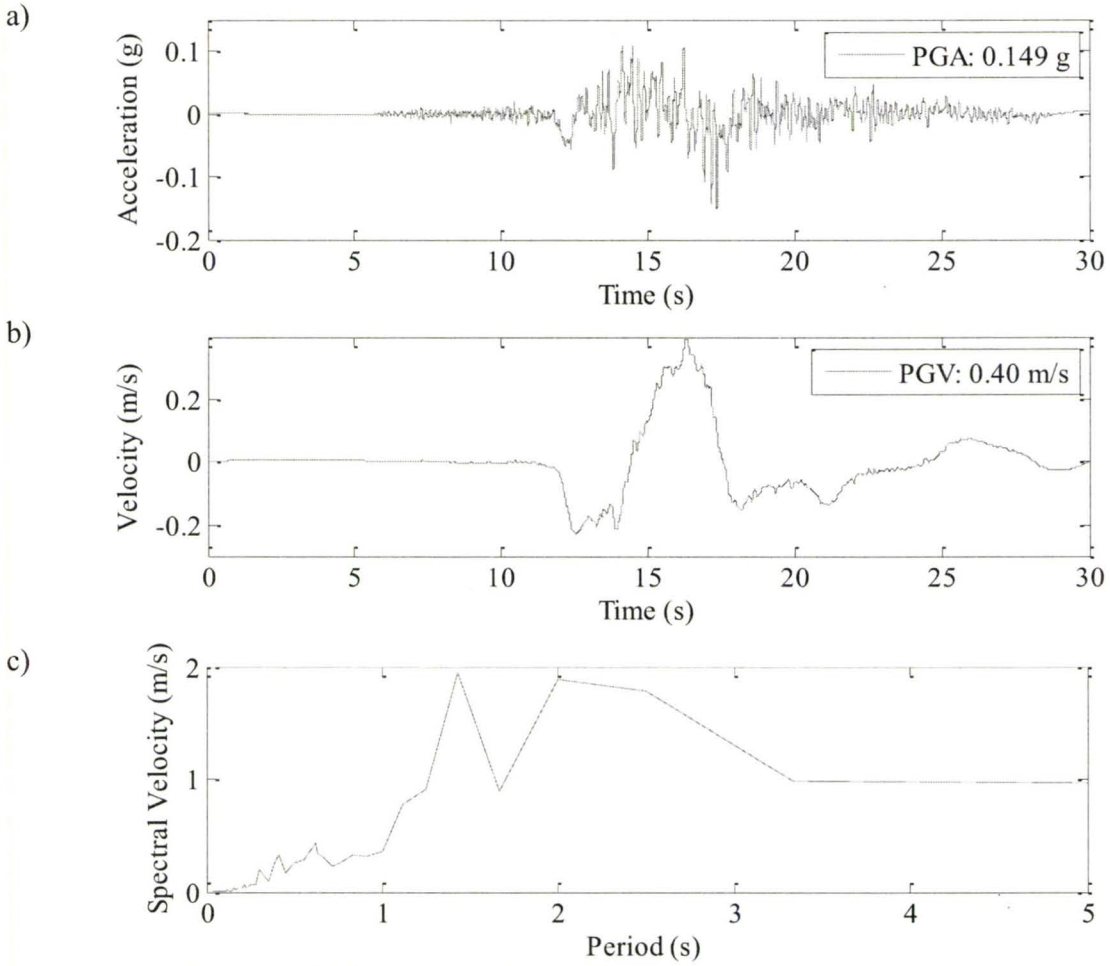

Figure 3. 13 Kocaeli 1999 (Arcelik) ground motion, A/V<1

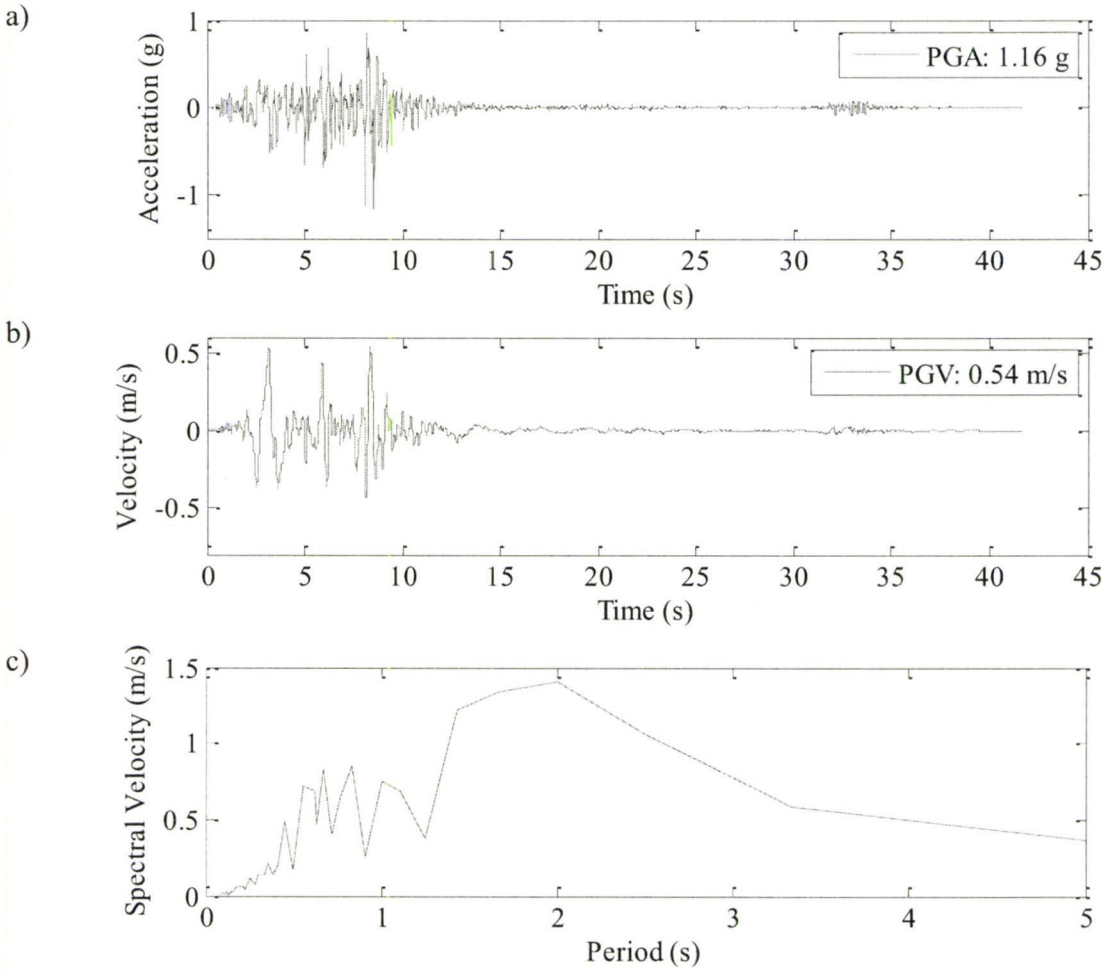

Figure 3. 14 San Fernando 1971 (279 Pacoima Dam) ground motion, A/V>1

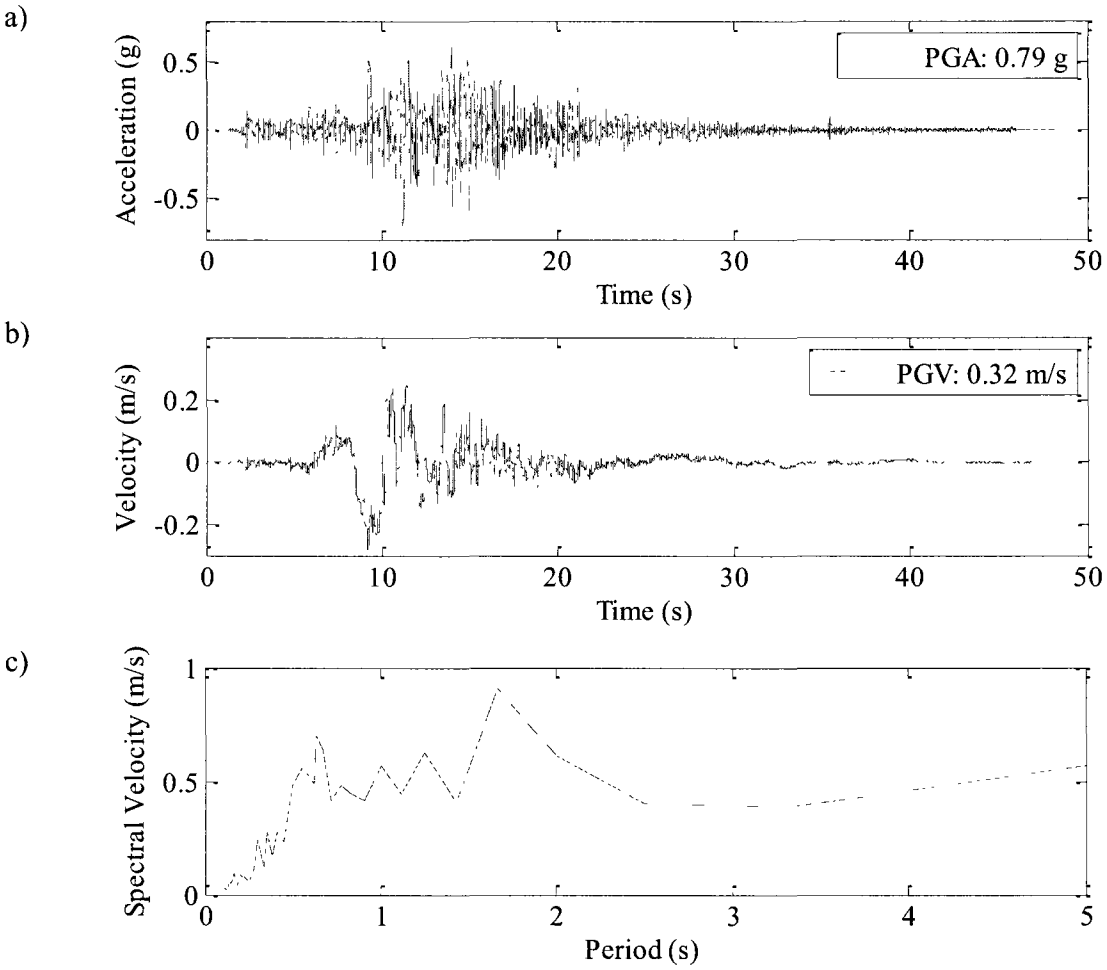

Figure 3. 15 Landers 1992 (24 Lucerne) ground motion, A/V>1

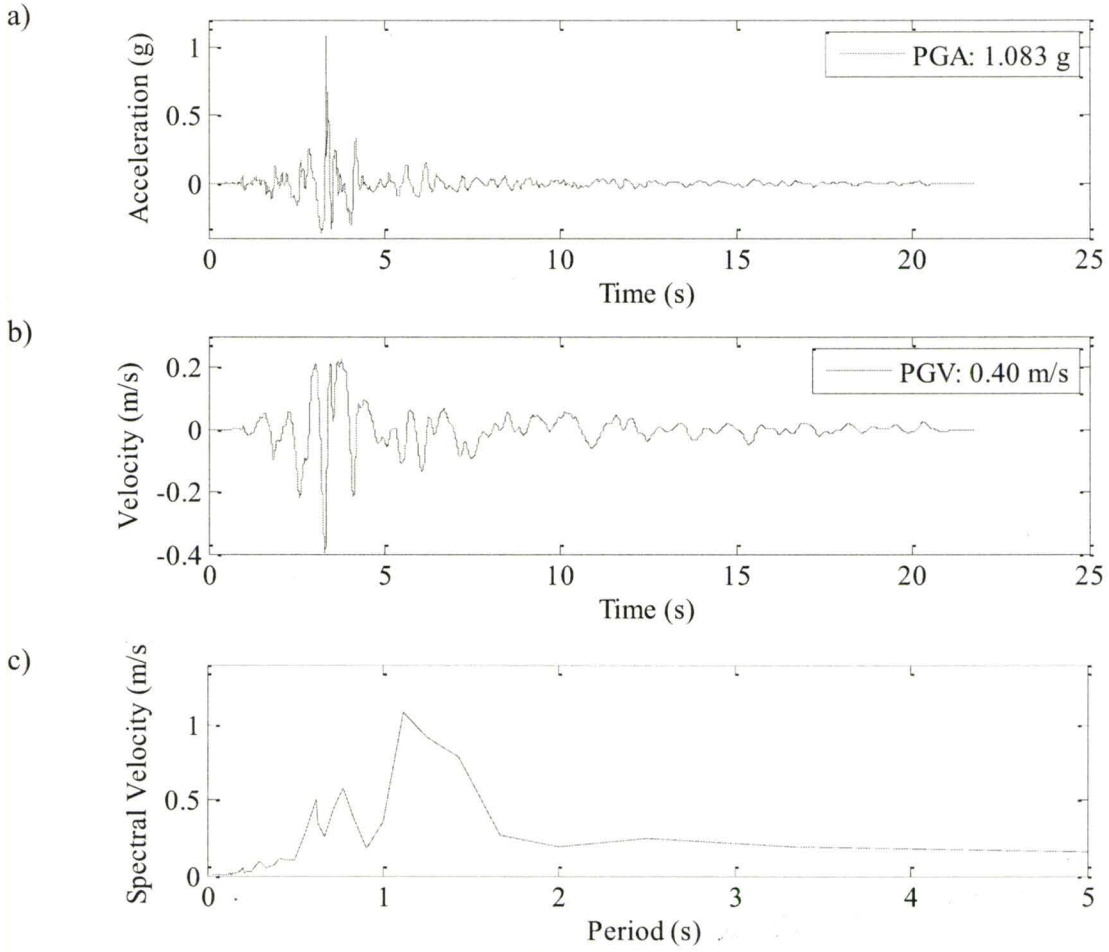

Figure 3. 16 Coalinga 1983 (1651 Transmitter Hill) ground motion, A/V>1

4. NON-LINEAR TIME-HISTORY ANALYSIS OF LRB AND THEIR DESIGN

4.1. INTRODUCTION

In this chapter, the model description for this study is first reviewed and results of nonlinear time-history analyses are presented. Using these results, three types of isolator design charts identified as, n-chart, r-chart and regression-based-chart, are created. An example is used to examine the accuracy of the new design method compared with the currently employed method.

4.2. NON-LINEAR TIME-HISTORY ANALYSIS

The nonlinear time-history analysis on a SDOF system was carried out using SAP2000 Nonlinear version 14 (Computers and Structures, 2010). A total of 10752 nonlinear time-history analyses was performed. The isolators were modeled using the SAP2000 NLLink two-joint link element. The maximum top joint displacement and maximum base joint shear force are examined. The details are explained in the subsequent sections.

Model Description

A SDOF system is used to model the isolation system. As illustrated in Fig.4.1, a lumped mass is supported by an isolation system, which is represented using a bilinear spring and a viscous damper with 5% damping ratio.

In practice, LRB is modeled by a bilinear model. As shown in Fig.4.2, a bilinear model is defined by three parameters: the elastic shear stiffness (k_1), the post-elastic stiffness (k_2),

and the characteristic strength (Q_y). For LRBs, the relation between the design parameters and the LRB configurations are explained as follows (Buckle, et al., 2006) :

Characteristic Strength (Q_y)

As shown in Fig.4.3, the characteristic strength is where the hysteretic loop intersects with the force axis. Its value can be calculated from the yield strength.

$$Q_y = F_y\left(1 - \frac{k_2}{k_1}\right) \qquad \text{.....4. 1}$$

where

F_y = yield strength of LRB

k_1 = elastic shear stiffness

k_2 = post-elastic shear stiffness

Yield Strength (F_y)

The yield strength is determined by the size of the lead core contained in the LRB. It is to ensure the structural rigidity under normal service load (i.e. traffic and wind load). The design relation is:

$$F_y = \frac{1}{\varphi} f_{yl} \frac{\pi d_L^2}{4} \qquad \text{.....4. 2}$$

where

f_{yl} = shear yield stress of the lead (10 MPa)

d_L = diameter of the lead core

φ = load factor accounting for creep in lead = 1.0 for dynamic loads

The requirement of LRB yield strength is specified as a percentage to the structure weight (w) in AASHTO (AASHTO, 1999). This yield strength to weight ratio (F_y/w) is represented as n in this study. Four values were considered for *n*, they are 2%, 5%, 10% and 20 %. When *n* exceeds 20%, the LRBs might not yield under design earthquakes and thus higher values should be avoided.

Post-elastic Stiffness (k_2)

Two slopes (k_1 and k_2) are needed to define a hysteretic loop for LRB (Fig. 4.2). They must ensure a long enough period to avoid the strong earthquake energy and short enough period to satisfy the serviceability requirement respectively (i.e. the wind load and the traffic load) (Park et al., 2002). The post-elastic stiffness (k_2) is determined by the rubber stiffness (k_r) primarily and an extra 10% is added for the contribution of the yielded lead core. The rubber stiffness is found using Equation 4.3. Combining Equation 4.3 and 4.4, it is found that the value of k_2 is directly influenced by the size of rubber bearing, as it is directly proportional to the rubber surface area and inversely proportional to the rubber height. The natural periods corresponding to these stiffnesses can be found using Equation 4.5 and Equation 4.6.

$$k_r = \frac{GA_b}{h_r} \qquad \text{.....4. 3}$$

$$k_2 = 1.1k_r \qquad \text{.....4. 4}$$

$$T_1 = 2\pi\sqrt{\frac{m}{k_1}} \qquad \text{.....4. 5}$$

$$T_2 = 2\pi\sqrt{\frac{m}{k_2}} \qquad \text{.....4. 6}$$

where

T_1 = period of motion calculated based on k_1

T_2 = period of motion calculated based on k_2

m = equivalent SDOF mass

G = shear modulus of rubber (1 MPa)

h_r = height of rubber

Note: To prevent roll-out, the height (h) of LRB should be lower than its diameter with the height corresponding to the maximum allowable design displacement (Naeim and Kelly, 1999).

$$A_b = \frac{\pi(d_b^2 - d_L^2)}{4} \qquad \text{.....4. 7}$$

where

d_L= diameter of the lead plug

d_b= the diameter of bonded rubber

Elastic Stiffness (k_1)

The elastic loading and unloading stiffness (k_1) is the first slope of the hysteretic loop (Fig. 4.3). The value of k_1 can be found from available hysteresis loops from laboratory tests or as a multiple of k_2. Values of post-to-pre elastic stiffness ratio ($r=k_2/k_1$) have been

suggested in different studies. Skinner et al (1993) suggested 1/9 to 1/16 (0.11 to 0.06), while Naeim and Kelly (1999) recommended 1/10 to 1/21 (0.1 to 0.05) for LRBs. The actual value of r will be updated after laboratory prototype tests. In practice, LRB is most often associated with r =1/10. For example, LRBs used in the William Clayton Building and the Wellington Press Building have r=1/10 (Skinner, et al., 1993). In this study, three values, r=0.05, 0.10 and 0.15 are considered.

Energy Dissipation

One of the main purposes of employing a LRB is to dissipate earthquake energy. The energy dissipated per cycle of the hysteretic loop (E_h) when the lead has yielded, is calculated as:

$$E_h = 4Q_y(d_m - d_y) \qquad \text{.....4. 8}$$

where

d_m= maximum shear displacement

d_y= yield displacement

4.3. RESULTS AND DISCUSSION

The results of nonlinear time-history analyses are presented using a bilinear spectrum. The vertical axis shows the displacement or shear force response of the isolator unit and the horizontal axis shows the period of the isolated system (T_I). Seven values of T_I, ranging from 0.6 seconds to 4.4 seconds are considered. For each T_I, three values of r and four values of n are considered. In total there are 5040 (20x3x7x4x3) nonlinear time-history analyses performed for Group A earthquakes and 5712 (17x4x7x4x3) nonlinear

time-history analyses performed for Group B earthquakes. The mean plus one standard deviation (84.1 percentile) of the response displacement and shear force are plotted against T_1 in two ways, namely r-charts and n-charts. The schematic of constructing r-chart and n-chart is shown in Fig. 4.3. Over 200 spectra are generated. Since responses are found to have similar trends over different shaking intensities, only representative PGAs of 0.5*g* and 1.0*g* are presented. The grouped n-charts are shown in Fig.4.4 to Fig.4.7 and grouped r-charts are shown in Fig.4.8 to Fig.4.11 for displacement and shear responses, respectively. The responses for A/V<1 earthquakes are shown in the left columns and the responses for A/V>1 earthquakes are shown in the right columns in each figure.

The n-chart is used to investigate the performance influence of n, which is determined by LRB lead content. Each n-chart consists of four curves, which have the same value of r and four different values of n. Each figure from Fig.4.4 to 4.7 shows three values of r.

The r-chart is used to investigate the response influence of r, which is determined by LRB rubber size. Each r-chart summarizes the responses of bilinear hysteretic loops with a particular value of r and three values of n. Fig.4.8 to 4.11, each displays three values of n.

It should be noticed that results for PGA under 0.5g are obtained using Group A records while results for PGA under 1.0g are obtained using Group B records. Their bilinear spectra will have similar trends, as will be illustrated in the following sections.

4.3.1. Response under A/V<1 Earthquakes

Nonlinear time-history results from A/V<1 records are shown on the left columns in Fig.4.4 to Fig.4.11 while the results from A/V>1 records are shown on the right columns. A/V<1 earthquakes produce higher responses in both displacement and shear force compared to what A/V>1 earthquakes produce. The differences in response are the resultant of long duration pulse-like content in A/V<1 records and acceleration spike content in A/V>1 records. It should be noticed that increase in displacement response of A/V<1 earthquakes is substantial (Fig. 4.4 and Fig 4.6), while the increase in shear response is not as distinct (Fig. 4.5 and Fig. 4.7). This can be explained considering the nature of analyzed bilinear models, which have relatively low post-pre elastic stiffness ratios (r). Under earthquake excitation, these lower slopes (low post-elastic stiffness) draw larger variations over displacement response comparing to shear response.

The recommended maximum displacement for an elastomeric isolator is the height of the isolator unit (Naeim and Kelly, 1999). A LRB designed for A/V<1 earthquakes, therefore, must have larger dimensions in both height and area to achieve the same level of isolator performance and stability.

4.3.2. Influence of the Yield Strength to Weight Ratio (n)

For LRBs, the value of n is directly proportional to the yield strength (F_y) and therefore the size of the lead core (Equation 4.2). The influence on the hysteretic loop due to the lead size change is shown in Fig.4.12a.

For both A/V<1 and A/V>1 earthquakes, the displacements are generally found to decrease as n increases for all T_1 and r (Fig.4.4 and Fig.4.6). This trend occurs because an increased n will result in higher energy dissipated per cycle, as the dissipated energy is most influenced by the yield strength (F_y) following Equation 4.8.

The shear force is found to decrease as n increases in A/V<1 earthquakes, for T_1 less than about 1.5 sec (Fig.4.5 A/V<1 and Fig. 4.7 A/V<1). This relation is found reversed as T_1 gets higher than about 1.5 sec. For the A/V>1 earthquakes, it is observed that shear force increases as the ratio n increases. Intuitively, the maximum displacement and shear force from the three models should occur in the same order along both axes. For instance:

- A higher displacement (d_m) will correspond to a higher shear force (F_m) for the same hysteretic loop (Fig. 4.3).
- A higher damping will result in smaller responses of both displacements and shear forces.

However, these expectations are not upheld by the nonlinear time-history analysis. Due to the nature of earthquakes, plastic offset will be experienced. In other words, the hysteretic loop will not constantly repeat from the original position. As shown in Fig.4.13, qualitatively drawn hysteretic loops have the same value of T_1 and r but different values of n. The hysteretic loop with n of 5% produces the largest displacement but the smallest shear force, since it starts from a different position (around d_{10} mark) comparing to the others (n of 20% and 10%), which start from the origin. This indicates that damping

might not have an equal effect on both displacement and shear force responses when high nonlinearity is involved. These observations indicate that the elastic theory does not reflect the nonlinear responses and should be applied to seismic response analysis with caution.

Overall, an increase of n (directly proportional to the lead size) can produce a reduction in the displacement response. Thus in LRB design, when the design is more restricted by the displacement requirements, one solution is to increase the lead content.

4.3.3. Influence of Post-Pre Elastic Stiffness Ratio (r)

In LRBs, the value of r (k_2/k_1) is determined by the rubber area and height for the same k_1 using Equation 4.3 and Equation 4.4. For the same k_1, the changes made to the hysteretic loop when the rubber dimensions changed are shown in Fig. 4.12b. As the rubber height increases or the rubber area decreases, the r value will decrease.

The shear force is found to increase as the value of r increases (Fig.4.9 and Fig.4.11). However, very limited influence is found over the displacement response and for high values of n, the influence of r is not noticeable (Fig.4.8 and Fig.4.10). Therefore, in LRB design, when the shear force is the design restriction, one solution is to decrease the rubber area or increase the height.

4.3.4. Influence of the Earthquake Selection and Scaling

Group A and B records are scaled to the same PGA and PGV and the 84.1 percentile results of the two group results are compared. The representative results from PGA of 0.5g and PGV of 30cm/s are presented in Fig.4.14 and Fig.4.15, where the model has n=2% and r=0.1. The blue series represents the results of Group A and the red series represents the results of Group B. In general these lines follow a similar pattern.

Fig.4.14 and Fig.4.15 show the displacement and shear response results obtained from earthquake scaling done to PGA and PGV, respectively. Fig.4.15 shows that the results obtained from Group A and Group B are almost identical. This supports one of the views in literature that PGV is a better parameter to identify damage potential.

4.4. DESIGN OF LRB

A displacement-based method reviewed in Naeim and Kelly (1999) was found a better method over currently available methods (Wesolowsky, 2001). It is found to be accurate in modeling as it is capable to model the complete hysteretic loop. The procedure of Naeim and Kelly (NK) method will be explained. Design accuracy comparisons of NK method and a proposed Chart Method are made.

4.4.1. Naeim and Kelly (NK) Method

The NK method is a versatile method. It allows the designer to define a wide range of post-to-pre elastic shear stiffness (k_2/k_1) ratio (r). For LRB, Naeim and Kelly (1999) suggested post-to-pre elastic shear stiffness ratios in the range of 1:10 to 1:21. The

fundamental objective of this method is to define a bilinear hysteretic loop of LRB. As shown in Fig.4.2, when the design displacement (d_m), the design force (F_m) and the ratio of k_2/k_1 are chosen, the hysteretic loop can be defined by locating the Q_y. This process is done by simplifying the bilinear model to an equivalent visco-elastic model, which is often called an equivalent linear model. The hysteretic loops of the simplified force-displacement relation and viscous damper are shown in Fig.4.16. The effective (secant) stiffness (k_{eff}), which is calculated based on the anticipated maximum displacement and force, is used to simplify the isolator stiffness. The amount of damping inherent in the bilinear behaviour is simplified as a viscous damper. The mathematical equations are explained as follows:

Effective Stiffness and Period

The high non-linearity inherent in bilinear isolator causes the isolated period to vary at different loading stages. Therefore, an effective isolated period is used to represent the isolated period of motion at the maximum displacement. It is calculated based on the effective stiffness (k_{eff}), which is obtained by dividing the maximum horizontal force, F_m, by the corresponding displacement, d_m. The effective stiffness and period are expressed as follows:

$$k_{\text{eff}} = \frac{F_m}{d_m} = \frac{Q_d + k_2 d_m}{d_m} = \frac{Q_d}{d_m} + k_2 \qquad \text{.....4. 9}$$

$$T_{eff} = 2\pi \sqrt{\frac{m}{k_{eff}}} \qquad \text{.....4. 10}$$

Equivalent Viscous Damping

The energy dissipated per cycle of a viscous damper (E_v) is calculated using the following equation:

$$E_v = 2\pi k_{eff} {d_m}^2 \beta_e \quad \text{.....4. 11}$$

The energy dissipated per hysteretic cycle (E_h) was previously (Equation 4.8) defined as:

$$E_h = 4Q_d(d_m - d_y)$$

An equivalent critical damping ratio (β_e) is used to represent hysteretic damping. To obtain β_e, the following equation is used:

$$\beta_e = \frac{E_h}{E_v} = \frac{4Q_d(d_m - d_y)}{2\pi k_{eff} {d_m}^2 \beta_e} = \frac{2Q_d(d_m - d_y)}{\pi d_m (Q_d + k_2 d_m)} \quad \text{.....4. 12}$$

Incorporating with the equivalent visco-elastic model, the procedure of the NK method following ASCE 7 (2002), is adopted as follows:

1. Design displacement (d_m) and Design force are (F_m) chosen
2. The effective stiffness is calculated at the design displacement and the design force. Note that design displacement and force are the maximum values using Equation 4.9

$$k_{eff} = F_m / d_m$$

3. The effective period is calculated at the maximum displacement using Equation 4.10

$$T_{eff} = 2\pi \sqrt{m / k_{eff}}$$

4. If the design displacement (d_m) is chosen to satisfy the minimum lateral displacement (D_D). The damping required is calculated following Step 4 and 5.

$$B_D = \frac{gS_{D1}T_{eff}}{4\pi^2 D_D} \quad \text{.....4. 13}$$

where

S_{D1} = maximum considered 5% damped spectral acceleration at a period of one sec, in units of g

B_D = numerical coefficient related to the effective damping (β_e) of the isolation system at the design displacement

5. Find the effective damping ratio (β_e) for calculated B_D from Table.4.1

6. The energy dissipated per viscous damping cycle (E_v) and the energy dissipated per bilinear hysteresis cycle (E_h) are found from the area within their hysteretic loops as shown in Fig.4.3 using Equation 4.8 and Equation 4.9

$$E_v = 2\pi k_{eff} {d_m}^2 \beta_e$$

$$E_h = 4Q_d(d_m - d_y)$$

7. Equating E_v and E_h and rearranging to find Q_d

$$Q_d = \frac{\pi k_{eff} {d_m}^2 \beta_e}{2(d_m - d_y)} \quad \text{.....4. 14}$$

8. Neglecting d_y to find the first approximation of Q_d

$$Q_d = \frac{E_v}{4d_m} \quad \text{.....4. 15}$$

9. Use the approximation of Q_d in the following rearrangement of Equation

$$k_2 = k_{eff} - Q_d/d_m \quad \text{.....4. 16}$$

10. Calculate d_y using

$$d_y = \frac{Q_d}{k_1 - k_2} \quad \text{.....4. 17}$$

11. Recalculate $Q_d$using Equation 4.14

12. Repeat step 9 through 11 until the solution converges

13. The final value of d_y is used to calculate the yielding force (F_y)

$$F_y = k_1 d_y \quad \text{.....4. 18}$$

The final results of k_2 and F_y can be used to determine the rubber bearing and lead sizes, respectively. In routine office design, the NK method is typically used; However, studies have found that this process becomes less accurate as the nonlinearity increases (Dicleli and Buddaram, 2007; Hwang, 1996; Hwang and Chiou, 1996).

4.4.2. Design Using Chart Method

Logarithmic regression analysis is applied to the 84.1 percentile displacement results and the shear results shown in Fig.4.4 to Fig.4.7. The analyzed displacement and shear responses are plotted against the horizontal axis, which is the weight to elastic stiffness ratio (w/k_1). This type of chart is called as regression-based-chart, which can be adopted for two applications: LRB Design and LRB performance evaluation. When it is adopted for design application, (namely Chart Method), it simplifies the design procedure, as the displacement and shear responses are read from charts. When this design procedure is adopted in a reversed order, the performance of different sized LRBs can be evaluated. The displacement and shear regression-based-charts are shown in Fig. 4.17 to Fig.4.20. The details of the design procedure and its implementation are explained as follows.

If the displacement and shear force in the isolator are the design considerations, the methodology of adopting the Chart Method is to first select one set of LRB hysteretic loop design parameters, which is a coordinate (w/k_1, r, n) in the charts, to meet one of the design requirements (i.e. displacement). Subsequently, the shear force corresponding to the selected set of parameters is checked to ensure the shear force requirement is satisfied. The procedure is as follows:

1. Define the design earthquake intensity (PGA or PGV)
2. Design displacement (d_m) and Design force are (F_m) chosen
3. Find d_m from Fig.4.17
4. Identify the corresponding coordinate of (r, n, w/k_1)
5. With the same r, n and w/k_1, find the corresponding shear force to weight ratio in the vertical axis of Fig. 4.18.
6. Obtain the shear force by multiplying the supported weight (w) by the ratio found in step 5.
7. Check the shear force obtained from the step 6 with the design force (F_m).
8. If the design requirements are satisfied, record the values of r, n and w/k_1. Otherwise, perform iteration on steps 3 through 7.
9. The values of k_1, k_2 and F_y can be calculated using the following equations:

$$k_1 = w \cdot \left(\frac{w}{k_1}\right)^{-1} \quad \text{.....4. 19}$$

$$k_2 = r \cdot k_1 \quad \text{.....4. 20}$$

$$F_y = n \cdot w \quad \text{.....4. 21}$$

4.4.3. Design Example

A hypothetical example is employed to illustrate the design of isolator and to compare the design accuracy of the NK Method and the Chart Method under four circumstances: relatively large and small weights to be isolated under moderate and severe ground motions, respectively.

Example: Assume soil/foundation-interaction is neglected and the anticipated earthquake will not be affected by the forward directivity focusing. A 25000kN and a 10000kN rigid frame are to be isolated under PGA of 0.5g and PGA of 1.0g. The design allowances under each circumstance are as follows:

- Under PGA of 0.5g, the displacement and shear response limits are 0.25m and 3500 kN, respectively.
- Under PGA of 1.0 g, the displacement and shear response limits are 0.7m and 3500 kN, respectively.

Design a LRB system (total yield strength and total stiffness) to satisfy the each corresponding level of performance.

Solution: For preliminary design of LRB, the post-to-pre elastic stiffness ratio (r) is chosen as 0.1. The values used in each step of design are summarized in Appendix B. The design prepared by the NK Method and the Chart method are listed in the Table 4.2. The design performances are tested under four arbitrarily selected A/V<1 earthquake records (Table 4.3). The response time-histories of isolators designed using the NK

Method and the Chart Method are presented in Fig. 4.21 to Fig.4.24 and Fig.4.25 to Fig. 4.28, respectively.

4.4.4. Discussion on the Design

NK Method is found able to provide satisfactory designs under most circumstances (Fig.4.21, 4.22 and 4.24). However, for the circumstance where 25000kN is to be isolated under PGA of 1.0g earthquakes, the design provided using the NK Method exceeds the shear force design limit (Fig. 4.23b). The cause of this design inaccuracy is the high inherent equivalent damping (25%) as shown in Appendix B accordingly. This is consistent with the findings from other studies, where the design accuracy is found to decrease as the nonlinearity increases (Dicleli and Buddaram, 2007; Hwang, 1996; Hwang and Chiou, 1996). The Chart Method, on the other hand, is able to provide consistent design accuracy in all circumstances tested (Fig. 4.25 to 4.28). In addition to the enhanced design accuracy, the Chart Method is found a superior method in LRB design for the following reasons.

Firstly, the anticipated displacement and shear force for a certain shaking intensity are read. This makes the Chart Method simple to use. For instance in this example: A 25000kN frame is to be isolated. The design earthquake is taken as PGA 0.5g and A/V>1. When a 0.25 m design displacement is selected, the satisfactory r, n and w/k_1 are found as a coordinate (0.1, 5%, 0.5) from Fig.4.17 (b) A/V>1. The same coordinate in the Fig.4.18 (b) A/V>1, corresponds to a shear force of 3500 kN (14% of the weight). Thus the system can be designed based on this coordinate (0.1, 5%, 0.5) and the isolator unit is likely to

have less than 0.25m displacement and less than 3500kN. The design parameters F_y, k_1 and k_2 can be then calculated using Equation 4.19 to 4.21.

Secondly, it should be noticed that using the NK Method, the design accuracy relies on the estimated viscous damping ratio. As provided in the Equation 4.13, regardless of the accuracy of this equation, this damping ratio is dependent on the design displacement. Thus, design experience is required to address a feasible design displacement at the beginning of the design. Otherwise, the design is iterative and convergence is not guaranteed. However, using the Chart Method, design accuracy is not governed by the design experience.

Thirdly, the isolator designed using Chart Method is compact in size (Table 4.2). This reduces the cost of the isolator unit and it also makes placing the isolator at locations with limited area possible (i.e. bridge piers).

Lastly, using the Chart Method, the designer is able to evaluate the performance of available isolator sizes and determine whether they can satisfy the design requirements. For example, if one available isolator dimensions is, 0.25m in height, 1.0m in diameter and 0.3m in diameter of lead core. This isolator unit has a k_2/k_1 ratio of 0.1. A design can apply the Chart Method readily. The values of r, n and w/k_1 are calculated as (0.1, 11%, 0.4). The corresponding responses for such design are read from Fig.4.17& 4.18 (b) A/V>1 as 0.20m in displacement and 3500 kN for the shear force. Compareing these values with the design requirements, 0.25m of displacement and 3500 kN of shear force,

this isolator meets the preliminary design requirements and therefore can be adopted. Considering the costs of manufacturing custom isolator moulds can be substantial, using this available size can help minimize such costs.

4.5. CONCLUSIONS

4.5.1. Performance Assessment on LRB Design Parameters

Based on this chapter, general conclusions are drawn about the influence of the design parameters:

- An increase of lead size causes an increase of yield strength. Such a change has impacts on both displacement and shear force responses. The increase of lead causes a decrease in displacement responses in general situations. The corresponding shear force, however, does not have a general trend. This suggests that when displacement is the design limitation, one option is to increase the lead size.
- An increase of rubber size causes an increase of post-elastic stiffness. The increased post-elastic stiffness has significant influence over the shear force response. The shear force is found to increase as the post-elastic stiffness increases. The corresponding change over the displacement is found to be negligible. This suggests that when shear force is the design limitation, one solution is to reduce the rubber size.

4.5.2. Proposed Chart Method

Using the regression-based results, a new design method for LRB was developed.

- Compared with the NK Method, the Chart Method has a simple design procedure. It also provides consistent design accuracy under different design circumstances.

- Using the Chart Method, commercially available bearing sizes can be evaluated to determine whether they can meet the design requirements. Using an available isolator size can significantly reduce the costs of LRB moulds.

Table 4. 1 Damping Coefficient (ASCE-7, 2002)

Effective Damping Ratio (β_e)	Damping Coefficient (B_D)
$\leq 2\%$	0.8
5%	1.0
10%	1.2
20%	1.5
30%	1.7
40%	1.9
$\geq 50\ \%$	2.0

Table 4. 2 Design parameters obtained from both methods

	10000 kN				25000 kN			
	PGA 0.5g		PGA 1.0g		PGA 0.5g		PGA 1.0g	
	NK's	Chart	NK's	Chart	NK's	Chart	NK's	Chart
Elastic stiffness (k_1) (kN/m)	133365	20000	105783	5882	105783	50000	249999	14706
Post-elastic stiffness (k_2) (kN/m)	13336.5	2000	10578.3	588.2	10578.3	5000	24999.9	1470.6
Yield strength (F_y) (kN)	184	500	950	1000	950	1250	4615	2500
Rubber diameter (m)	1.98	0.81	2.96	0.79	1.79	1.27	4.57	1.24
Lead diameter (m)	0.16	0.26	0.35	0.36	0.35	0.4	0.77	0.57
Height (m)	0.25	0.25	0.7	0.7	0.25	0.25	0.7	0.7

Table 4. 3 Earthquakes used for design comparison

Earthquake Name	Year	Station	Mw	Closest Distance (km)	PGA (g)	PGV (m/s)	A/V
CAPE MENDOCINO	1992	89005 Cape Mendocino	7.1	8.5	1.497	0.127	1.36
NORTHRIDGE	1994	24207 Pacoima Dam	6.7	8	1.285	0.104	1.44
NORTHRIDGE	1994	24436 Tarzana, Cedar Hill	6.4	17.5	1.779	0.114	1.94
MORGAN HILL	1984	57217 Coyote Lake Dam	6.2	0.1	1.298	0.808	1.96

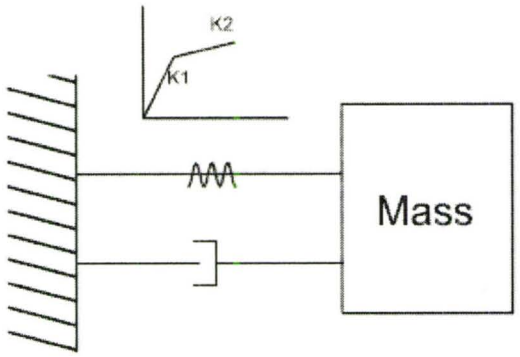

Figure 4. 1 Model of LRB Isolation System

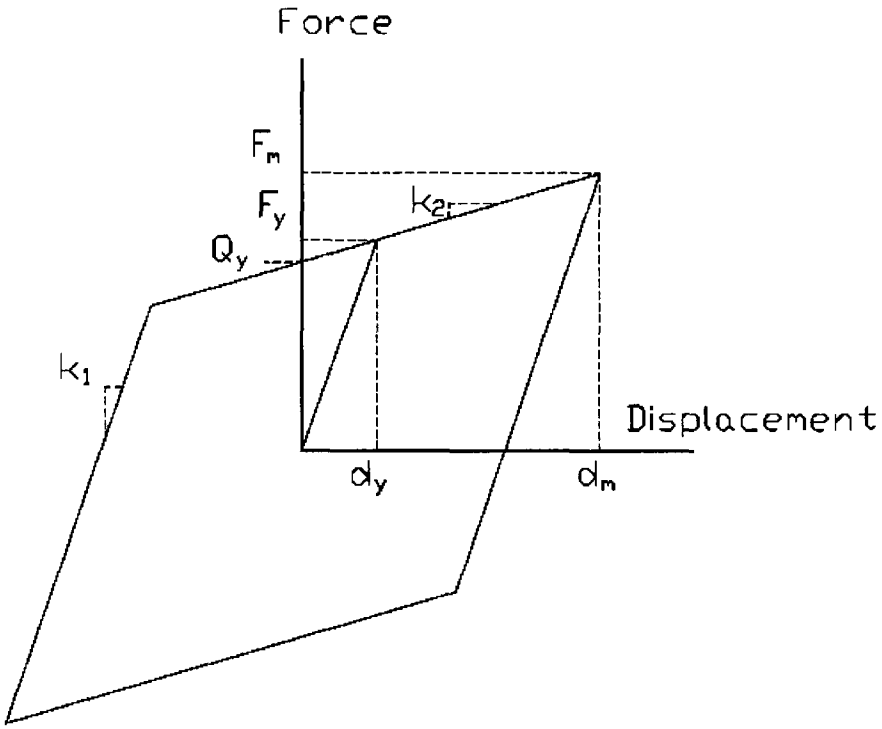

Figure 4. 2 Bilinear hysteretic loop

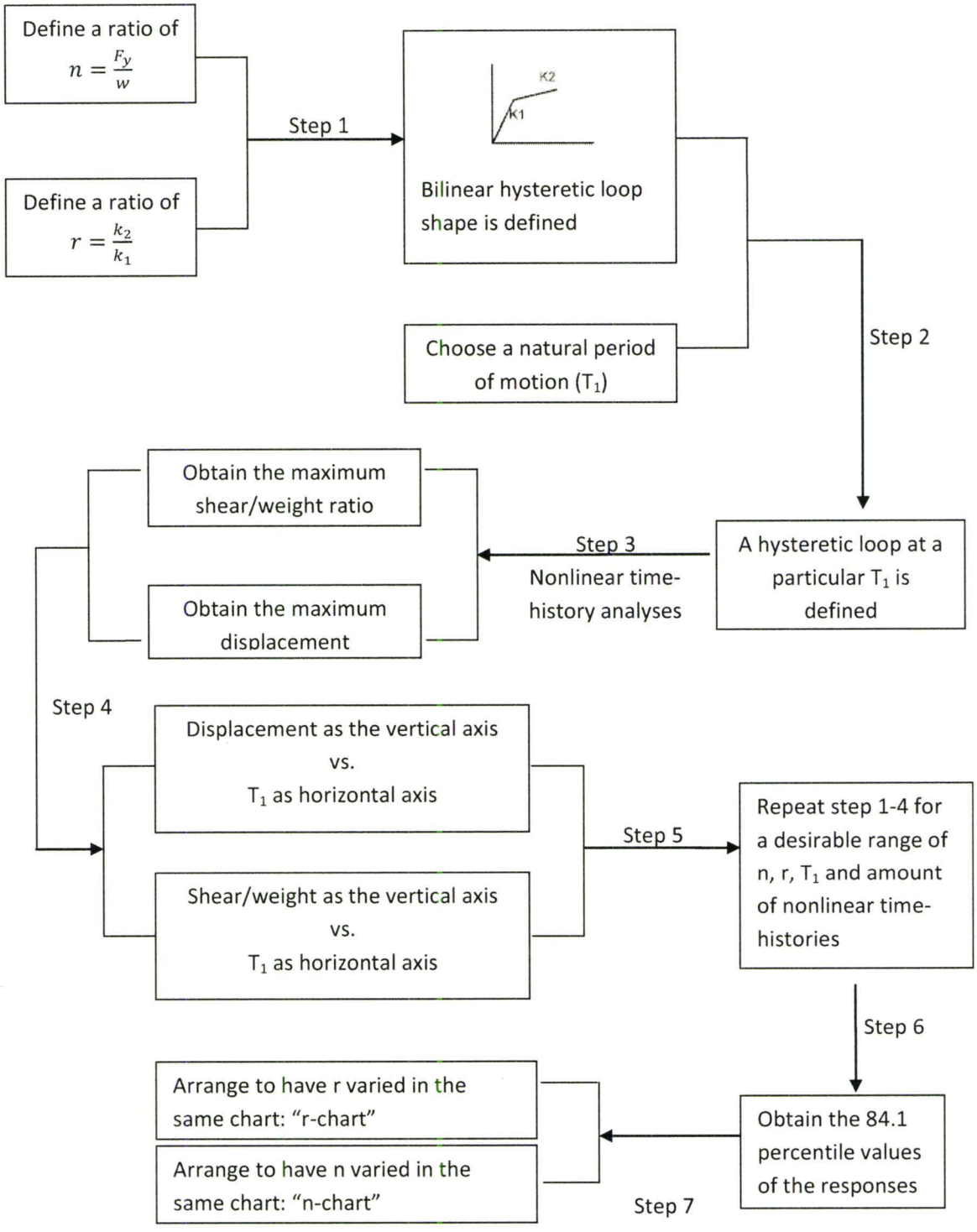

Figure 4. 3 Schematic flow chart of constructing the r-chart and n-chart

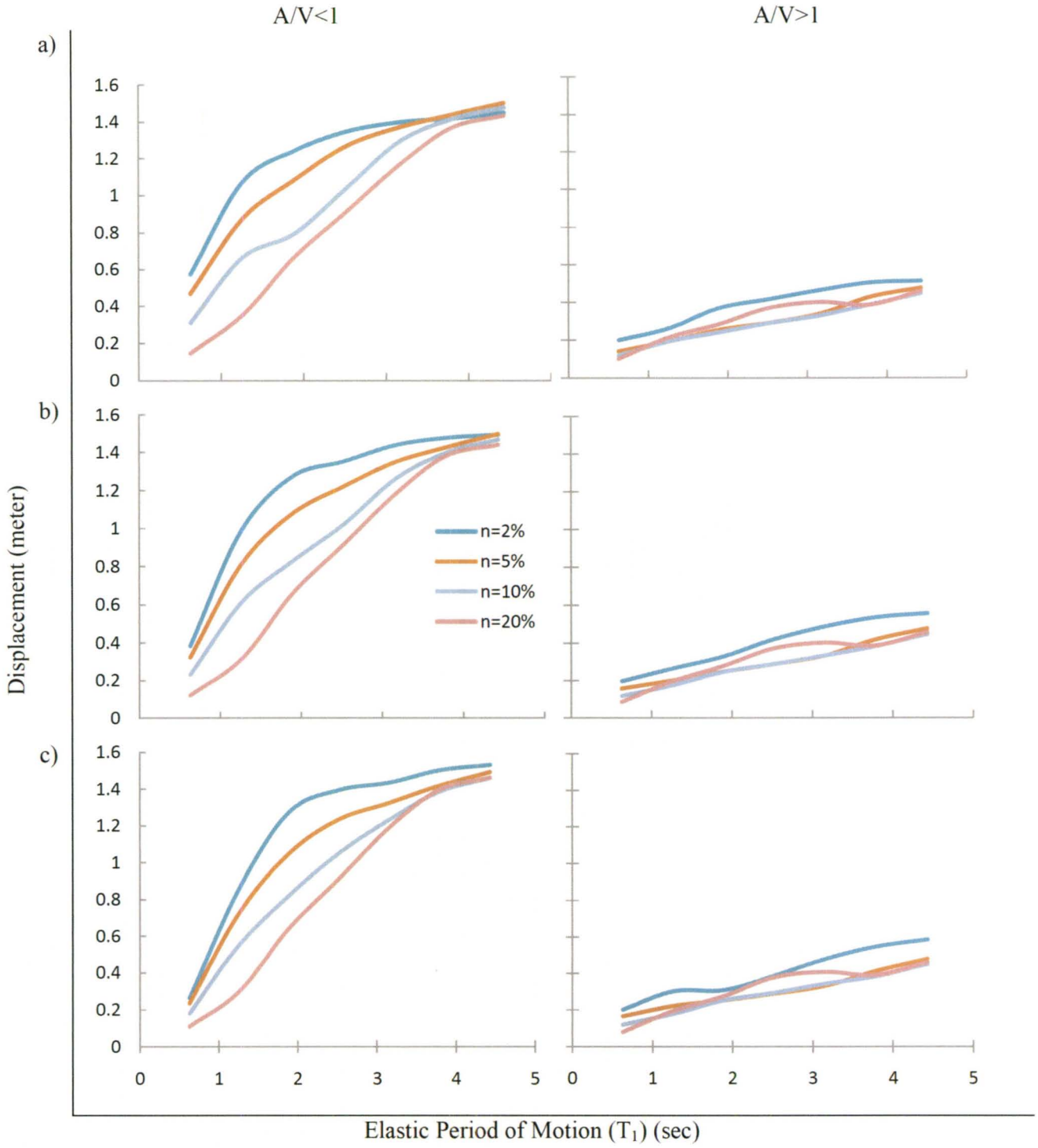

Figure 4. 4 Displacement n-chart at PGA of 0.5 *g*; produced using Group A : a) r=0.05; b) r=0.10; c) r=0.15

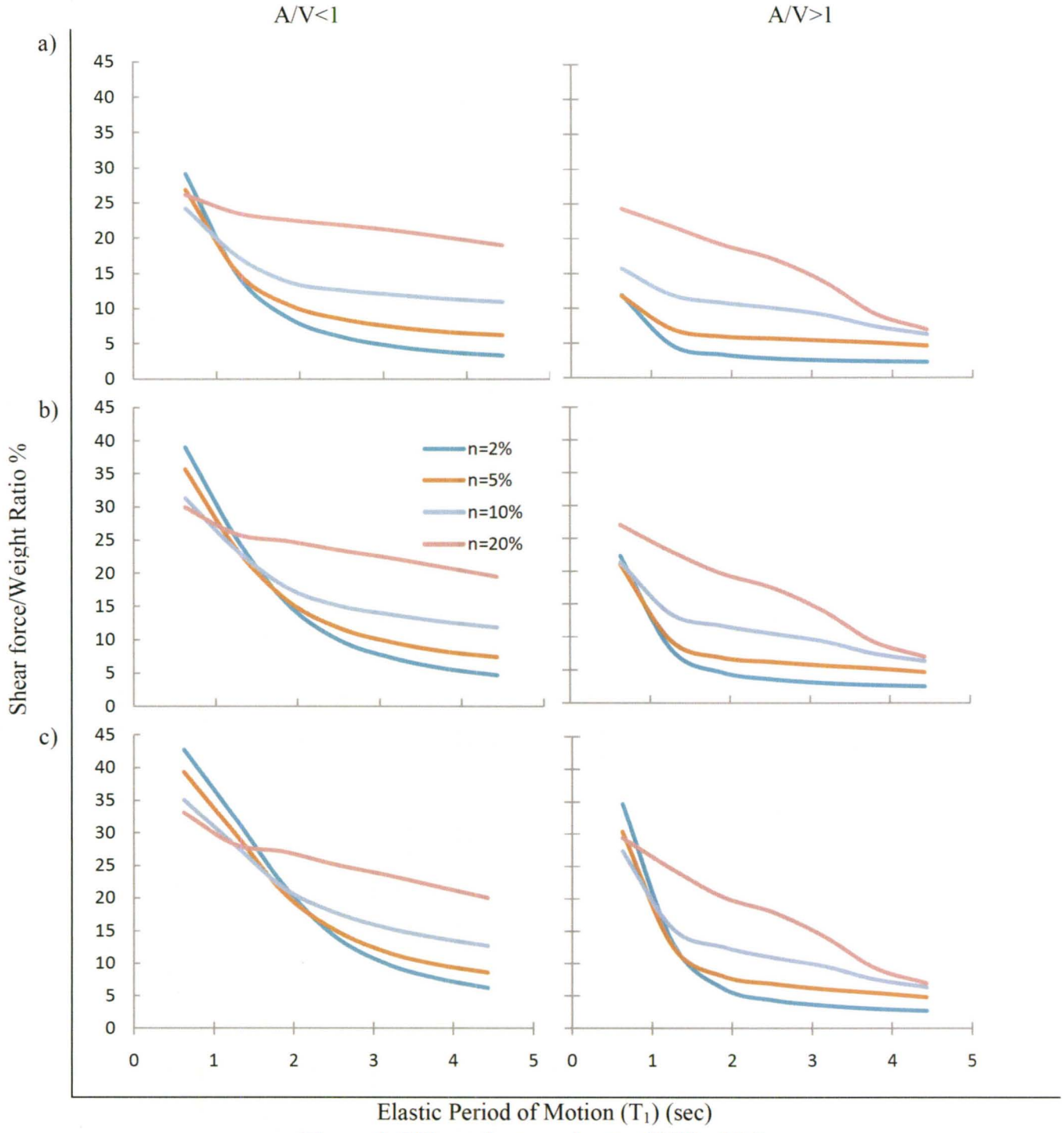

Figure 4. 5 Shear force n-chart at PGA of 0.5 *g*; produced using Group A: a) r=0.05; b) r=0.10; c) r=0.15

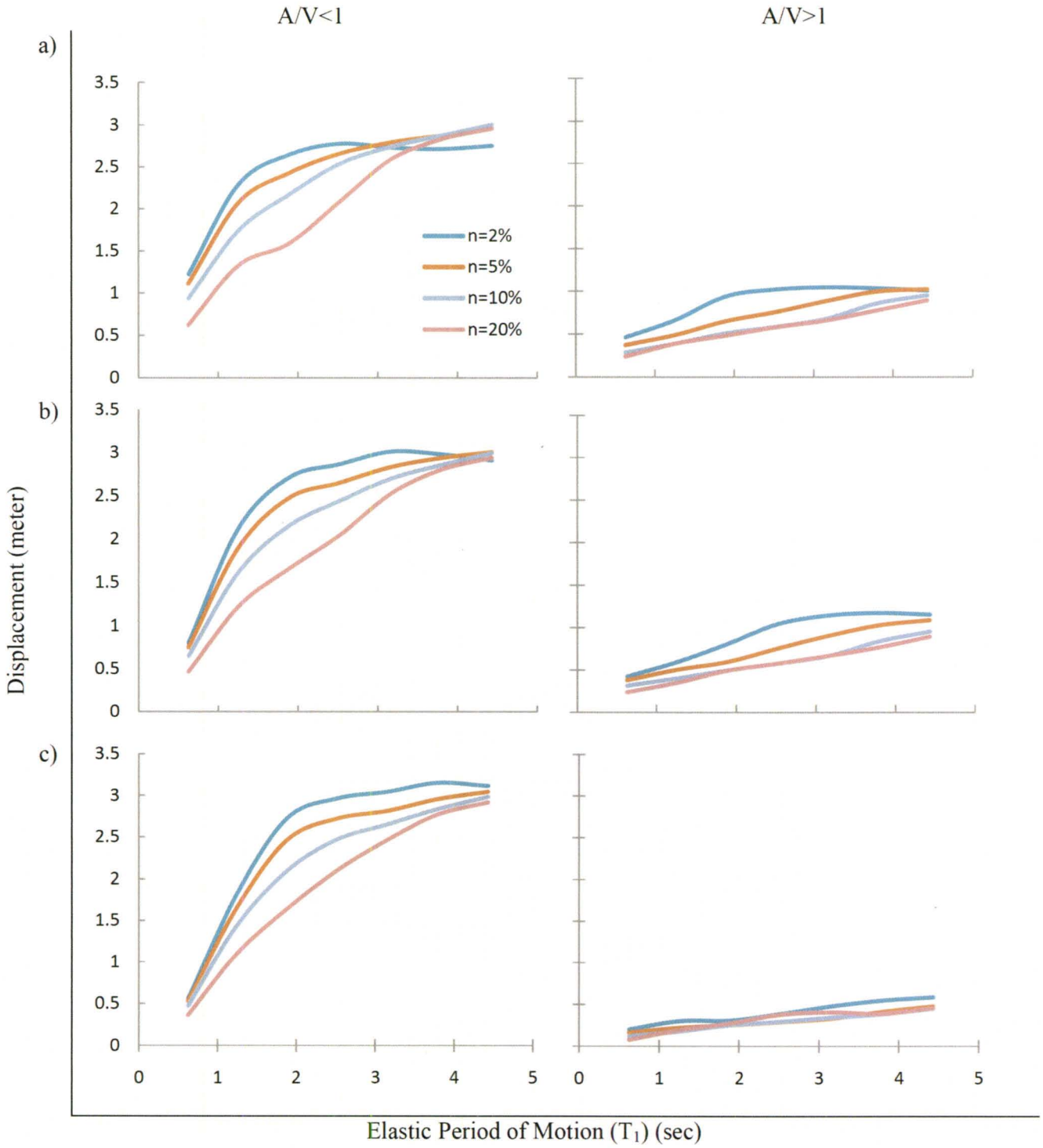

Figure 4. 6 Displacement n-chart at PGA of 1.0 *g*; produced using Group A: a) r=0.05; b) r=0.10; c) r=0.15

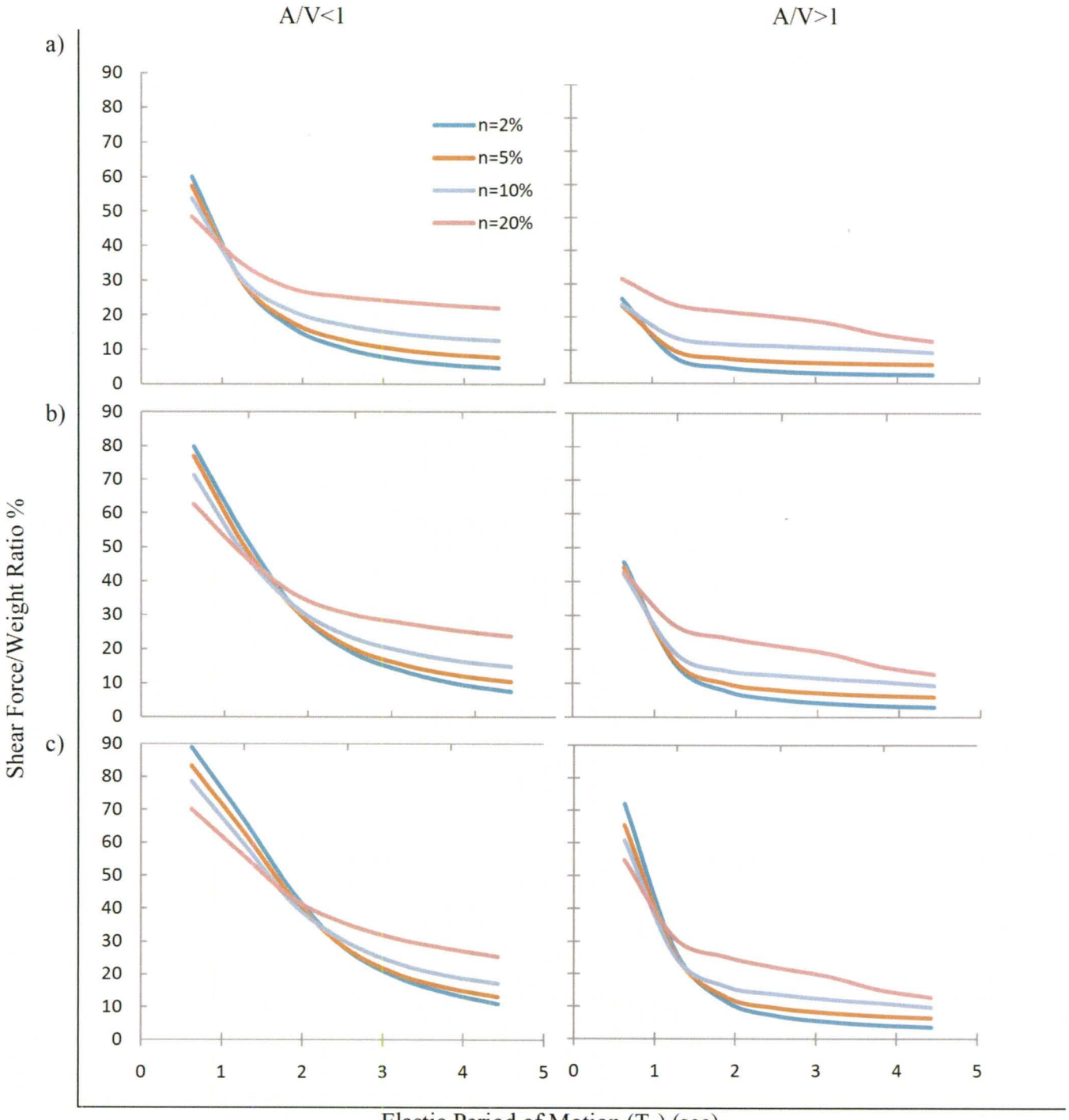

Figure 4. 7 Shear force n-chart at PGA of 1.0 *g*; produced using Group B: a) r=0.05; b) r=0.10; c) r=0.15

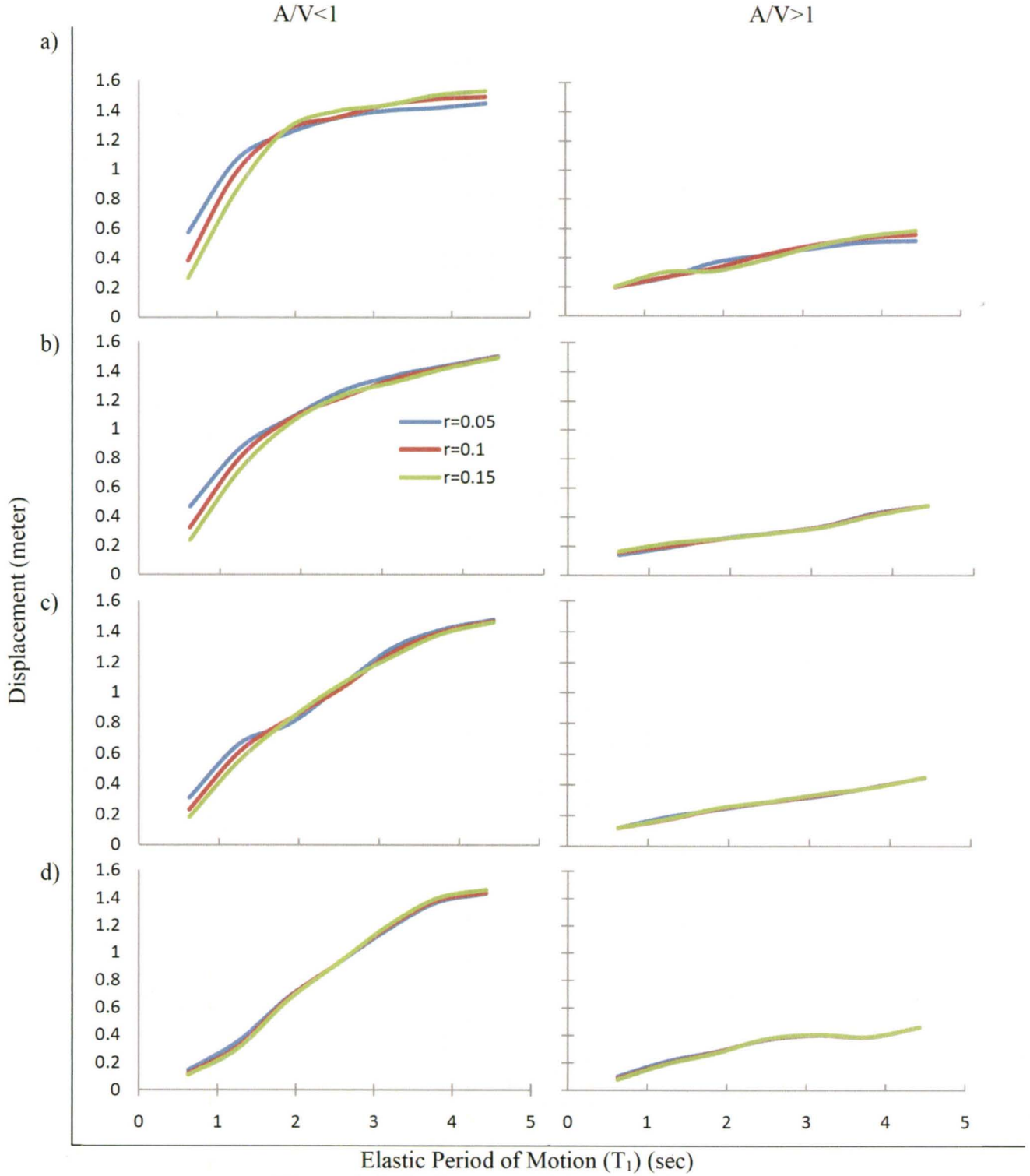

Figure 4. 8 Displacement r-chart at PGA of 0.5 *g*; produced using Group A: a) n=2%; b) n=5%; c) n=10%;d) n=20%

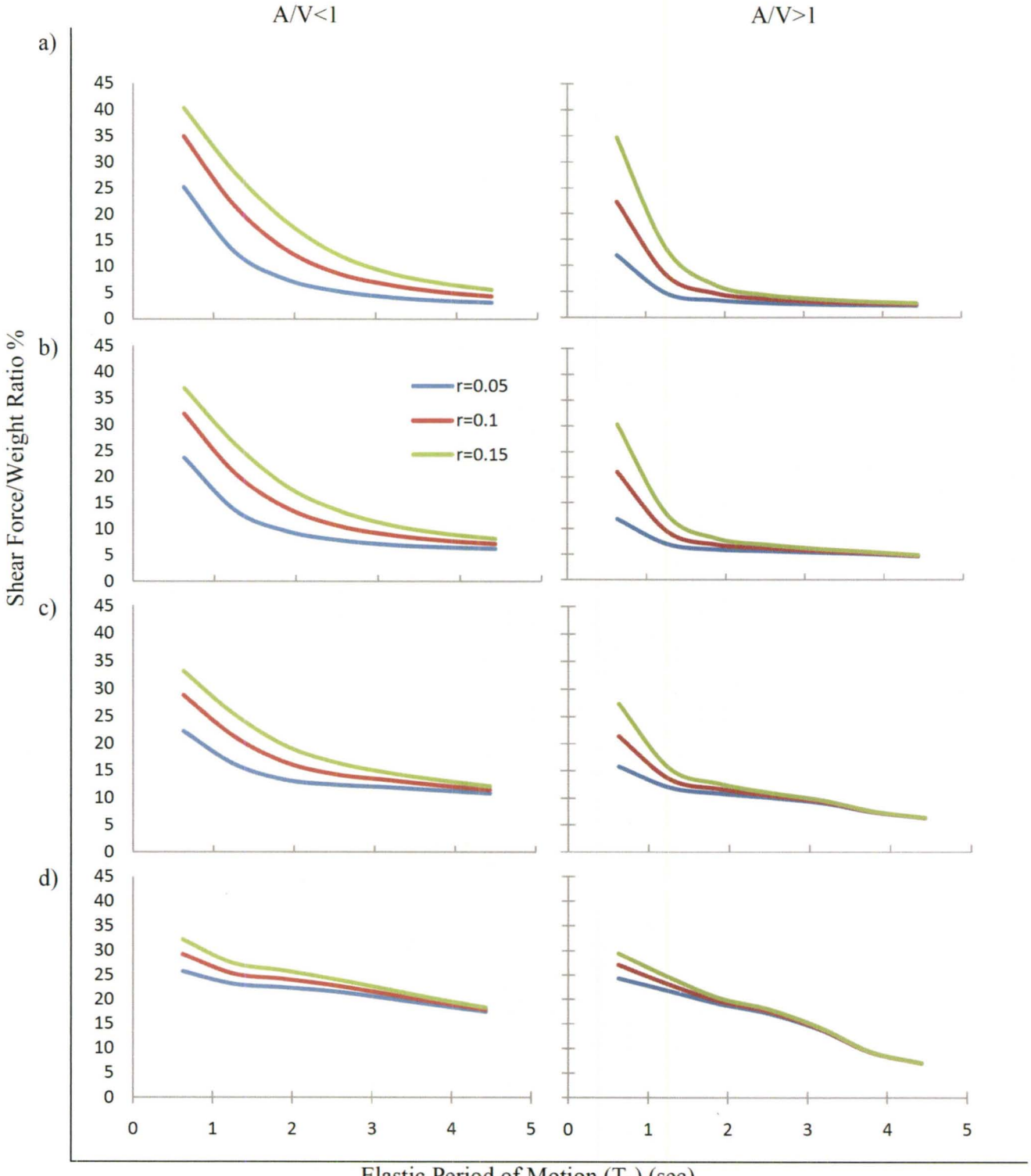

Figure 4. 9 Shear force r-chart at PGA of 0.5 *g*; produced using Group A: a) n=2%; b) n=5%; c) n=10%; d) n=20%

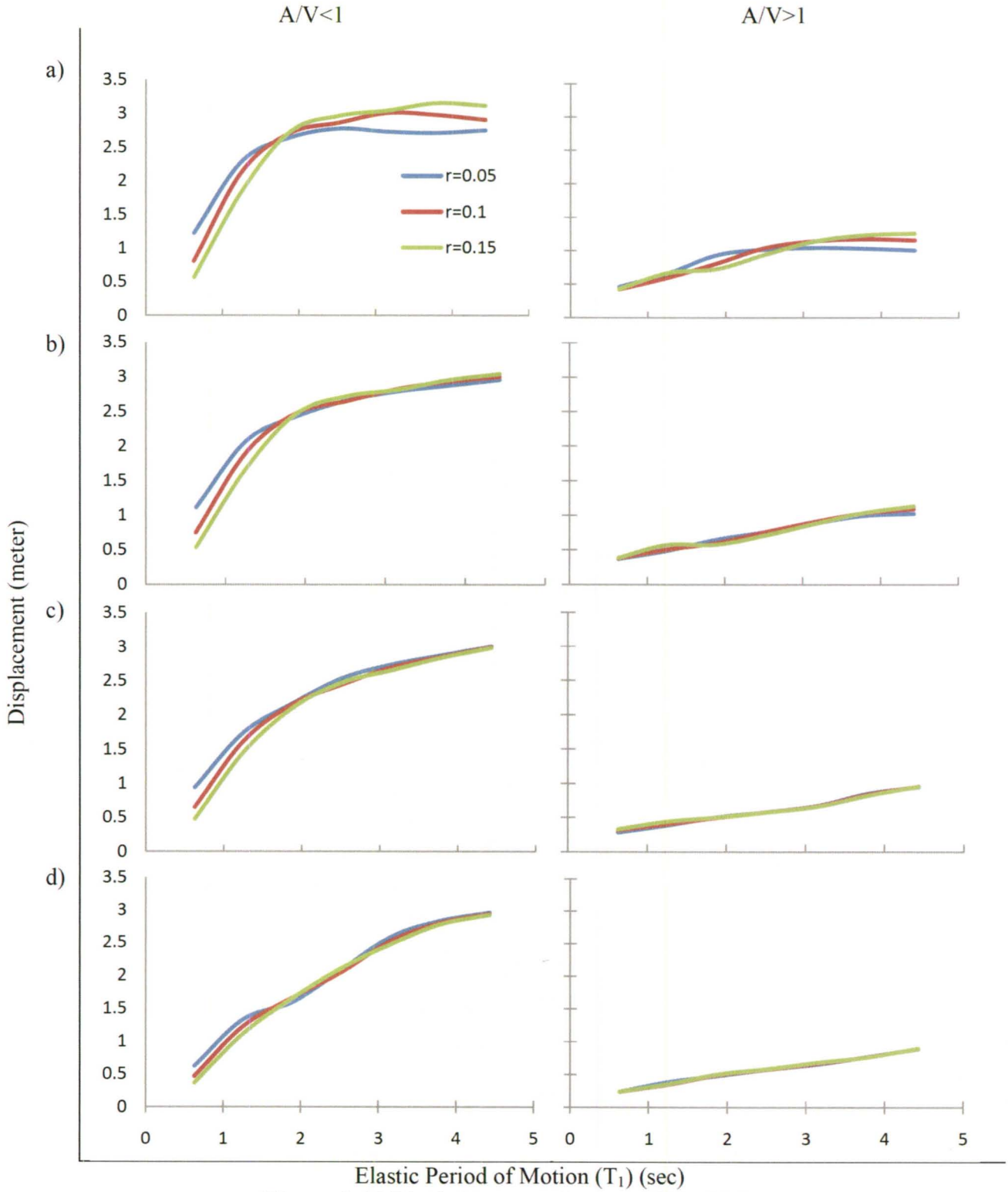

Figure 4. 10 Displacement r-chart at PGA of 1.0 *g*; produced using Group B: a) n=2%; b) n=5%; c) n=10%;d) n=20%

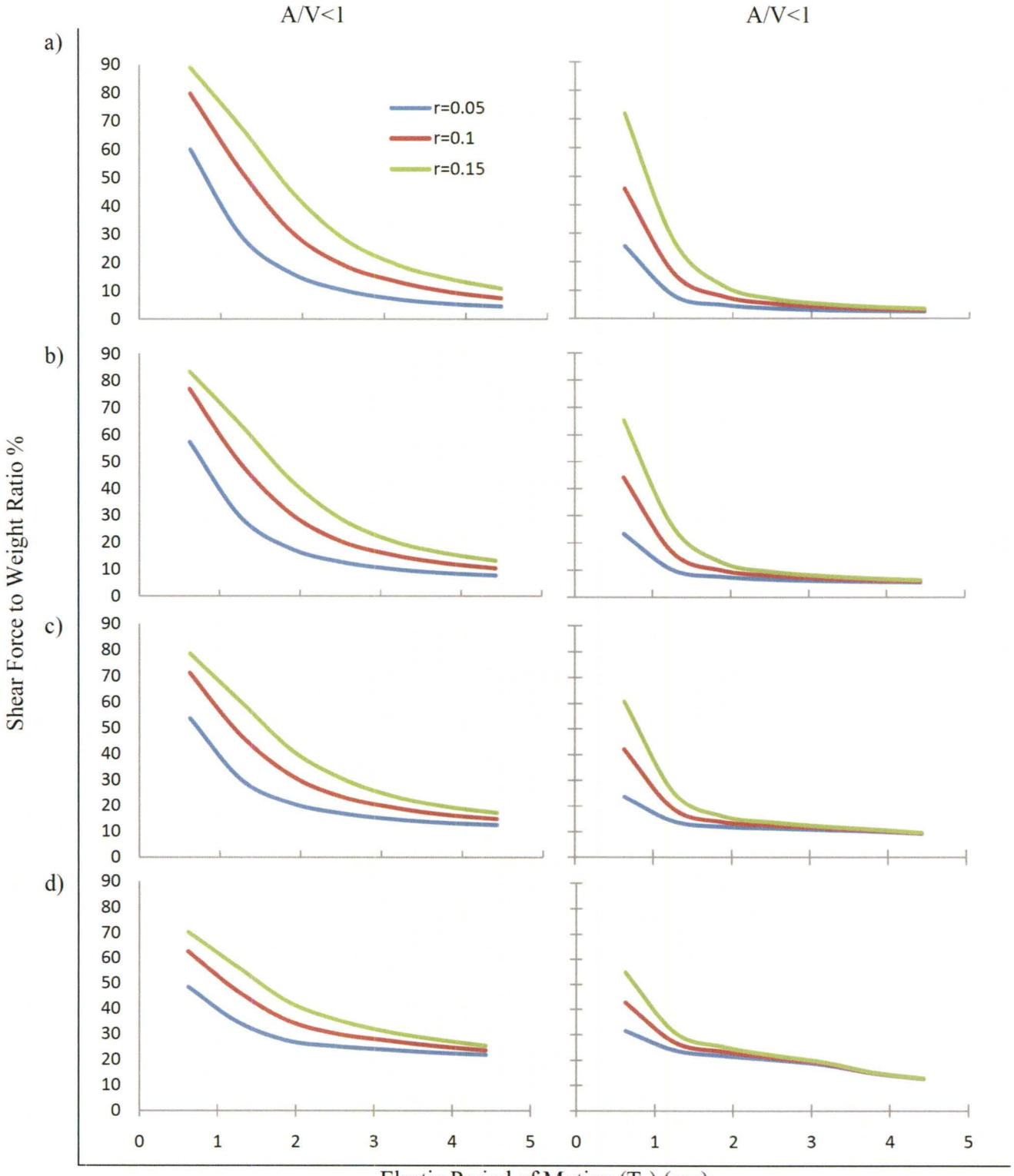

Figure 4. 11 Shear force r-chart at PGA of 1.0 *g*; produced using Group B: a) n=2%; b) n=5%; c) n=10%;d) n=20%

a)

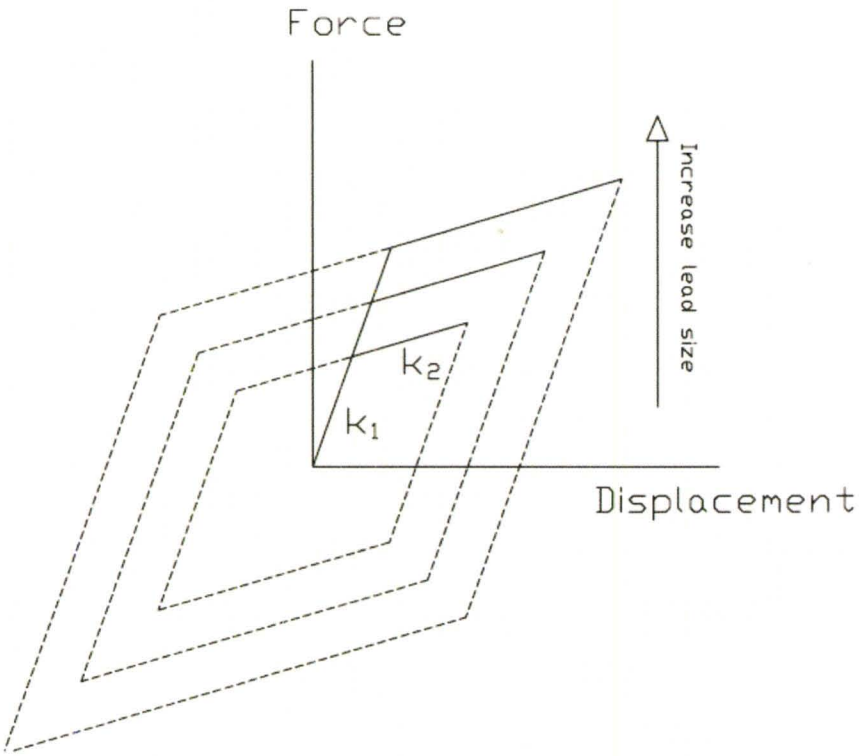

b)

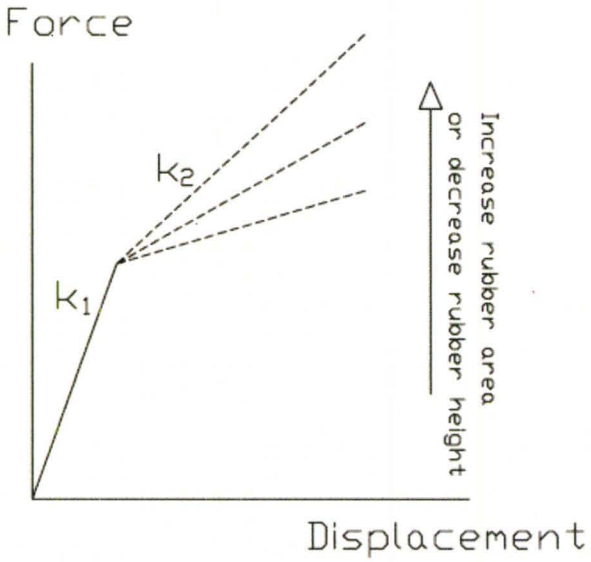

Figure 4. 12 Influence of LRB dimension on the hysteretic behaviour
a) Influence of lead size b) influence of rubber size

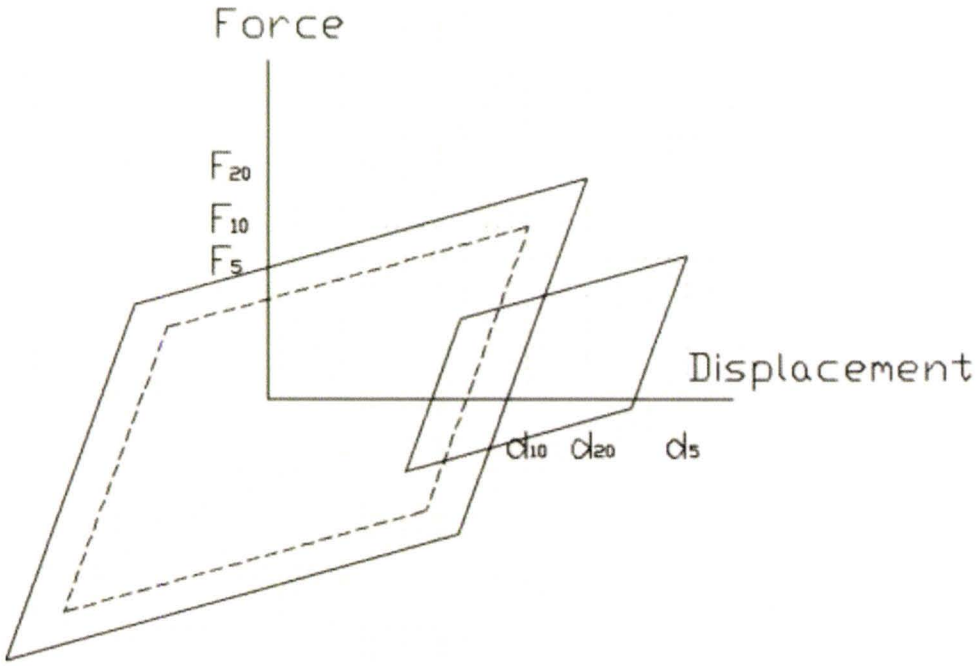

Figure 4. 13 Simplified explanation of nonlinear time-history analysis

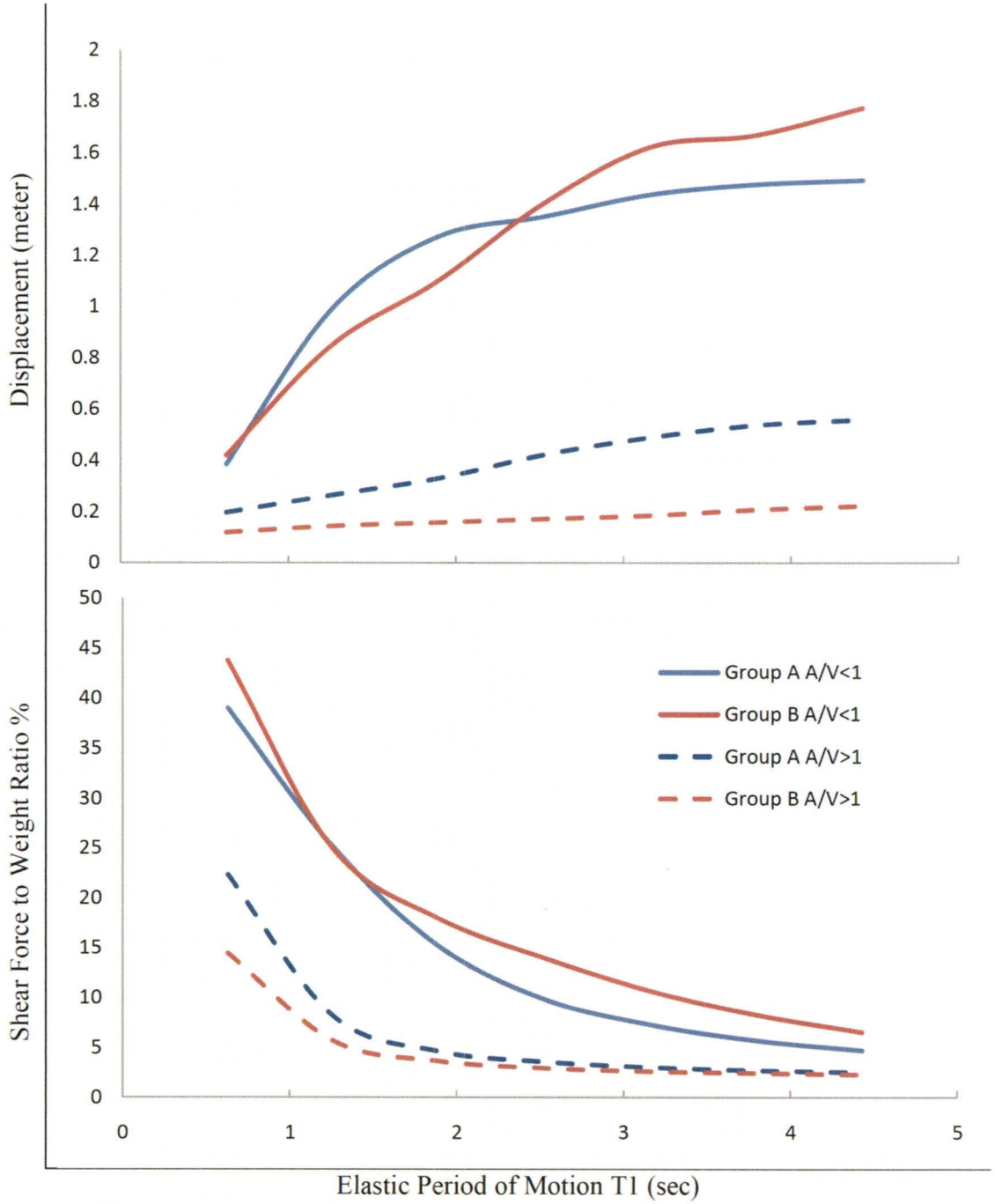

Figure 4. 14 Response comparison on exchanged groups at PGA of 0.5 *g*

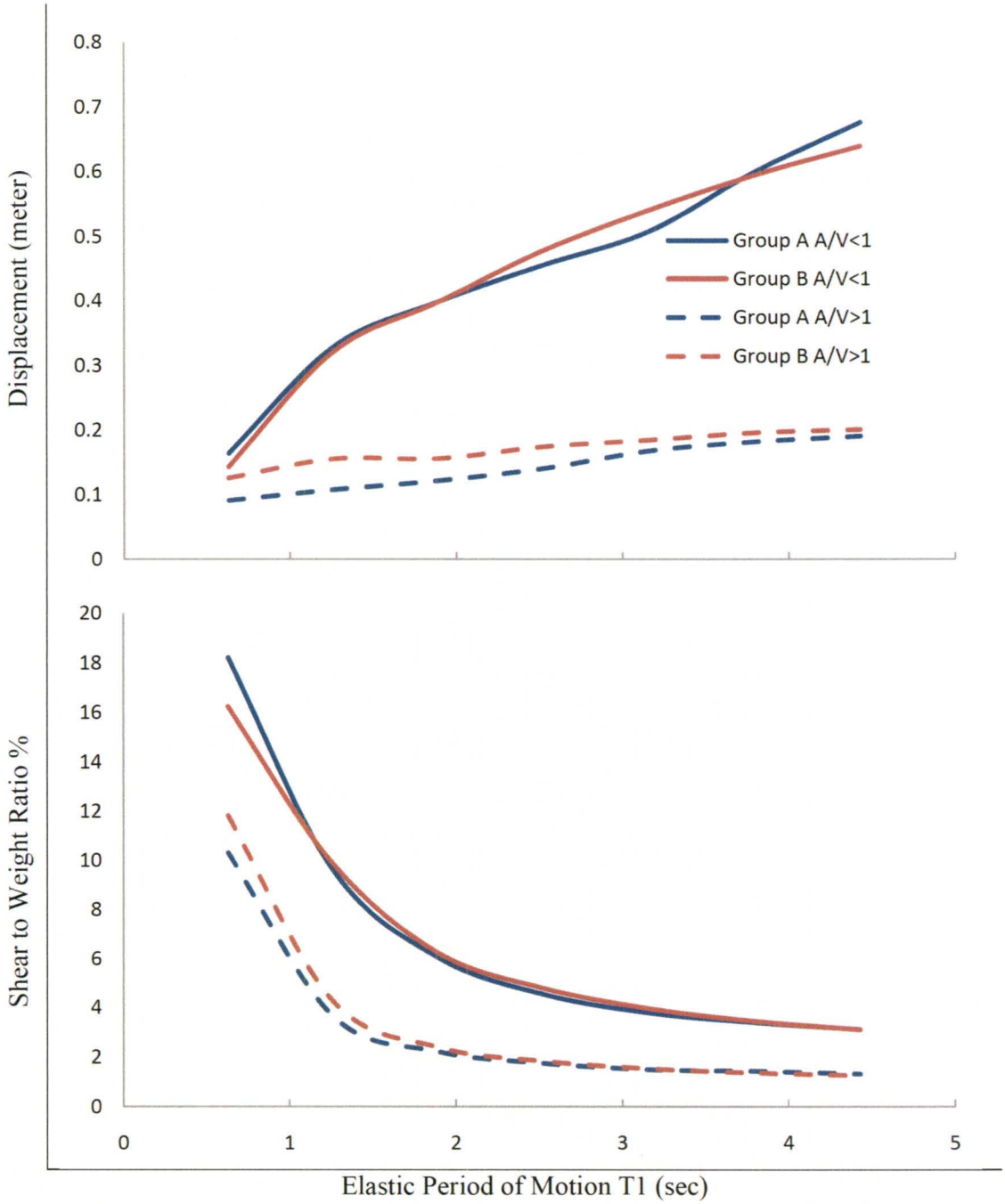

Figure 4. 15 Response comparison on exchanged groups at PGV of 30 cm/s

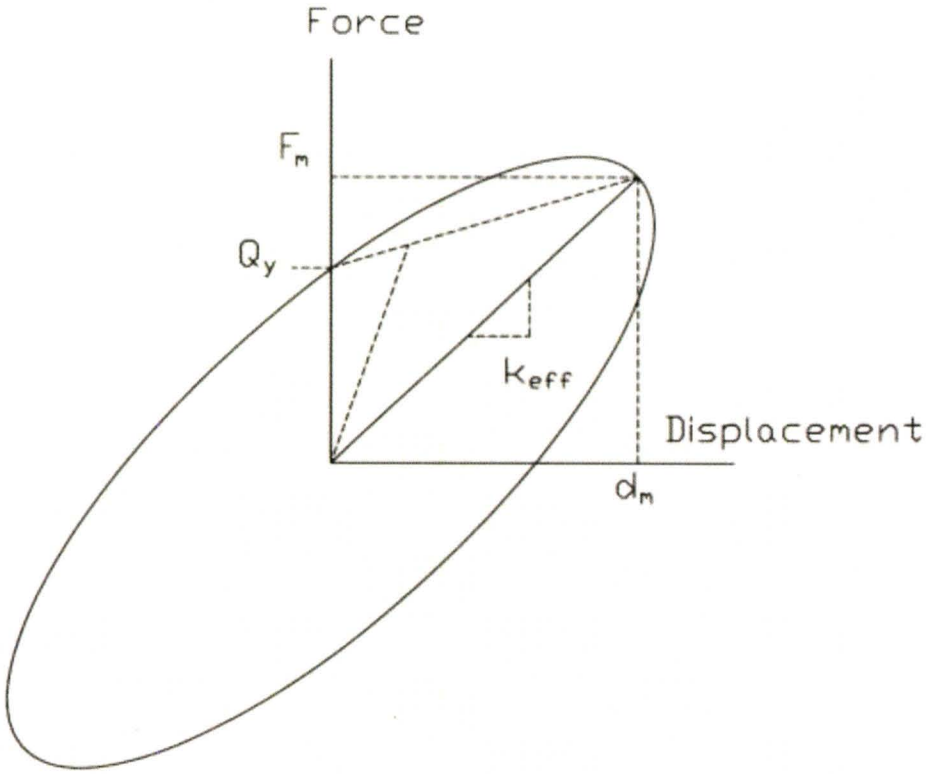

Figure 4. 16 Equivalent visco-elastic relation

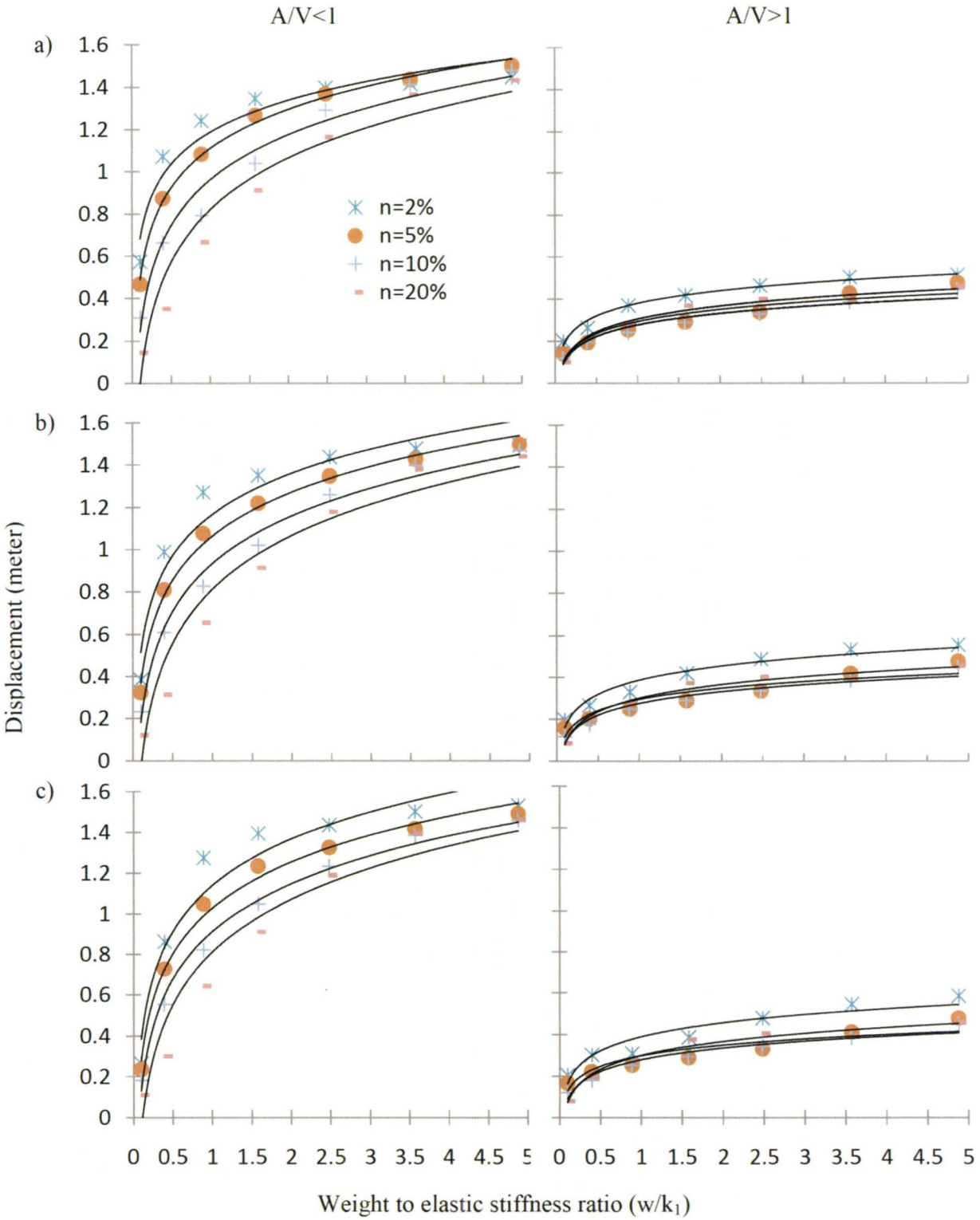

Figure 4. 17 Regressed displacement response at PGA of 0.5 *g*; produced using Group A: a) r=0.05; b) r=0.10; c) r=0.15

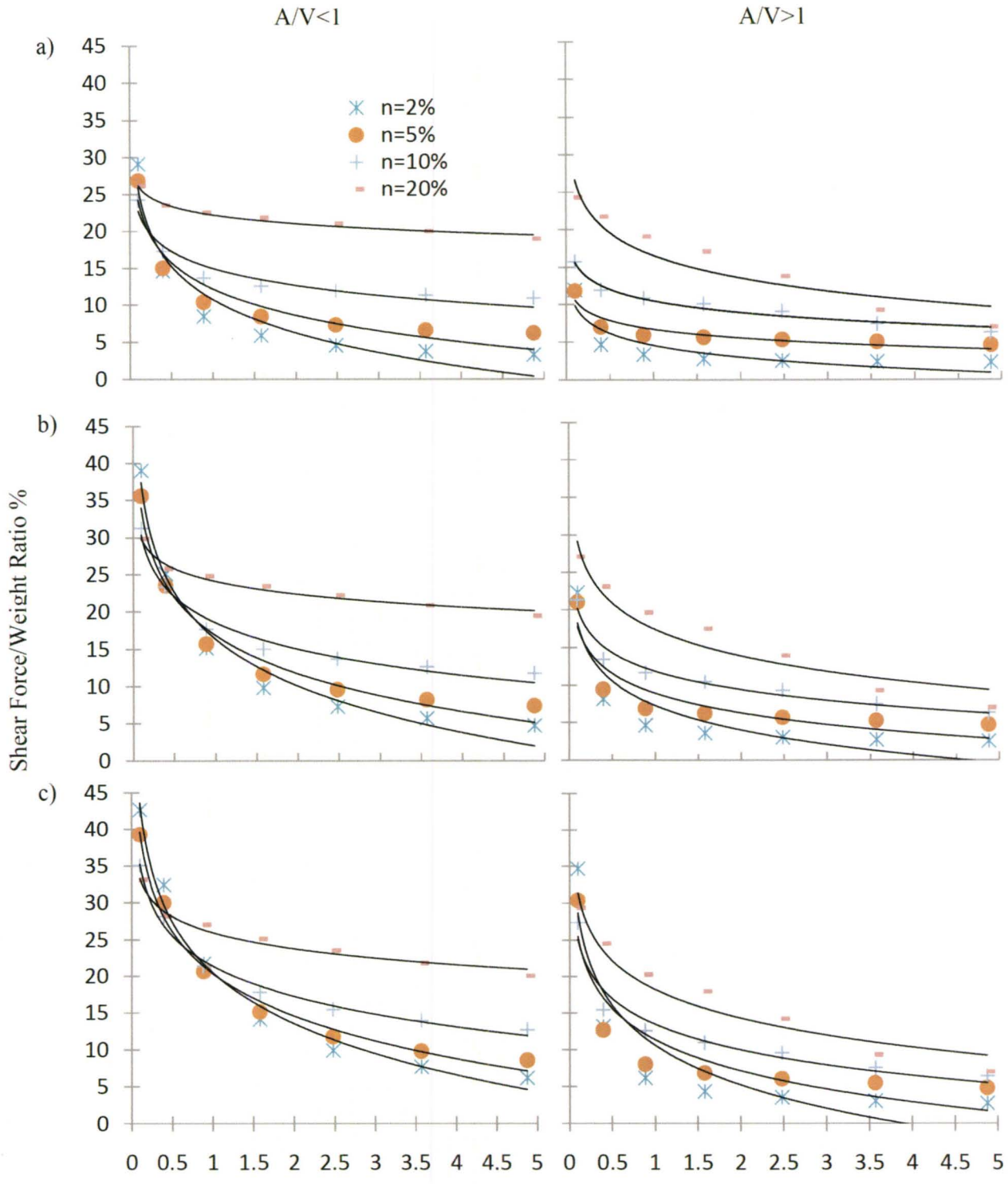

Figure 4. 18 Regressed shear response at PGA of 0.5 *g*; produced using Group A: a) r=0.05; b) r=0.10; c) r=0.15

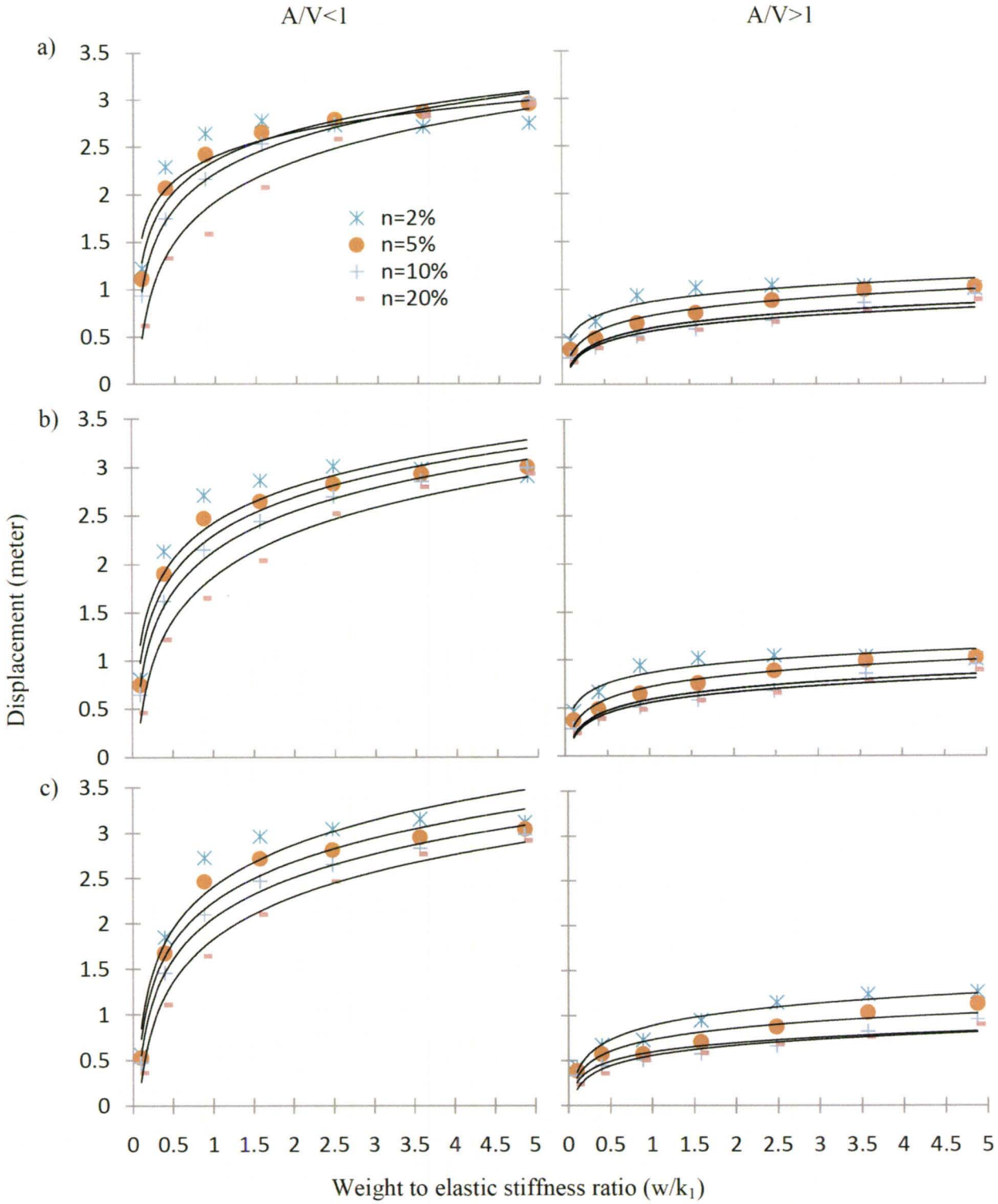

Figure 4. 19 Regressed displacement response at PGA of 1.0 *g*; produced using Group B: a) r=0.05; b) r=0.10; c) r=0.15

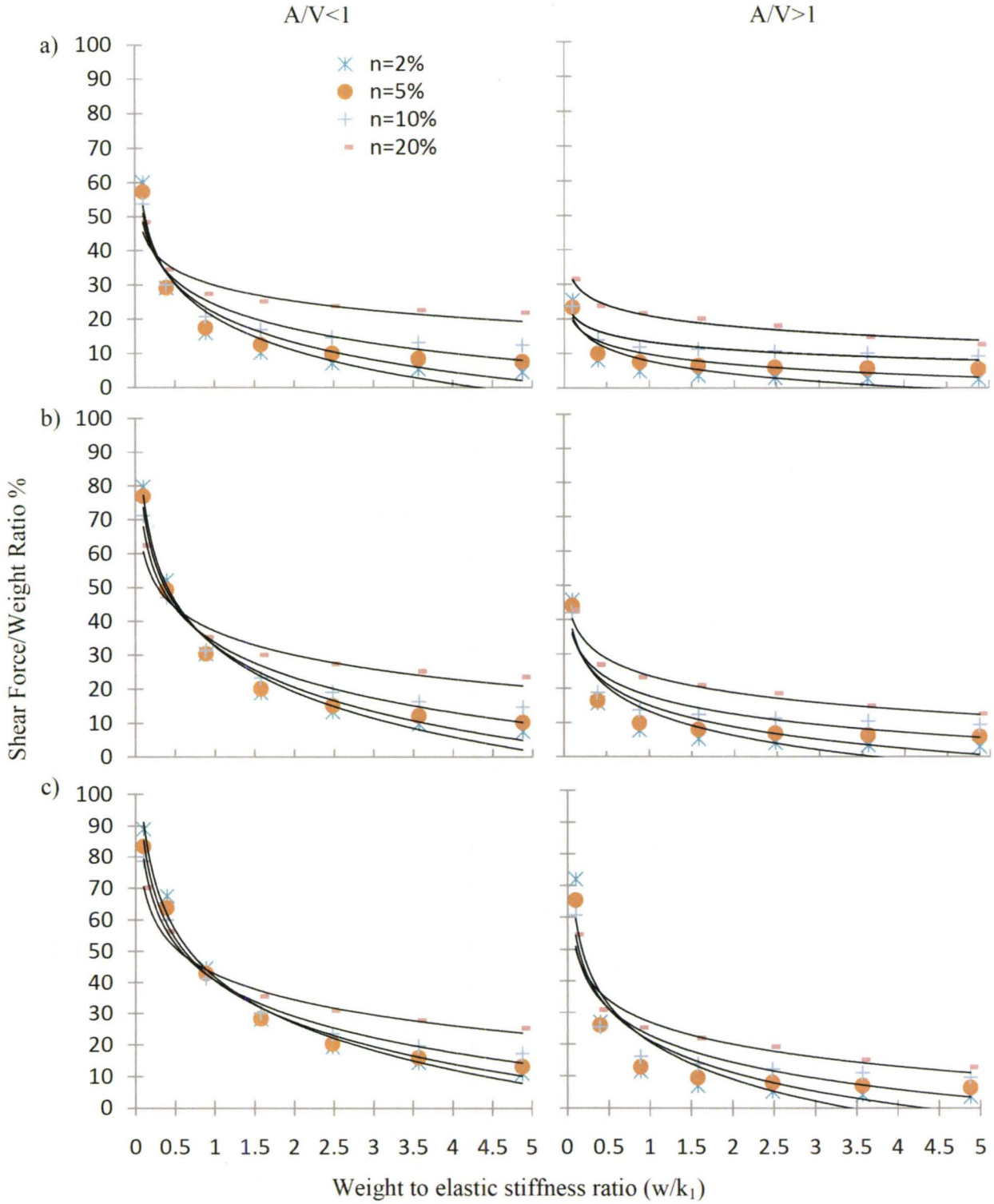

Figure 4. 20 Regressed shear response at PGA of 1.0 *g*; produced using Group B: a) r=0.05; b) r=0.10; c) r=0.15

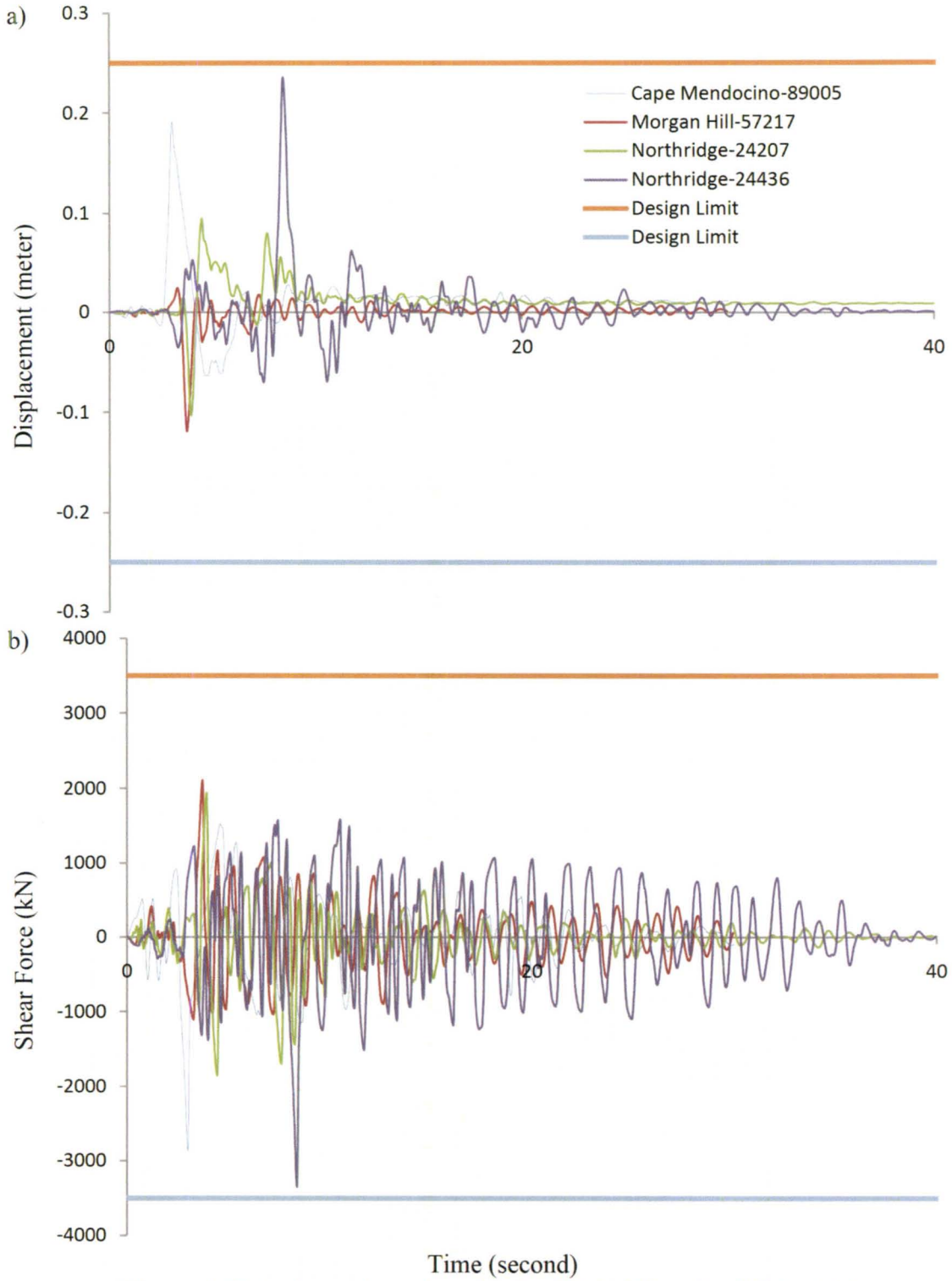

Figure 4. 21 Isolator time-histories for 25000 kN under PGA of 0.5 g, NK method: a) displacement b) shear force

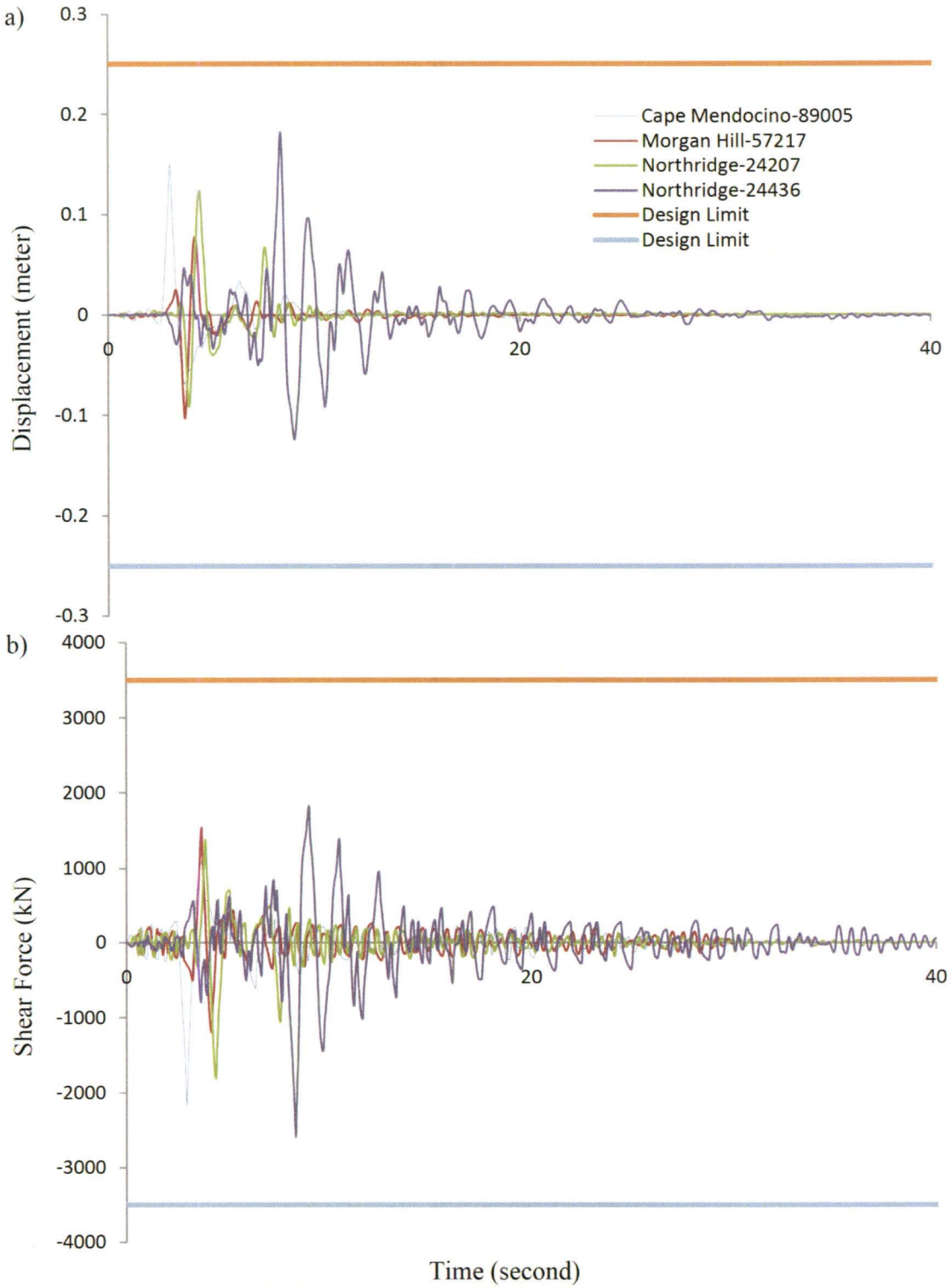

Figure 4. 22 Isolator time-histories for 10000 kN under PGA of 1.0g, NK method: a) displacement b) shear force

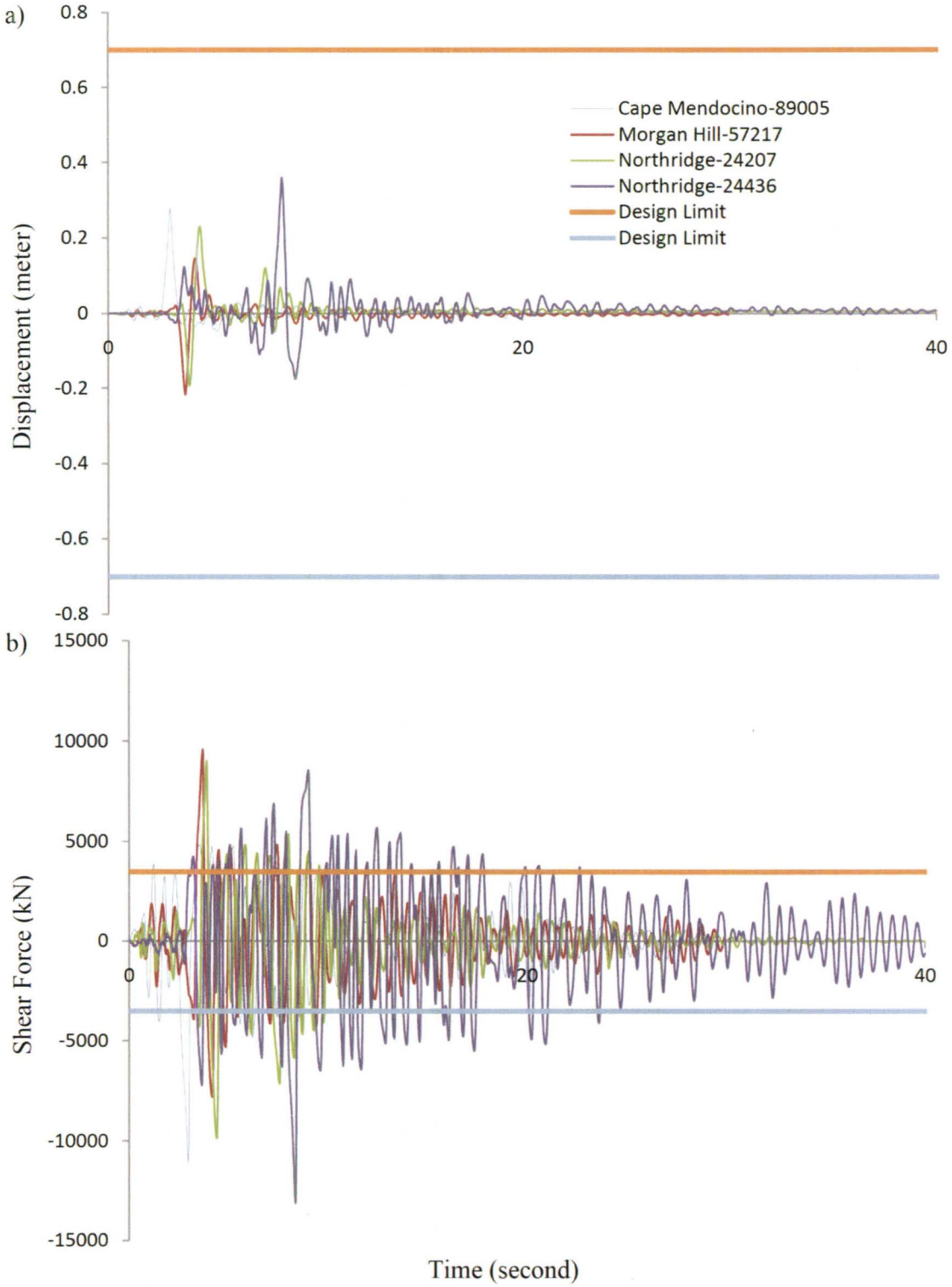

Figure 4. 23 Isolator time-histories for 25000 kN for PGA of 1.0g NK method: a) displacement b) shear force

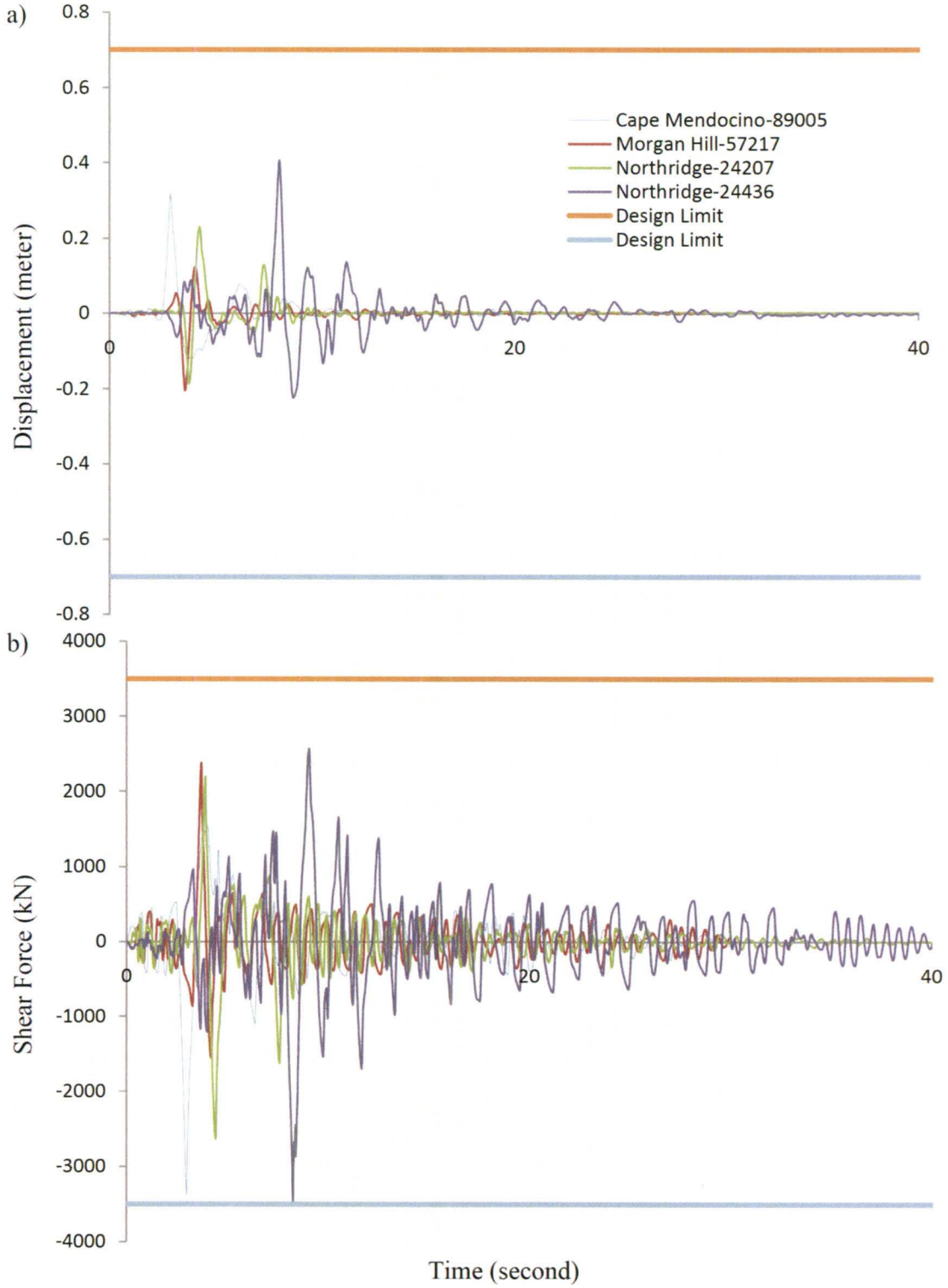

Figure 4. 24 Isolator time-histories for 10000 kN under PGA of 1.0g, NK method: a) displacement b) shear force

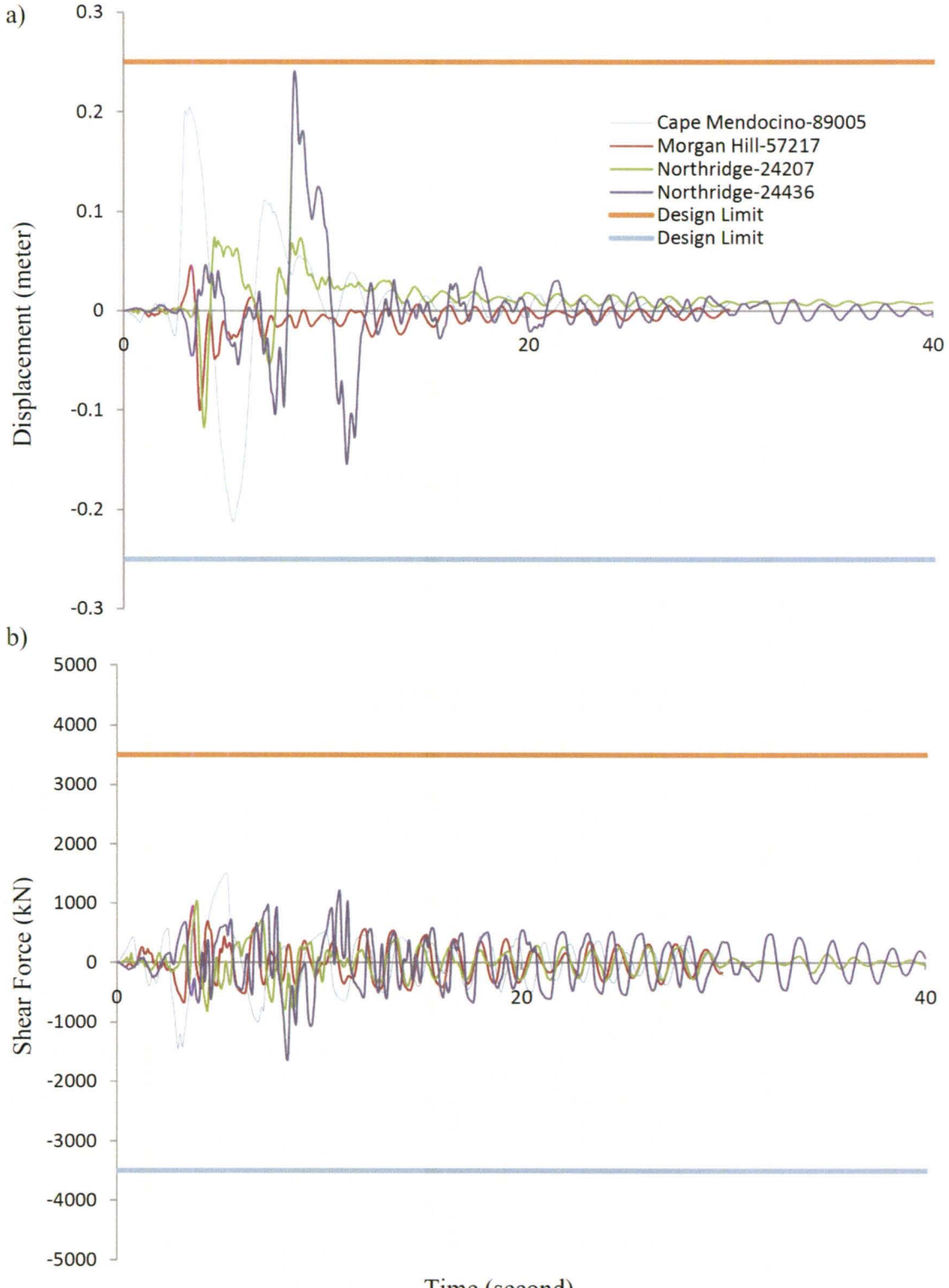

Figure 4. 25 Isolator time-histories for 25000 kN under PGA of 0.5g, Chart method: a) displacement b) shear force

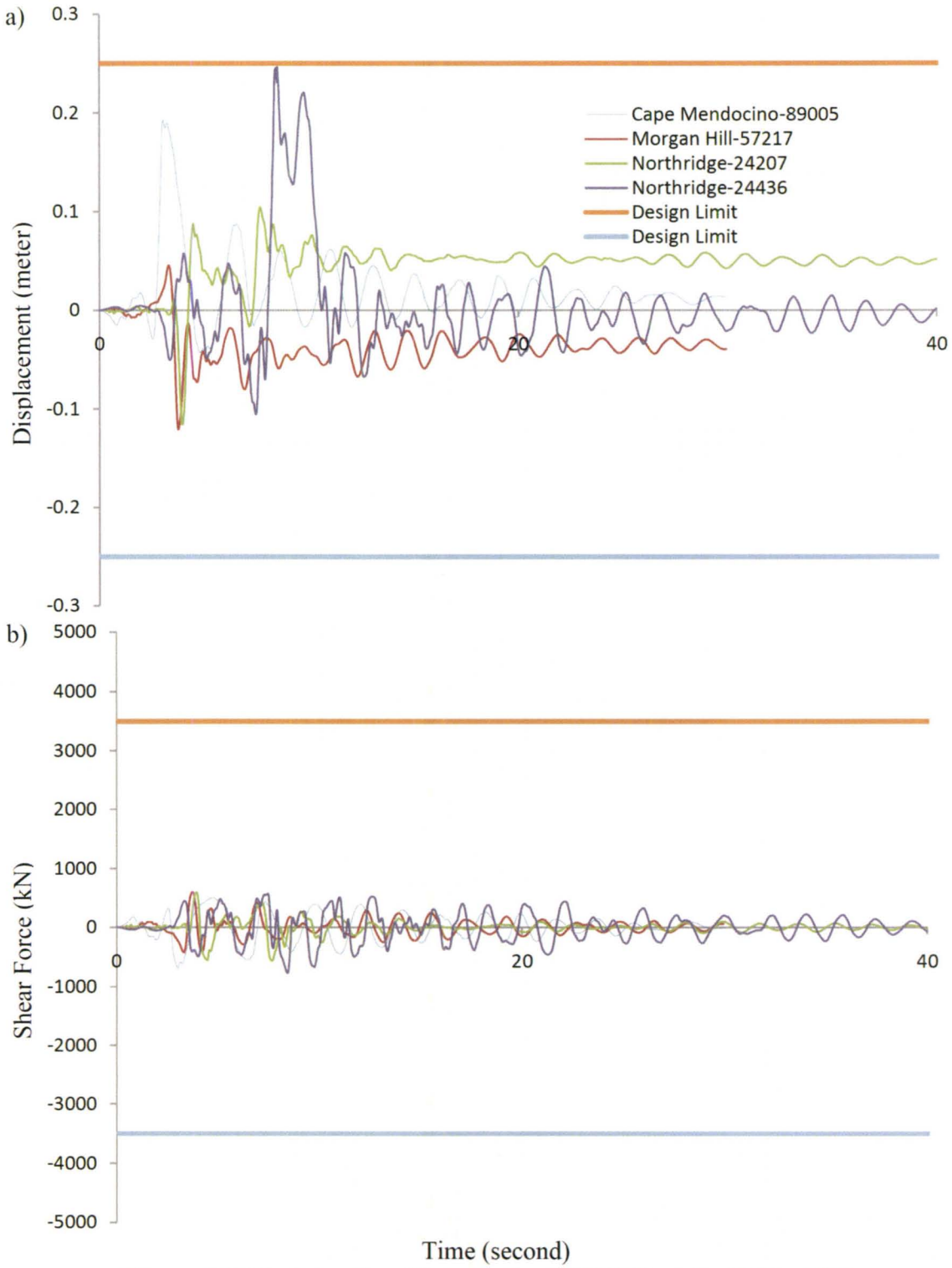

Figure 4. 26 Isolator time-histories for 10000 kN under PGA of 0.5g, Chart method: a) displacement b) shear force

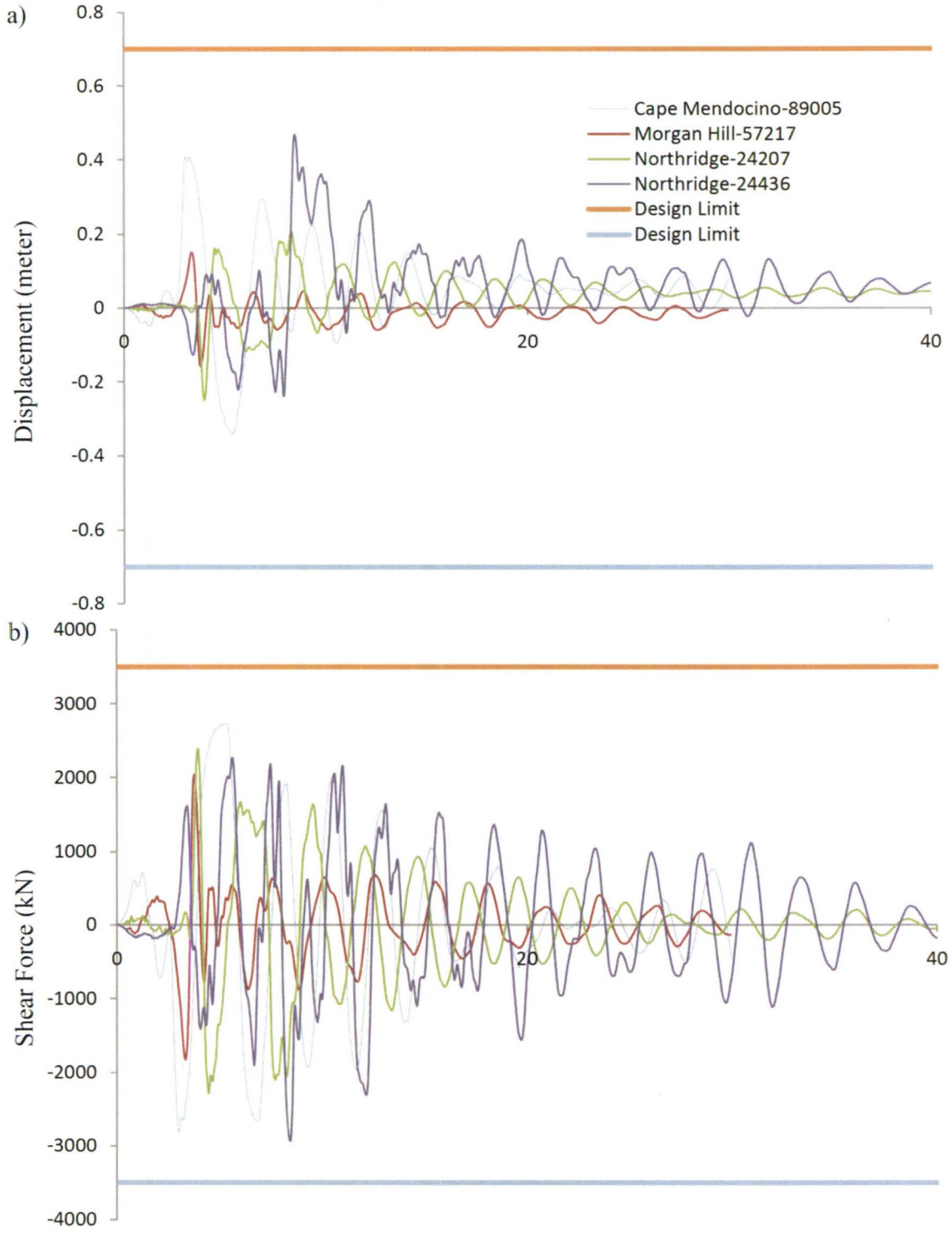

Figure 4. 27 Isolator time-histories for 25000 kN under PGA of 1.0g, Chart method: a) displacement b) shear force

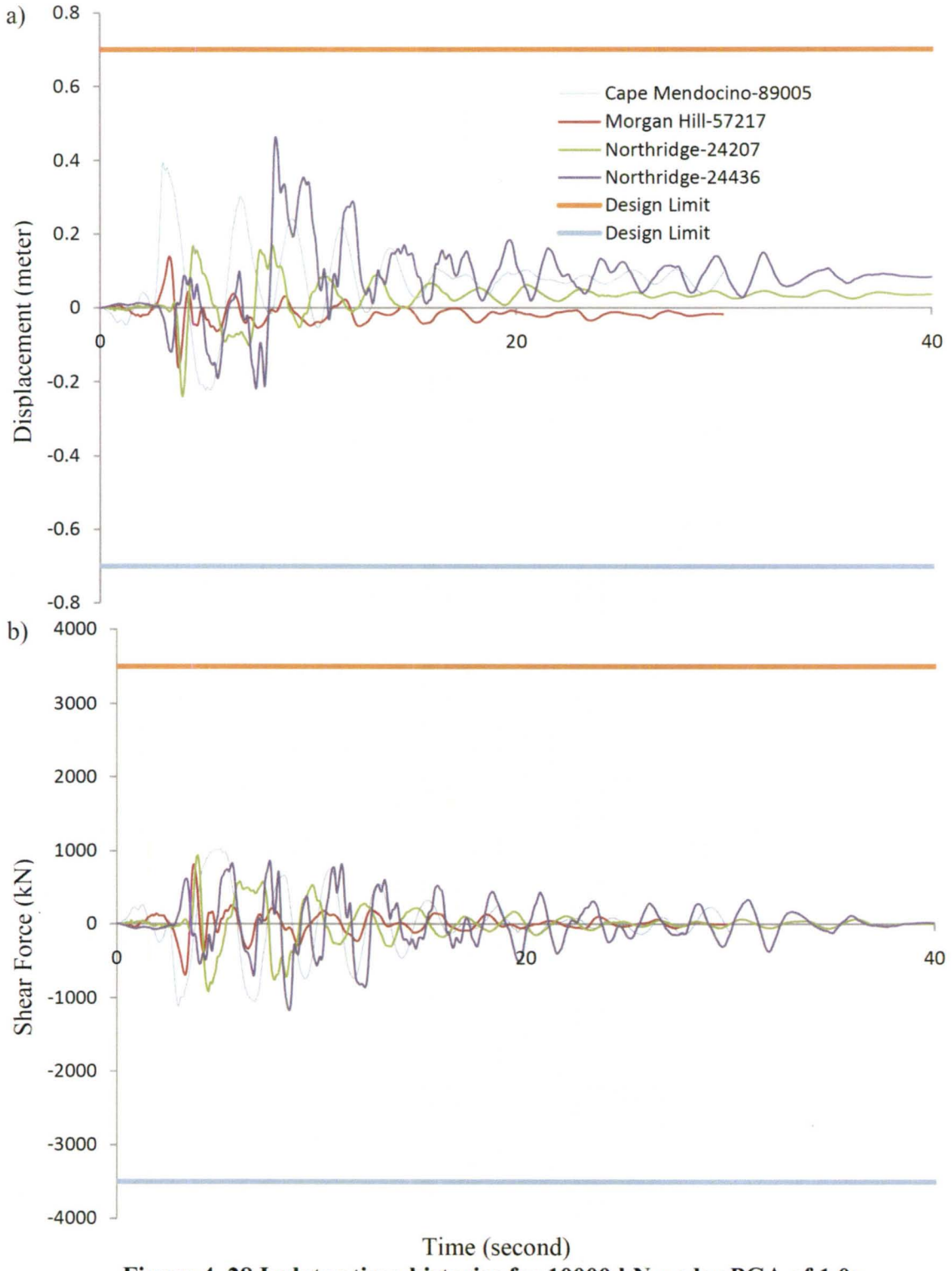

Figure 4. 28 Isolator time-histories for 10000 kN under PGA of 1.0g, Chart method: a) displacement b) shear force

5. CONCLUSION

5.1. SUMMARY

This study had two objectives: 1) to investigate the influence of LRB design parameters using nonlinear time-history analysis, and 2) to propose a simple LRB design method.

In the first part, basic concepts in earthquake time-history analysis were reviewed, including earthquake time-history characteristics, time-history selection and scaling. Two assumptions were made: 1) A/V<1 is used to indentify ground motions affected by earthquake forward directivity. 2) the 84.1 percentile responses of different groups of scaled-input nonlinear time-history analyses are similar, when the records fall into the same A/V category. Two groups of earthquakes totalling 37 records were selected considering PGA and PGV. Records in each group were separated into categories of A/V<1 and A/V>1. Both PGA and PGV were considered for earthquake scaling.

The second part carried out a nonlinear performance assessment of LRB. Over ten thousand nonlinear time-history analyses were performed. The performance of LRBs with multiple combinations of yield strength, elastic and post-elastic stiffness were tested. The response influence of each parameter was tested using bilinear spectra. The results verified the two assumptions made in the first part. A regression-based-chart was used to develop a new LRB design method. The design procedure and design accuracy were compared with the NK method.

5.2. CONCLUSIONS

Earthquake Selection and Scaling

- The results from Chapter 4 indicate that PGV is a better parameter for earthquake damage potential measurement, which supports what others have observed.
- A low A/V indicates that an earthquake time-history may be affected by forward directivity. Records with A/V<1 have long duration pulse-like waves and the spectrum velocity concentrates at 2-3 seconds. LRB responses with A/V<1 earthquakes are substantially higher than those subjected A/V>1 earthquakes.
- The similar response trend shown in Fig. 4.14 and in Fig. 4.15 verifies that when the probabilistic approach is used, earthquake time-history selection does not play an important role.

Design Parameter Influence and Implementation

- The LRB displacement decreases as the lead size increase. However, the corresponding shear force response does not have a general trend. Thus one solution to control the displacement is to increase the lead content ratio.
- An increase in rubber size causes an increase in the shear force response. The corresponding change in the displacement response is negligible. To control the shear force, one solution is to reduce the rubber size and the corresponding displacement will have negligible change.
- For nonlinear seismic response, a higher lead content does not necessarily provide equivalent damping effect on displacement and shear force responses. A higher

displacement does not necessarily correspond to a lower shear force. A lot of care needs to be used when a linearization approach is applied to seismic analysis.

Application of Chart Method

- Compared with the conventional methods, the Chart Method has improved accuracy. Unlike the more conventional method, the design accuracy does not depend directly on the design experience and the procedure is simpler.
- The Chart Method can be also applied in evaluating the suitability of commercially available LRB sizes. Using an available size can significantly reduce the costs of LRB mould construction.

5.3. RECOMMENDATIONS FOR FUTURE RESEARCH

This study only considered the behaviour of the isolator unit. It is based on the assumption that the isolator is placed on stiff supports and the supported mass is rigid. In reality, the situation can be more complex. Thus for future research, the following directions are suggested:

- Substructure or superstructure stiffness interaction can be integrated to the bilinear spectrum by incorporating an additional axis considering the stiffness.
- The concept of using a bilinear spectrum in design can be carried into other bilinear modeled systems.
- Mathematical interaction equations between responses and design parameters are worthwhile to be determined quantitatively.

- From the observation found in this study, the design accuracy might be different at different nonlinearity levels. Due to time constraints and scope of study, this was not considered herein. A study can be taken towards the design accuracy at different effective damping levels.

REFERENCES

AASHTO. (1999). *Guide Specifications for Seismic Isolation Design*. American Association of State Highway and Transportation Officials. Washington, D.C

Amiri, GG, and Dana, FM. (2005). Introduction of the Most Suitable Parameter for Selection of Critical Earthquake. *Computers & Structures, 83*(8-9), 613-626.

ASCE-7. (2002). *Minimum Design Loads for Buildings and Other Structures*. American Society of Civil Engineers. New York, NY

Bailey, James S., and Allen, Edmund W. (1988). Seismic Isolation Retrofitting: Salt Lake City and County Building. *APT Bulletin, 20*(2), 33-44.

Beskos, DE, and Anagnostopoulos, SA. (1997). *Computer Analysis and Design of Earthquake Resistant Structures: a Handbook*. Computational Mechanics Publications. Southampton, UK

Bleiman, D. , Kim, S. (1993). Base Isolation of High Volume Elevated Water Tanks. *Proceedings of a Seminar on Seismic Isolation, Passive Energy Dissipation and Active Control, ATC-17-1*.

Boatwright, J, Thywissen, K, and Seekins, LC. (2001). Correlation of Ground Motion and Intensity for the 17 January 1994 Northridge, California, Earthquake. *Bulletin of the Seismological Society of America, 91*(4), 739.

Bommer, Julian J., and Acevedo, Ana Beatriz. (2004). The Use of Real Earthquake Accelerograms as Input to Dynamic Analysis. *Journal of Earthquake Engineering, 8*, 43 - 91.

Bray, Jonathan D., and Rodriguez-Marek, Adrian. (2004). Characterization of Forward-Directivity Ground Motions in the Near-Fault Region. *Soil Dynamics and Earthquake Engineering, 24*(11), 815-828.

Buckle, I.G. , and Mayes, RL. (1990). Seismic Isolation: History, Application, And Performance-A World View. *Earthquake Spectra, 6*(2), 161-201.

Buckle, I.G., Constantinou, Michael C, Dicleli, Mirat, and Ghasemi, Hamid. (2006). *Seismic Isolation of Highway Bridges*. University at Buffalo. NY

Buckle, I.G., Lee, G. , and Liang, Z. (2003). Toward the Next Generation of Response Modification Technologies for Highway Bridges. *Proceedings of the ACI International Conference- Seismic Bridge Design and Retrofit for Earthquake Resistance*.

Carballo, Jorge Eduardo, and Cornell, C. Allin. (2000). Probabilistic Seismic Demand Analysis: Spectrum Matching And Design. *Department of Civil and Environmental Engineering, Stanford University, Report No. RMS-41*.

Chapman, MC. (1995). A Probabilistic Approach to Ground-Motion Selection for Engineering Design. *Bulletin of the Seismological Society of America, 85*(3), 937.

Chopra, Anil K., and Chintanapakdee, Chatpan. (2001). Comparing Response of SDF Systems to Near-Fault and Far-Fault Earthquake Motions in the Context of Spectral Regions. *Earthquake Engineering & Structural Dynamics, 30*(12), 1769-1789.

Computers and Structures, Inc. (2010). *SAP2000 v.14 Analysis Reference Manual*. Computers and Structures, Inc. Berkeley, CA

Dicleli, Murat, and Buddaram, Srikanth. (2006). Improved Effective Damping Equation for Equivalent Linear Analysis of Seismic-Isolated Bridges. *Earthquake Spectra, 22*(1), 29-46.

Dicleli, Murat, and Buddaram, Srikanth. (2007). Comprehensive Evaluation of Equivalent Linear Analysis Method For Seismic-Isolated Structures Represented by SDOF Systems. *Engineering Structures, 29*(8), 1653-1663.

Excel, MS. (2007). *User's Manual for Excel Macro*. Microsoft Cooperation. Redmond, Washington

FEMA-356. (2000). *Prestandard and Commentary for the Seismic Rehabilitation of Buildings*. Federal Emergency Management Agency. Washington,D.C

Higashino, M, and Okamoto, S. (2006). *Response Control and Seismic Isolation of Buildings*. Taylor and Francis, London, NY

Hwang, J. S. (1996). Evaluation of Equivalent Linear Analysis Methods of Bridge Isolation. *ASCE Journal of Structural Engineering, 122*(8), 972-976.

Hwang, J. S., and Chiou, J. M. (1996). An Equivalent Linear Model of Lead-Rubber Seismic Isolation Bearings. *Engineering Structures, 18*(7), 528-536.

Hwang, J. S., and Sheng, L. H. (1993). Effective Stiffness and Equivalent Damping of Base-Isolated Bridges. *ASCE Journal of Structural Engineering, 119*(10), 3094-3101.

Hwang, J. S., and Sheng, L. H. (1994). Equivalent Elastic Seismic Analysis of Base-Isolated Bridges with Lead-Rubber Bearings. *Engineering Structures, 16*(3), 201-209.

Hwang, J. S., Sheng, L. H., and Gates, J. H. (1994). Practical Analysis of Bridges on Isolation Bearings with Bi-Linear Hysteresis Characteristics. *Earthquake Spectra, 10*(4), 705-727.

IBC. (2006). *International Building Code*. International Code Council, Inc. Country Club Hills, IL

Iervolino, Iunio, and Cornell, C. Allin. (2005). Record Selection for Nonlinear Seismic Analysis of Structures. *Earthquake Spectra, 21*(3), 685-713.

Iwan, WD. (1997). Drift Spectrum: Measure of Demand for Earthquake Ground Motions. *ASCE Journal of Structural Engineering, 123*(4), 397-404.

Jangid, R. S., and Kelly, J. M. (2001). Base Isolation for Near-Fault Motions. *Earthquake Engineering & Structural Dynamics, 30*(5), 691-707.

Jangid, RS, and Datta, TK. (1995). Performance of Base Isolation Systems for Asymmetric Building Subject to Random Excitation. *Engineering Structures, 17*(6), 443-454.

Kaka, SLI, and Atkinson, GM. (2004). Relationships between Instrumental Ground-Motion Parameters and Modified Mercalli Intensity in Eastern North America. *Bulletin of the Seismological Society of America, 94*(5), 1728.

Kalkan, E, and Chopra, AK. (2010). Practical Guidelines to Select and Scale Earthquake Records for Nonlinear Response History Analysis of Structures. *US Geological Survey Open-File Report*, 1068.

Kelly, JM. (1986). Aseismic Base Isolation: Review and Bibliography. *Soil Dynamics and Earthquake Engineering, 5*(4), 202-216.

Malhotra, P. K. (1999). Response of Buildings to Near-Field Pulse-Like Ground Motions. *Earthquake Engineering & Structural Dynamics, 28*(11), 1309-1326.

Naeim, F, and Kelly, J (1999). *Design of Seismic Isolated Structures: from Theory to Practice*. Wiley. New York, NY

Naeim, Farzad, Alimoradi, Arzhang, and Pezeshk, Shahram. (2004). Selection and Scaling of Ground Motion Time Histories for Structural Design Using Genetic Algorithms. *Earthquake Spectra, 20*(2), 413-426.

Park, KS, Jung, HJ, and Lee, IW. (2002). A Comparative Study on Aseismic Performances of Base Isolation Systems for Multi-Span Continuous Bridge. *Engineering Structures, 24*(8), 1001-1013.

Robinson, WH, and Greenbank, LR. (1976). An Extrusion Energy Absorber Suitable for the Protection of Structures During an Earthquake. *Earthquake Engineering & Structural Dynamics, 4*(3), 251-259.

Skinner, RI, Robinson, WH, and McVerry, GH. (1993). *An Introduction to Seismic Isolation*. John Wiley and Sons. New York

The University of Waikato. (2007). William Clayton Building. Retrieved from http://www.sciencelearn.org.nz/Contexts/Earthquakes/Sci-Media/Images/

Vlack, LHV. (1989). *Elements of Materials Science and Engineering*. Addison-Wesley. New York

Wald, DJ, Quitoriano, V, Heaton, TH, and Kanamori, H. (1999). Relationships between Peak Ground Acceleration, Peak Ground Velocity, and Modified Mercalli Intensity in California. *Earthquake Spectra, 15*, 557.

Walters, M., Elsesser,E.,Allen,E.W. (1986). Base Isolation of the Existing City and County Building in Salt Lake City. *Proceedings of a Seminar and Workshop on Base Isolation and Energy Dissipation, ATC-17*.

Wesolowsky, Michael J. (2001). *Design and Application of Seismic Isolators and Supplemental Dampers for Cable-Stayed Bridges.* M.A.Sc Thesis, McMaster University, Hamilton, Ontario.

APPENDIX A: SAP2000 INPUT FOR ISOLATORS FOR POST-TO-PRE STIFFNESS RATIO OF 0.1

Isolators

```
Link=Rubber    LinkType="Rubber Isolator"
  Mass1=300,000 kg
  Link=Rubber    DOF=R1    Fixed=Yes
  Link=Rubber    DOF=R2    Fixed=Yes
  Link=Rubber    DOF=R3    Fixed=Yes
```

Table A. 1 Input for "Rubber isolator" with n=0.1, r=2%

Period(s)	Isolator Property Input								
0.63	Link=Rubber	DOF=U2	Fixed=No	NonLinear=Yes	TransKE=29608	TransCE=0	TransK=29608	TransYield=58.9	Ratio=.1
1.26	Link=Rubber	DOF=U2	Fixed=No	NonLinear=Yes	TransKE=7402	TransCE=0	TransK=7402	TransYield=58.9	Ratio=.1
1.90	Link=Rubber	DOF=U2	Fixed=No	NonLinear=Yes	TransKE=3289	TransCE=0	TransK=3289	TransYield=58.9	Ratio=.1
2.53	Link=Rubber	DOF=U2	Fixed=No	NonLinear=Yes	TransKE=1850	TransCE=0	TransK=1850	TransYield=58.9	Ratio=.1
3.16	Link=Rubber	DOF=U2	Fixed=No	NonLinear=Yes	TransKE=1185	TransCE=0	TransK=1185	TransYield=58.9	Ratio=.1
3.80	Link=Rubber	DOF=U2	Fixed=No	NonLinear=Yes	TransKE=822	TransCE=0	TransK=822	TransYield=58.9	Ratio=.1
4.43	Link=Rubber	DOF=U2	Fixed=No	NonLinear=Yes	TransKE=604	TransCE=0	TransK=604	TransYield=58.9	Ratio=.1

Table A. 2 Input for "Rubber isolator" with n=0.1, r=5%

Period(s)	Isolator Property Input								
0.63	Link=Rubber	DOF=U2	Fixed=No	NonLinear=Yes	TransKE=29608	TransCE=0	TransK=29608	TransYield=147.15	Ratio=.1
1.26	Link=Rubber	DOF=U2	Fixed=No	NonLinear=Yes	TransKE=7402	TransCE=0	TransK=7402	TransYield=147.15	Ratio=.1
1.90	Link=Rubber	DOF=U2	Fixed=No	NonLinear=Yes	TransKE=3289	TransCE=0	TransK=3289	TransYield=147.15	Ratio=.1
2.53	Link=Rubber	DOF=U2	Fixed=No	NonLinear=Yes	TransKE=1850	TransCE=0	TransK=1850	TransYield=147.15	Ratio=.1
3.16	Link=Rubber	DOF=U2	Fixed=No	NonLinear=Yes	TransKE=1185	TransCE=0	TransK=1185	TransYield=147.15	Ratio=.1
3.80	Link=Rubber	DOF=U2	Fixed=No	NonLinear=Yes	TransKE=822	TransCE=0	TransK=822	TransYield=147.15	Ratio=.1
4.43	Link=Rubber	DOF=U2	Fixed=No	NonLinear=Yes	TransKE=604	TransCE=0	TransK=604	TransYield=147.15	Ratio=.1

Table A. 3 Input for "Rubber isolator" with n=0.1, r=10%

Period(s)	Isolator Property Input								
0.63	Link=Rubber	DOF=U2	Fixed=No	NonLinear=Yes	TransKE=29608	TransCE=0	TransK=29608	TransYield=294.35	Ratio=.1
1.26	Link=Rubber	DOF=U2	Fixed=No	NonLinear=Yes	TransKE=7402	TransCE=0	TransK=7402	TransYield=294.35	Ratio=.1
1.90	Link=Rubber	DOF=U2	Fixed=No	NonLinear=Yes	TransKE=3289	TransCE=0	TransK=3289	TransYield=294.35	Ratio=.1
2.53	Link=Rubber	DOF=U2	Fixed=No	NonLinear=Yes	TransKE=1850	TransCE=0	TransK=1850	TransYield=294.35	Ratio=.1
3.16	Link=Rubber	DOF=U2	Fixed=No	NonLinear=Yes	TransKE=1185	TransCE=0	TransK=1185	TransYield=294.35	Ratio=.1
3.80	Link=Rubber	DOF=U2	Fixed=No	NonLinear=Yes	TransKE=822	TransCE=0	TransK=822	TransYield=294.35	Ratio=.1
4.43	Link=Rubber	DOF=U2	Fixed=No	NonLinear=Yes	TransKE=604	TransCE=0	TransK=604	TransYield=294.35	Ratio=.1

Table A. 4 Input for "Rubber isolator" with n=0.1, r=20%

Period(s)	Isolator Property Input								
0.63	Link=Rubber	DOF=U2	Fixed=No	NonLinear=Yes	TransKE=29608	TransCE=0	TransK=29608	TransYield=588.6	Ratio=.1
1.26	Link=Rubber	DOF=U2	Fixed=No	NonLinear=Yes	TransKE=7402	TransCE=0	TransK=7402	TransYield=588.6	Ratio=.1
1.90	Link=Rubber	DOF=U2	Fixed=No	NonLinear=Yes	TransKE=3289	TransCE=0	TransK=3289	TransYield=588.6	Ratio=.1
2.53	Link=Rubber	DOF=U2	Fixed=No	NonLinear=Yes	TransKE=1850	TransCE=0	TransK=1850	TransYield=588.6	Ratio=.1
3.16	Link=Rubber	DOF=U2	Fixed=No	NonLinear=Yes	TransKE=1185	TransCE=0	TransK=1185	TransYield=588.6	Ratio=.1
3.80	Link=Rubber	DOF=U2	Fixed=No	NonLinear=Yes	TransKE=822	TransCE=0	TransK=822	TransYield=588.6	Ratio=.1
4.43	Link=Rubber	DOF=U2	Fixed=No	NonLinear=Yes	TransKE=604	TransCE=0	TransK=604	TransYield=588.6	Ratio=.1

Legend:

DOF	Degree of Freedom (U1= local X dir., U2= local Y dir., U3= local Y dir., R1=rotation around local X dir., R2=rotation around local Y dir., R3=rotation around local Z dir.
TransKE	Effective Stiffness (Linear analysis required)
TransCE	Equivalent Damping (Linear analysis required)
TransK	Pre Elastic Stiffness (Non-linear analysis required)
TransYield	Yield Force
Ratio	Post-Pre Stiffness Ratio

Units are in kN and meters

APPENDIX B:

DESIGN VALUES USED IN THE NK METHOD AND THE CHART METHOD

Values used in the NK method

25000 kN under PGA of 0.5 g

Fu	3500.00	kN			
Dd	0.25	m			
Keff	14000.00	kN/m			
W	25000.00	kN			
Teff	2.68	secs			
Sd	0.50	g			
B	1.33	damping	15%		
Ev	824.67	kN.m			
k_2/k_1	0.1				
Q	K2	K1	Dy	Q	Fy
824.6680716	10701.33	107013.28	0.01	853.91	916.30
853.91	10584.34	105843.42	0.01	855.34	948.79
855.34	10578.65	105786.50	0.01	855.41	950.37
855.41	10578.37	105783.69	0.01	855.41	950.45

10000 kN under PGA of 0.5 g

Fu	3500.00	kN			
Dd	0.25	m			
Keff	14000.00	kN/m			
W	10000.00	kN			
Teff	1.70	secs			
Sd	0.50	g			
B	0.84	damping	3%		
Ev	164.93	kN.m			
k_2/k_1	0.1				
Q	K2	K1	Dy	Q	Fy
164.9336143	13340.27	133402.66	0.001	165.84	183.26
165.84	13336.62	133366.20	0.001	165.85	184.27
165.85	13336.60	133365.99	0.001	165.85	184.28
165.85	13336.60	133365.99	0.001	165.85	184.28

25000 kN under PGA of 1.0 g

Fu	3500.00	kN
Dd	0.70	m
Keff	5000.00	kN/m
W	25000.00	kN
Teff	4.49	secs
Sd	1.0	g
B	1.59	damping
Ev	3848.45	kN.m

25%

k_2/k_1	0.1				
Q	K2	K1	Dy	Q	Fy
1374.446786	24999.73	249997.25	0.01	3944.84	1527.16
3944.84	24999.21	249992.11	0.02	4138.71	4383.16
4138.71	24999.17	249991.72	0.02	4154.11	4598.57
4154.11	24999.17	249991.69	0.02	4155.34	4615.68

10000 kN under PGA of 1.0 g

Fu	3500.00	kN
Dd	0.70	m
Keff	5000.00	kN/m
W	10000.00	kN
Teff	2.84	secs
Sd	1.00	g
B	1.01	damping
Ev	923.63	kN.m

6%

k_2/k_1	0.1				
Q	K2	K1	Dy	Q	Fy
329.8672286	9999.93	99999.34	0.004	331.60	366.52
331.60	9999.93	99999.34	0.004	331.61	368.45
331.61	9999.93	99999.34	0.004	331.61	368.46
331.61	9999.93	99999.34	0.004	331.61	368.46

Values used in the Chart method

25000 kN under PGA of 0.5 g

Fm	3500.00	kN	14% of the weight	
D_d	0.25	m		
W	20000.00	kN		
S_d	0.5	g		
k_2/ k_1	0.1			
w/k_1	0.5		k_1	50000kN/m
F_y/w	5%		F_y	1250 kN

10000 kN under PGA of 0.5 g

Fm	3500.00	kN	14% of the weight	
D_d	0.25	m		
W	10000.00	kN		
S_d	0.5	g		
k_2/ k_1	0.1			
w/k_1	0.5		k_1	20000kN/m
F_y/w	5%		F_y	500 kN

25000 kN under PGA of 1.0 g

Fm	3500.00	kN	14% of the weight	
D_d	0.70	m		
W	20000.00	kN		
S_d	0.5	g		
k_2/ k_1	0.1			
w/k_1	1.7		k_1	14706kN/m
F_y/w	10%		F_y	2500 kN

10000 kN under PGA of 1.0 g

Fm	3500.00	kN	14% of the weight	
D_d	0.70	m		
w	10000.00	kN		
S_d	0.5	g		
k_2/ k_1	0.1			
w/k_1	1.7		k_1	5882kN/m
F_y/w	10%		F_y	1000 kN